11-14-2017

Experimental Study of High-Temperature Range Latent Heat Thermal Energy Storage

Chatura Wickramaratne
University of South Florida, chaturaw@mail.usf.edu

Experimental Study of High-Temperature Range Latent Heat Thermal Energy Storage

by

Chatura Wickramaratne

A dissertation submitted in partial fulfillment
of the requirements for the degree of
Doctor of Philosophy
Department of Mechanical Engineering
College of Engineering
University of South Florida

Major Professor: Yogi Goswami, Ph.D.
Elias Stefanakos, Ph.D.
Jaspreet Dhau, Ph.D.
Rasim Guldiken, Ph.D.
Sarath Witanachchi, Ph.D.

Date of Approval:
November 2, 2017

Keywords: Macro-encapsulation, PCM, Spherical EPCM, Capsule sealing, Cylindrical capsule, Flow conditioners

DEDICATION

I dedicate this work to my parents, Mahinda Wickramaratne and Thusita Wickrmaratne, my sister, Nisayuri Gunatilake, and my uncle, Sunil Weerasekara, for their relentless support and encouragement towards my educational accomplishments.

ACKNOWLEDGMENTS

First of all, I would like to express my sincere gratitude to my advisor, Dr. D. Yogi Goswami, for providing me this opportunity to pursue higher studies in the field of engineering. His guidance, inspiration, and words of encouragement helped me in numerous ways throughout my stay at Clean Energy Research Center (CERC). I am very grateful for the constant support and guidance I received from Dr. Jaspreet Dhau. I would also like to appreciate Dr. Elias Stefanakos, for his years of sound advice, and my committee members, Dr. Rasim Guldiken and Sarath Witanachchi, for their support and encouragement.

I would take this opportunity to thank my friends in CERC, Rajeev, Arun, Francesca, Mehdi, Eydhah, Barry, Philip, Abhinav, Tanvir, Rachana, Saumya, Saeb, Jamie, Yanyang , Antionos, for their support and help. I would like to thank Dr. Jotshi, Dr. Krakow, Dr. Mujumdar, Dr. Ram, Dr. Rahman, Mr. Garretson, Mrs. Barbara Graham, and Mr. David Goslin who helped me in the course of my stay in Clean Energy Research Center. I would like to acknowledge Dr. Dubey, all my professors and support staff at the mechanical engineering department for their support. I'm thankful for the Advanced Research Projects Agency-Energy (ARPA-E) for their financial support towards the research that I was involved in.

I am forever grateful to Samantha Wijewardane and Thejaka Amila Jayasekara, who were instrumental in directing me to the path of higher studies. Finally, I am grateful to my mother, father and all my family members for their unconditional support throughout my life.

TABLE OF CONTENTS

LIST OF TABLES

LIST OF FIGURES

ABSTRACT

Among all thermal energy storage (TES) systems, latent heat thermal energy storage (LHTES) attracts high interest due to its high energy density and high exergetic efficiency. Due to the high enthalpy of fusion and low cost, inorganic salts are becoming popular as phase change materials and are used as the storage media in LHTES systems. The main drawbacks for the inorganic salts are their low thermal conductivity and high reactivity above 500°C. Therefore, designing a cost-effective containment at these conditions with longevity is a challenge. Macro-encapsulation of the PCM is one way to solve both the PCM containment issue as well as the low thermal conductivity problem. However, finding a practically viable encapsulation technique is a challenge especially for temperatures above 500°C.

In the present study, encapsulation techniques were investigated for two temperature ranges; 500°C – 600°C and 600°C above. Metallic encapsulation was adopted for the 500°C – 600°C temperature. Commercially available, low-cost carbon-steel tubes were used, and the encapsulation shape was cylindrical. A 200µm coating of Ni was applied to strengthen the corrosion resistance. For temperatures above 600°C, a novel approach involving the use of ceramic materials was investigated for encapsulating chloride based PCMs. Low-cost ceramics with excellent thermal and chemical stability under molten-salt conditions were identified as the encapsulants. The influence of sintering temperature on the reactivity of feldspar, ball clay, kaolin and the mixture thereof with molten sodium chloride was investigated. The results were used to

develop an optimum ceramic capsule fabrication procedure, using a green ceramic body followed by sintering at 1190°C. An innovative sealing process of in-situ layered eutectic formation was introduced. Sealing was performed at a temperature above the eutectic melting point of the salt mixture but below the individual melting points of each salt. The fabricated capsule survived more than 500 thermal cycles without showing degradation in its thermo-physical properties. Alumina (99%) based capsule containing NaCl-KCl was tested successfully for 1000 thermal cycles with a PCM weight loss of less than 5%.

A lab-scale setup was designed and constructed to test an industry scalable LHTES system suitable for supplementing heat to a steam-powered cycle. Metallic cylindrical capsules were used with a eutectic of sodium sulfate (Na_2SO_4) and potassium chloride (KCl), which melts at 515^{o}C, as the PCM for energy storage. This system was modeled and validated with experimental measurements. The calculated ratio of exergy to energy efficiency was around 89% (for 380-535^{o}C). Flow irregularities were found due to a bend in the flow channel. Therefore, flow conditioners were investigated. A modified system with the flow conditioners and radiation shields showed 98% exergy to energy efficiency ratio (for 495-535^{o}C). The overall efficiency of the system, however, was found to be low due to the heat losses from the storage tank.

Finally, a novel design of a TES system using spherical capsules is proposed with additional enhancement gained from the experimental work on the lab-scale LHTES system. The innovation of this design lies in the manufacturing process to forms multiple spherical capsules using sheet metals. The adoptability of this technique for higher or lower temperature LHTES applications depends on the properties of the selected sheet metal. Any formable sheet metal can be used depending on the compatibility with PCM and HTF.

CHAPTER 1: INTRODUCTION

Many renewable energy sources are restricted by their intermittent nature. In many cases, they are supplemented with non-renewable energy sources. For instance, solar thermal energy is limited by the sun's availability. However, use of thermal energy storage (TES) can provide assurance and reliability for it to stand alone as a power source. With the growing global renewable energy generation, the need for low-cost thermal energy storage has become inevitable.

Common types of TES technologies currently available include sensible heat thermal energy storage (SHTES) and latent heat thermal storage (LHTES)[1]. Kuravi et al. [2] gave a review of the technologies and systems for thermal energy storage in solar thermal power plants. LHTES is more attractive as it provides a higher energy density and, therefore, requires less storage material compared to SHTES [3–5]. Latent heat storage also has the capability to provide stored energy at a nearly constant temperature, which corresponds to the phase transition temperature of the phase change material (PCM) and results in maintaining high exergetic efficiency [6–9].

Low-temperature TES, operating in a temperature range below 200^{o}C, has been widely studied for building heating and cooling applications [10–12], Hasnain et al. reviewed the advantages and disadvantages of most common thermal energy storage technologies for cooling and heating applications[13,14]. Sharma et al. discussed the use of TES in solar cooking, solar water heating, and air-heating applications [5].

High-temperature TES can play a vital role in solar thermal power [15,16]. Use of high-temperature TES in waste heat recovery and hydrogen production was examined by Maruoka, N et al. [17] . Kuravi et al. [2] and Tian et al. [18] discussed the importance of integration of TES systems with concentrated solar power plants (CSP) and other renewable energy production technologies. A major part of research in this field is focused on identifying and characterizing new PCMs [19–22]. Kenisarin [23] investigated high-temperature phase change materials, ranging from 120˚C to 1000˚C, and discussed the compatibility of PCMs with encapsulation materials. Agyenim et al. [24] reviewed the progress of latent heat thermal energy storage systems over the last three decades by investigating various PCMs, heat transfer and enhancement techniques. Furthermore, they discussed the importance of geometry and configuration of the PCM container. Drawbacks of LHTES discussed here include low heat transfer properties of PCM and limitations in encapsulation at elevated temperatures [24].

One of the main concerns related to LHTES is its long charging and discharging times leading to inefficient energy retrieval and higher system losses. The main reason for this is the low thermal conductivity of PCMs [23,25]. Many techniques have been proposed to improve the thermal conductivity of PCMs[25–29]. Inclusion of expanded graphite or carbon nanotubes in a PCM material can increase its thermal conductivity [30,31]. Micro and macro-encapsulation techniques also increase the heat transfer rate [32–34]. Alam et al. [34,35] tested a lab-scale packed bed system of spherical capsules for a temperature range of 286-326˚C. They used a polymer-based macro-encapsulation technique to form capsules of sodium nitrate PCM which melts at 306˚C.

Finding cost-effective yet reliable encapsulation techniques becomes difficult with the increase of operating temperature. Ceramics are quite efficacious in high-temperature applications as they are less prone to corrosion under high-temperature molten-salt conditions (hot corrosion) than metals and metal-alloys [36]. Even though ceramics provide high corrosive resistance, finding a cost-effective encapsulation technique is still challenging [37–40]. Metallic encapsulation with surface coating was found to be reliable and cost-effective for temperatures below 600˚C [40,41].

Most of the experimental research has been done for low-temperature LHTES applications even though there is considerable focus on high-temperature range applications.

1.1 TES Design Requirements

The important parameters for the design of a TES system include, storage density, capacity, charging and discharging rates and efficiencies. In order to design a smooth and efficient system, certain requirements must be fulfilled [42]:

- Compatibility of storage medium in the operating temperature range
- High energy density in the storage material
- Good heat transfer between the heat transfer fluid (HTF) and the storage medium
- Mechanical and chemical stability of the storage material
- Compatibility of HTF, heat exchanger, and storage medium
- Complete reversibility in charging/discharging cycles and no degradation of TES materials as well as equipment.
- Cost effective system
- Low system heat losses

- Ease of operation

1.2 TES Material

Depending on the energy absorption/ retrieval process of TES material, there are three forms of Thermal Energy Storage,

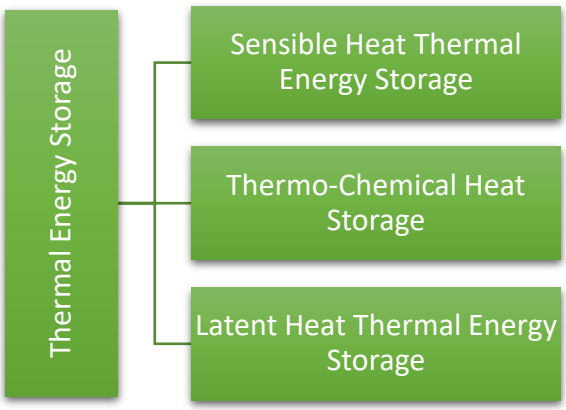

Figure 1.1 TES categorization

1.2.1 Sensible Heat Thermal Energy Storage (SHTES)

In a SHTES system, the storage material stores or releases heat while the material phase remains unchanged. The energy storage capacity of a SHTES system depends on the total mass of the storage material, its specific heat and the temperature change in the material. SHTES technologies have been are the most common commercially available in the power plant sector [2]. Sensible heat TES media can be either liquid or solid. Specific energy, energy density, full cycle (round trip) efficiency, expected lifetime and cost are some of the key parameters in a SHTES system [43,44].

Molten salts are commonly used in SHTES for central receiver tower type of solar thermal power systems [45]. Molten salts, while being non-toxic and non-flammable, are compatible with the working temperatures of the present high-pressure power plants. The molten salts have received considerable attention other than solar power generation as they are already used in the chemical and metallurgical industries as heat-transfer fluids [46]. The most common commercially available salts is known as solar salt, 60% of NaNO3 and 40% of KNO3, that melts at 221^{o}C [47]. Apart from the liquid phase materials, solids like concrete and ceramics have been widely studied due to their low costs, good thermal conductivities and moderate specific heats [48].

Even with some disadvantages, sensible heat materials are currently applied in solar thermal plant applications. Molten salts have a relatively high freezing point which limits their operating temperature range in a system [49]. They require maintaining high outlet temperatures thus, high heat losses, and more expensive piping and materials. The sensible portion of thermal energy is rarely fully utilized due to the required temperature difference as a heat transfer driving force. The low energy density of sensible heat materials results in large volumes or quantities of sensible heat materials and consequently, higher storage costs.

1.2.2 Thermo-Chemical Heat Storage

Thermo-chemical storage systems adopt a reversible endothermic/exothermic chemical reaction to store and release heat. The effective reversibility of the chemical reaction determines the efficiency of the system. The main advantage of thermo-chemical heat storage is its high energy density compared to other storage options. SnO_x/Sn and ammonia system have been mostly examined for chemical storage systems [50,51]. Regardless of its high energy density,

thermo-chemical heat storage is considered to be an expensive method as it is still in the initial stages of development.

1.2.3 Latent Heat Thermal Energy Storage (LHTES)

Latent heat thermal energy storage (LHTES) stores energy by absorbing or releasing the latent heat when a storage material undergoes a phase change. LHTES systems based on phase change materials (PCMs) with solid-liquid phase transition are considered to be more efficient in comparison to solid-solid and liquid-vapor transitions [28].

LHTES has attracted attention due to its advantages like high energy density, high exergetic efficiency, and moderate cost. Present examined uses of PCMs for thermal storage mainly involve low to moderate temperatures (below 300^{o}C). Although the use of PCM in High-temperature LHTES has been studied for solar power plant applications, it has not yet been commercially used [16,52].

Most of the PCMs used in high-temperature LHTES have low thermal conductivities and as a result, exhibit low charging and discharging rates [25,27,53]. Therefore, new heat transfer enhancement techniques are needed to make LHTES commercially viable.

There are three main components of a LHTES system[28],

1. PCM suitable for the desired operating temperature range
2. Encapsulation method for the PCM
3. Heat exchanger (heat transfer mechanism between TES material and HTF)

When designing a Latent heat TES system, the first step of the design stage is the selection of a suitable PCM. Characteristics and importance of PCM to the latent heat TES will be discussed in detail in the next chapter.

1.3 Research Objectives

As mentioned in the earlier section, there is very little research on high-temperature range (above 500°C) LHTES systems. The main focus of this study is to examine and develop a LHTES system for high-temperature applications. A considerable amount of research has been done on PCMs [19–22], but insufficient work has been reported in the literature on encapsulation techniques for the high-temperature range. Therefore, the objectives of this research are:

1. Design and develop an encapsulation method for phase change materials used for high-temperature thermal energy storage (500°C above)
2. Experimentally analyze the system performance of high-temperature thermal energy storage system

The research challenge associated with the first objective is to fabricate a practically viable encapsulation technique for a high-temperature PCM. Volume expansion of high-temperature PCM can be even over 20%. Careful selection of an encapsulation material is important along with the method of encapsulation for the stability and durability of the PCM storage system.

It is evident from the past studies that most of the experimental work on LHTES has been carried out for low temperature PCMs (0-60°C) [24]. There is hardly any experimental data for LHTES system over 500°C. The second objective focuses on the testing and evaluation of a lab-scale LHTES system for applications over 500°C. The research challenge of this objective was minimizing the system losses and neutralizing the flow imbalances inherent to a compact lab-scale arrangement and to overcome uneven heating and cooling inside the TES system.

In chapter two, a literature review of heat transfer enhancement techniques and encapsulation methods are discussed. Phase change materials and their advantages are also discussed briefly in the chapter.

Chapter three investigates the encapsulation of PCMs and compatibility of ceramic as a shell material. Chapter three also provides a discussion on the dependency of the porosity and reactivity on the sintering temperature, capsule sealing and metal encapsulation. A novel approach to the sealing of eutectic mixtures is presented and experimentally validated.

Chapter four discusses the construction of a lab-scale LHTES system with cylindrical PCM capsules and experimental study of its performance at high temperature operating conditions. Radial and axial temperature variations are analyzed. The energy and exergy efficiencies of the system are calculated, and heat transfer issues are addressed.

In chapter five, a novel method is proposed considering the heat transfer as well as manufacturability. In addition, potential manufacturing techniques are discussed. Finally, conclusions based on the design and experimental study and recommendations for further study are summarized in chapter six.

CHAPTER 2: IMPORTANT PARAMETERS FOR LATENT HEAT THERMAL ENERGY STORAGE

Design of a LHTES system is based on the type of application, storage capacity, energy storing/extraction effectiveness and cost. Selection of a phase change material (PCM) as the storage medium plays a key role in the design of a LHTES system. Since the research is on encapsulated PCM storage, materials and method of encapsulation are also key parameters. Even though each parameter has its own selection criteria, the interaction and the compatibility of one another was considered in the design. Key parameter and their selection criteria are discussed in detail based on a review of the literature in this chapter.

2.1 Phase Change Materials (PCMs)

A PCM at first acts similar to sensible heat storage materials until its temperature increases to its phase change temperature, however, the amount of sensible heat stored is small. The main portion of the energy is stored in the phase change period, making the latent heat component significantly larger than the sensible heat portion.

The focus of this research is on solid-liquid transition system as liquid-gas or solid–gas phase transition is limited in TES systems due to the large volume changes associated with the phase transition [28]. These PCMs can be divided into organic materials and inorganic phase change materials [54].

2.1.1 Organic and Inorganic PCMs

In general, inorganic PCMs have higher latent heat energies as compared with organic materials, therefore, show higher storage capacity per unit volume. Thermal conductivity is comparatively better in inorganic materials and can get high operating temperatures because of the usually high phase transition temperatures. Inorganic PCMs are cheaper compared to organic PCMs [27]. However, there are some shortcomings with inorganic PCMs that need to be addressed. Inorganic PCMs are typically corrosive, especially to metals, thus leading to a short service life of the system [55]. Other problems with inorganic PCMs include phase segregation and supercooling, that can reduce the effectiveness of the TES system [56]. However, metals and metallic alloys show no phase segregation or supercooling and are suitable for high-temperature applications [57]. Containment is one of the key issues with metals as the volume changes on phase change can be fairly large in comparison with non-metals. Zalba et al. [58] highlighted the advantages and disadvantages of organic and inorganic PCMs as shown in Table 2.1.

Table 2.1 Advantages and disadvantages of PCMs [58]

	Inorganic PCMs	Organic PCMs
Advantages	• Greater phase change enthalpy	• Non-corrosive • Low supercooling • Chemical and thermal stability
Disadvantages	• Supercooling • Corrosion • Phase segregation • lack of thermal stability	• Low thermal conductivity • Flammability • Lower phase change enthalpy

2.2 Method of PCM Containment

To ensure a long lasting and efficient LHTES system, the method of PCM containment is critical. PCMs are typically placed in cylindrical [24,59,60] or rectangular shaped containers [24,61] . The most analyzed LHTES arrangement is the shell and tube configuration[62–65].

The method of PCM containment has a direct impact on the heat transfer rate of the overall system, thus affects the charge and discharge times and the thermal performance of the LHTES system. Appropriate PCM container geometry coupled with the right heat enhancement technique can provide a better overall performance for the LHTES system.

2.2.1 Heat Enhancement Techniques for LHTES

As stated earlier, most PCMs, except metals or metal alloys, have low thermal conductivity and as a result, would lead to slow charging and discharging rates. Thermal conductivity of non-metal PCMs usually falls below 0.6 W/m.K range [18,58]. Initial melting of a PCM in the charging cycle enables a natural convection driven process, thus making it comparatively faster than the discharging process [66]. The impact of having low thermal conductivity is prominent during the solidification process as it forms a solid layer at the inner surface of the capsule, thus making it a conduction driven process. Agyenim et al.[24] listed several techniques to improve the heat transfer rate for LHTES systems. Figure 2.1 shows the drawings and pictures of some of the heat transfer enhancement techniques that were reviewed in this study.

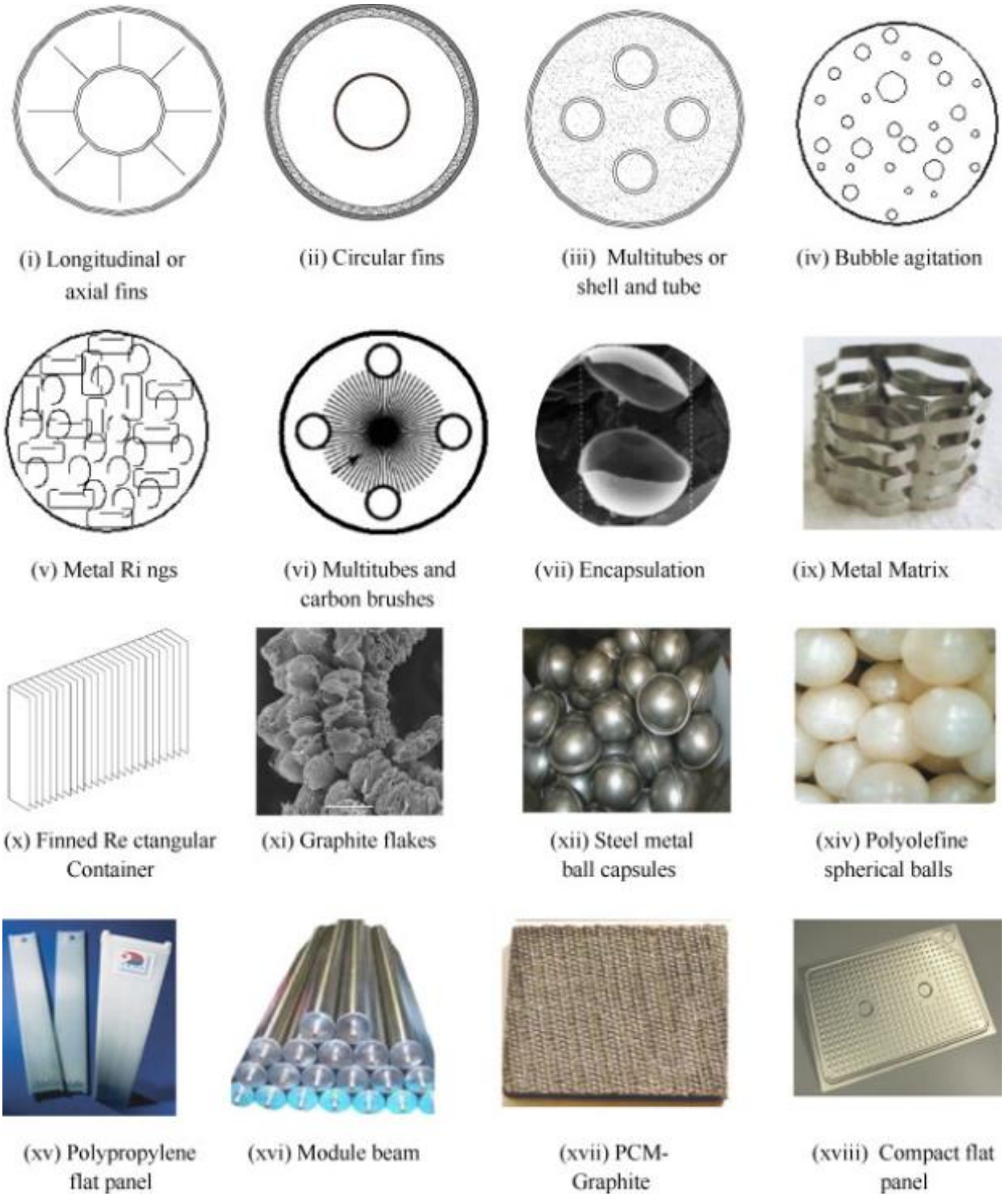

Figure 2.1 Various heat transfer enhancement techniques [16] (with permission)

Ibrahim et al. [67] separated the enhancement techniques into three categories and reviewed the recent developments in each category.

Table 2.2 Thermal enhancements for LHTES [67]

Heat transfer enhancement	Thermal conductivity enhancement	Combined techniques for heat transfer enhancement
• Embedded fins • Heat Pipes • Multiple PCMs • Encapsulation	• Dispersion of high conductivity nanoparticles • Porous materials • Low-density, high conductive materials	• Finned heat pipes • Combined heat pipe-metal foil • Fins with multiple PCMs

Out of all the techniques, the most popular enhancement technique is the use of extended surfaces such as fins.

2.2.1.1 Use of Fins

Due to the simplicity, low cost and ease of fabrication, a majority of the heat enhancement techniques have been based on fins. Fins are typically used to increase the effective heat transfer area between HTF and PCM and therefore enhance the thermal performance of TES system.

Thermal conductivity, corrosion potential with HTF/PCM, cost and density are usually the crucial parameters when it comes to the selection of fin materials [27]. Materials like aluminum, copper, and graphite foil are selected primarily for their high thermal conductivity (over 100 W/m.K), and materials like carbon steel are selected due to their low cost. Stainless steel is also used as a fin material because of its corrosion resistance [27].

Several studies have been done on fins of different configurations in LHTES systems. There are two standard configurations of fins in LHTES systems [67]:

1. Systems that involve heat storage and retrieval through a HTF
2. Systems that serve as a heat sink/reservoir through hot/cold boundary wall

In heat sink type-LHTES (no HTF), the fins are located inside the PCM. Even with the HTF, the fins are usually embedded in the material with the lower relative thermal conductivity, which in most cases is the PCM side [68].

Compared to other enhancement techniques, the amount of experimental studies carried out for fins is significant. Table 2.3 summarizes some of the experimental studies carried out for LHTES systems.

Table 2.3 Studies of heat transfer enhancement with fins

Fin geometry	System geometry	Fin material	Notes	Ref
Rectangular	Cylindrical	Aluminium	Solidification time was inversely proportional to the number of fins.	[69]
Rectangular	Rectangular	Steel	Close to 40% decrease in solidification time compared to the base case.	[70]
Rectangular	Rectangular	Aluminium alloy	Increasing the fin height and number of fins increased the thermal performance of the system.	[71]
Rectangular	Shell and tube	Copper	Fin length gives higher PCM charging rate.	[63]
Rectangular	Shell and tube	Brass	12.5%(inlet at 80°C) and 24.52%(inlet at 85°C) decrease in melting time compared to the base case.	[72]
Rectangular	Rectangular shell and tube	Aluminium	Increase in flow rate reduced both melting and solidification time whereas this drop is more significant for the melting than solidification.	[73]

Table 2.3 (continued)

Rectangular	Triplex concentric tubes(TTHX)	Copper	Melting time was decreased by 34.7% for the highest number of fin configuration compared to the base case.	[74]
Rectangular	TTHX	Copper	Solidification time was decreased by 35% highest number of fin configuration compared to the base case.	[75]
Rectangular	TTHX	Copper	The internal-external fin arrangement decreased the melting time by 43.3% compared to the base case.	[76]
Circular	Cylindrical tube	Stainless steel	Heat transfer coefficient was doubled with the use of thick-finned arrangement.	[77]
Circular	Shell and tube	Bronze	The amount of stored energy increases with the increase in fin radius and decrease in fin space.	[78]
Circular/longitudinal	Cylindrical tube	Copper	Enhancement of the heat transfer rate was high in longitudinal fin arrangement compared to the circular fin arrangement.	[79]
Spiral	Cylindrical tube	Copper	Thermal conductivity improvement was three times high compared to the base case.	[80]

All the fin arrangements described in the literature have used metallic PCM containers. Therefore, the tested operating temperatures were below 600^{o}C.

2.2.1.2 Use of Heat Pipes

A heat pipe (HP) can deal with high heat transfers as its operation involves phase change (evaporation and condensation). Some researches analyzed the improvement in charging and discharging processes of PCM with the use of HP [81–87]. Gravity assisted and wick assisted are some of the common types of heat pipes. Operating temperature range, geometric size, and configuration of the TES system are some of the key parameters for the selection of HPs for TES

systems. One typical configuration of storage systems that can adopt HPs for heat transfer enhancement is the shell and tube type TES.

A large number of numerical studies were carried out on analyzing the effect of HP configuration, orientation, and number of HPs on the thermal performance of LHTES systems, but the experimental studies were limited [81–83,85,87]. Robak et al. [84] experimentally compared the effect of HP and fins in a LHTES system and found that the overall melting rates for the heat pipe systems were, on average, 70% greater than the non-HP setup and 50% greater than the system with fins. Tiari et al. [88] used a primary central heat pipe with an array of secondary heat pipes for a PCM containing vertical cylindrical type container. Both melting and solidifying behaviors were analyzed with the use of photographic images as well as internal temperature measurements. Increasing the incoming hot HTF flow rate from 1.89 L/min to 7.57 L/min led to a 30% improvement in the charging process. Increasing the temperature of the incoming HTF from 63 °C to 73 °C during charging resulted in 55% reduction in the system's charging time. Both of the experimental works mentioned above are for low temperature applications. No experimental studies have been reported in the literature for high temperature applications using this technique.

2.2.1.3 Multiple PCM Systems

Having multiple PCMs in a LHTES system enables a nearly constant heat flux throughout the passage between the HTF and the PCMs. This arrangement improves the heat transfer of the overall system. Several PCMs of different melting temperatures are arranged in a decreasing order of their melting temperatures along the HTF flow direction during the charging process. The HTF flow direction is reversed during the discharging process moving the HTF through PCMs

in increasing order of their melting points which enables a nearly constant heat transfer rate from the PCM to HTF [66].

Table 2.4 summarizes some of the numerical and experimental studies of multiple PCMs in LHTES systems. It is evident that using multiple PCMs was beneficial when the difference between the charge and discharge temperatures increased.

Table 2.4 Studies of multiple PCMs in LHTES systems

PCM containment	Nature of work	No. of PCMs	Notes	Ref
Cylinder tubes	Numerical	5	30-35% improvement in charge-discharge rates were attained for six different operating temperature ranges.	[89]
Cylindrical tube	Numerical	3	The proposed method can improve the receiver performance in a solar dynamic power system and decrease the fluctuation of HTF temperature.	[90]
Shell and tube	Numerical	4	The selection of PCM fractions and their melting temperatures are important for the performance improvement.	[91]
Shell and tube	Numerical	2	Using multiple PCMs increased the heat transfer rate by an average of 57%.	[62]
Rectangular slabs	Numerical	3	The LHTES was used for air conditioning and higher COPs were obtained for shorter and thinner PCM slabs	[92]
Rectangular slabs	Numerical	2	The LHTES was used for air conditioning and higher COPs were achieved for higher inlet temperatures, while higher exergy efficiencies were achieved for lower inlet temperatures.	[93]
Shell and tube	Experimental	2	An average improvement of 19.36% was obtained in comparison with the single PCM arrangement.	[94]
Cylindrical capsules	Experimental	3	The amount of stored energy increased by 15%.	[95]
Cylindrical capsules	Experimental	3	Melting time reduction of 37–42% was obtained compared to the single PCM LHTES system.	[96]

Experimental studies of multiple PCMs in LHTES systems are limited in the literature. Farid et al. [95] constructed an experimental setup to test three different wax type PCMs (melting temperatures of 44°C, 53°C, and 64°C). They reported a 15% improvement with the multiple PCM configuration during the latent heat period. Peiro et al. [94] tested a cascaded system for a temperature range of 150-200°C. Hydroquinone, melting range of 165- 172°C, and d-Mannitol, melting range of 155-162°C were used as PCMs. The system with two PCMs arrangement showed a higher consistency in the HTF temperature change between the inlet and outlet. An average overall enhancement of 19.36% was obtained in comparison with the single PCM arrangement.

2.2.1.4 Dispersion of High Conductivity Nanoparticles

Dispersing nanoparticles in a PCM is one of the simplest and most effective ways to enhance its thermal conductivity [97]. Table 2.5 summarizes some of the experimental studies on thermal conductivity improvement of PCMs containing nanoparticles.

Table 2.5 Studies of nanoparticles use in PCM systems

Nanoparticle	PCM type	Notes	Ref
Aluminium powder	Paraffin	The charging duration was reduced by close to 60% for the mixture compared to the pure paraffin.	[98]
Al_2O_3 nanoparticles	*n*-octadecane	The natural convection heat transfer in the melted region degraded with the increase of nanoparticles.	[99]
TiO_2 nanoparticles	*n*-octadecane	The maximum improvement happened at 3 wt% of nanoparticles in the mixture. Increasing over 4 wt% reduced the thermal conductivity in the liquid phase.	[100]
Carbon nanotubes(CNTs) & nanofibers(CNFs)	Paraffin and soy wax	The enhancement of thermal conductivity is high in CNF mixtures in contrast to CNT mixtures.	[101]

Table 2.5 (Continued)

CNT	Palmitic(PA)–stearic acid(SA)	The thermal conductivity was increased by close to 20%, 26%, 26% and 30% for the CNT mass fractions of 5 wt%, 6 wt%, 7 wt% and 8 wt% respectively.	[102]
Single and multi-walled carbon nanotubes	Paraffin	A highest enhancement of close to 13% was achieved for the PCM containing single-walled carbon nanotubes.	[103]
Multi-walled carbon nanotubes(MWCNT)	Palmitic acid	Thermal conductivity improvement was 36% in the solid state and 56% in the liquid states for the mixture of 5 wt% MWCNT and PCM.	[126]
MWCNT	Paraffin	Thermal conductivity improvement was 35% in the solid state and 45% in the liquid states for the mixture of 2 wt% MWCNT and PCM.	[104]
MWCNT/graphite	Paraffin	MWCNTs were more effective compared to graphite as a thermal conductivity enhancer.	[105]
MWCNT/CNF/graphene nanoplatelets(GNPs)	Paraffin	PCM with GNPs showed the highest thermal conductivity enhancement of 164% at 5 wt%.	[106]
GNPs	Lauric acid	The thermal conductivity improvement by GNP(1 vol%) was close to 230% compared to the base case.	[107]
Cu nanowires	Tetradecanol	The overall thermal conductivity increased with the increase of Cu nanowires	[108]
CuO nanoparticles	KNO3/NaNO3/ KNO3-NaNO3 eutectic	Substantial improvements in thermal conductivity were achieved for both the eutectic salt and pure nitrate salts with the addition of nanoparticles.	[109]

The literature on experimental studies with nanoparticles on high-temperature LHTES is limited [96,109–113]. Myers et al.[96,114] analyzed the possibility of enhancing radiative heat transfer with a dispersion of infrared radiation (IR) absorbing particles in high-temperature

molten salt applications. They considered CuCl, $CoCl_2$, $FeCl_2$, and $NiCl_2$ as additives for the NaCl-KCl eutectic mixture, which has a melting temperature of 657°C. Their study showed that the IR range absorption in the PCM was increased due to the additives.

2.2.1.5 Enhancement with Porous Materials

Several studies have been done on thermal conductivity improvements by impregnation of PCMs into porous conductive materials [115–120]. Having a porous material with high thermal conductivity makes the overall thermal conductivity of the PCM-porous material combination higher than the pure PCM [119]. Aluminum foam and expanded graphite (EG) are widely used as porous materials to increase the thermal conductivity of PCMs. The improvement is mainly due to their high thermal conductivities and relatively low or medium densities [67]. A quite a few experimental studies were done on PCM-porous material composite systems, some of which are shown in Table 2.6.

Table 2.6 Studies of heat transfer enhancement by porous materials

Porous material	PCM material	Notes	Ref
Graphite matrix	Paraffin	Thermal conductivity of the composite matrix was 20 times greater than that of the pure PCM.	[119]
Aluminium foam	Paraffin	The inclusion of aluminum foam decreased the discharging duration by 42.42% and charging duration by 15.37%.	[121]
Graphite foams (GFs)	Paraffin	Thickness of ligaments and pore size of the foam are significant parameters in improving the thermal diffusivity and the storage capacity of the system.	[122]
Expanded graphite (EG)	Paraffin	Thermal conductivity was increased with the increase of mass fraction of EG(2-10%).	[123]
Compressed expanded natural graphite (CENG)	Paraffin	Thermal conductivity improvement of the paraffin/CENG composite was more than 28 times of the pure paraffin.	[124]

Table 2.6 (Continued)

Copper porous foam (CPF)	Eicosane ($C_{20}H_{42}$)	Thermal conductivity was increased from 0.423 W/mK to 3.06 W/mK.	[125]
Copper, steel alloy and EG	$NaNO_3$	Compared to the pure PCM, heat transfer rate was doubled during the solid phase but remained almost same in the liquid phase due to the weakening of natural convection	[126]
Copper foam, copper-steel alloy and EG	$NaNO_3$	heat transfer was improved by foams of copper and copper-steel alloy as well as EG.	[127]
EG	$LiNO_3$–KCl, $LiNO_3$–$NaNO_3$, $LiNO_3$–NaCl	Substantial improvements of thermal conductivity were achieved for the eutectic mixtures.	[128]
Copper foam, Nickel foam	$NaNO_3$-KNO_3	Inclusion of metal foam reduced the natural convection of the PCM composite mixture compared to the pure PCM system.	[129]

Most of the studies have been done on low-temperature applications. But the noticeable thing is the improvement in discharging time due to the solid phase thermal conductivity improvement. Natural convection was usually prominent during melting in the case of pure molten salt but it was weakened by the use of metal foams or porous materials. Therefore, the charging time improvement was negated due to the increase in the discharge time in many cases.

2.2.1.6 Dispersion of Low-density Materials

Metal particles are usually denser than the PCM and as a result distributing them in the PCM is hard. The enhancement expected from these metal particles would be hindered by having these particles settled at the bottom of the PCM container. One alternative technique is to use low-density high conductivity particles. Carbon fiber is one such substitute for high-density metal particles. Carbon fiber has relatively low density, and its thermal performance is in the same range as copper and aluminum [66].

Fukai et al. [130] experimentally tested the improvement of thermal conductivity in a carbon fiber-paraffin system. Carbon fibers were tested for two orientations; random and brush type. The brush type gave the best performance and it was found that the effect of fiber length on the thermal performance was minimal. Hamada et al. [131] tested the effects of carbon-fiber chips and carbon brushes in low-temperature *n*-octadecane PCM system and found that heat transfer improvement for the carbon brusher was higher than the fiber chips arrangement.

Like in the earlier cases, a majority of the studies were focused on the low-temperature applications.

2.2.1.7 Combined Techniques for Heat Transfer Improvement

The approach of combining two or more heat transfer techniques to achieve more enhancement in the overall thermal performance has become more popular in the recent past. Table 2.7 shows some of the experimental studies of combined heat transfer technique used in LHTES systems.

Table 2.7 Studies of combined heat techniques in LHTES systems

Combined methods	System geometry	Notes	Ref
Fins & heat pipe(HP)	Rectangular heat pipe heat exchanger	The rate of energy retrieval from the PCM was increased by 86% and the effectiveness of HP was increased by 24%.	[132]
Fins & HP	Rectangular heat pipe heat exchanger	The amount of energy stored was increased by 140% in the 12-HP configuration compared to the base case.	[133]
HP & metal foil	Cylindrical enclosure	Melting and solidification rates were doubled in contrast to the HP only system.	[134]

Table 2.7 (Continued)

Copper form & fins	Rectangular container	The thermal conductivity improvement was 3.7 times that of the system without fins.	[135]
HP & metal foam, HP & metal foil	Cylindrical enclosure	High melting and solidification rates were achieved with both HP with foil arrangement and HP with foam arrangement.	[136]
Macro-encapsulation & foam, Macro-encapsulation & sponge	Cylindrical capsules	The effective conductivity improvement with foam was 15% and with sponge was 32%.	[137]

This area of research is still developing, and so far a majority of the studies have been focused on finned-HP type enhancements. The combination of encapsulation with IR absorbing particles [96] was investigated and later adopted in this study to further improve the heat transfer of encapsulation.

2.2.2 Encapsulation

Encapsulation can overcome the low thermal conductivity of a PCM by reducing the path length and increasing the surface area for heat transfer. Encapsulation is typically done by covering the PCM with a suitable coating or shell material [33]. The use of proper encapsulation has the following advantages [138,139]:

- Enhancement of heat transfer rate by increasing the effective surface area
- Isolation of the PCM from HTF and the container vessel.
- Potential for greater exergetic efficiency with the use of a cascaded PCM arrangement
- Enhancement in thermal and mechanical stability of the system
- Reduction in tankage cost

Encapsulated phase change materials (EPCM) are small capsules with the PCM in its core [140]. Different shapes and sizes of EPCM have been adopted for different applications. Based on size, encapsulated PCMs can be classified into the following:

- Nano-encapsulation (0-1000 nm)
- Micro-encapsulation (1-1000 µm)
- Macro-encapsulation (above 1 mm)

Thermo-mechanical stability of the encapsulation and PCM is very important considering thermal cyclic loads that are typically associated with LHTES applications. Compared to macro-EPCM, nano-EPCM and micro-EPCM PCMs usually provide higher heat transfer rates in the charging and discharging cycles. However, the lower PCM-to-shell mass ratio significantly reduces the energy storage density, thus increasing the storage cost [141].

Substantial work has been done on EPCM for lower temperature applications (less than 300^{o}C). Thermal performance, stability and manufacturability of micro-EPCM and nano-EPCM were studied for low temperature applications [142–145]. Most of the studies on high temperature applications were based on macro-encapsulation. Table 2.8 shows some of the experimental studies of macro-encapsulation for LHTES systems operating in the temperature range of 300^{o}C or above.

In a recent study, Fukahori et al. [146] used a ceramic (alumina) as the encapsulation material for an application in the temperature range of 400-650^{o}C. They used an aluminum and silicon (25 wt%) mixture as the PCM which melts at 577^{o}C. An alumina (Al_2O_3) cup of one inch diameter, was sealed by slightly overlapping a cap also composed of alumina. A thin aluminum film with a thickness of 10µm was placed around the part of the cup where it would be in contact

Table 2.8 Experimental studies of macro-encapsulation for LHTES systems

Encapsulation		PCM	Operating range	Notes	Ref
Shape	Material				
Spherical	Polymer	NaNO3, KNO3-NaNO3	200°C - 330°C	Capsules were tested for over 1000 cycles with no degradation and weight loss.	[34,35]
Cylindrical	Silica	NaNO3	300°C - 500°C	Nonuniformity of coating resulted in capsule failure before 10 thermal cycles.	[147]
Cylindrical	Stainless steel	NaNO3, NaCl–MgCl2	350°C - 500°C	For a 100°C temperature difference, the latent heat of phase change contributed 57% and 75% to storage capacity for NaNO3 and NaCl–$MgCl_2$ respectively.	[148]
Cylindrical	Alumina	Aliminum-25wt% Silicon	400°C - 650°C	The capsules successfully survived for 100 thermal cycles.	[146]
Spherical	chromium and nickel	Copper	1050°C - 1150°C	The capsules successfully survived for 1000 thermal cycles.	[41]

with the cap. After placing the cap over PCM filled cup, the capsule was heated to over 660°C to melt the aluminum and seal the capsule. Phase change volume expansion was discussed and provisions were made to overcome the issue. However, the solid state expansion of the shell (silica) and the PCM, which is considerably high for aluminum, were not discussed. No leakage was reported for 100 thermal cycles (400-650°C).

Another high temperature range EPCM study was done by Zheng et al. [41]. They fabricated spherical capsules of 2mm diameter with copper as the PCM. Shell material was made from a combination of chromium and nickel, which were electroplated to a thickness of 100 µm

and 500 µm respectively. The capsules successfully survived 1000 thermal cycles. Both Fukahori et al. [146] and Zheng et al. [41] reported thermal cyclic durability, but did not consider the cost of encapsulation material or process.

CHAPTER 3: ENCAPSULATION OF PHASE CHANGE MATERIALS

3.1 Phase Change Material Selection

The selection of a PCM for TES application depends on many factors. Studies on a wide range of organic and inorganic PCMs have highlighted certain desired characteristics for efficient latent heat TES systems [5,28,58]. These characteristics are as follows:

- Melting temperature appropriate for the operating temperature range.
- High enthalpy of fusion
- High density
- High specific heat (both in solid and liquid state)
- Small volume change
- Low vapor pressure during the liquid state
- High thermal conductivity
- Congruent melting to avoid segregation of components (binary or ternary systems)
- Chemically stable, non-corrosive
- Non-toxic and non-flammable.
- High availability and low cost.
- No supercooling

The phase transition temperature of the PCM must match the operating temperature for the desired application. High enthalpy of fusion and high density would provide a high energy per

volume of PCM material. This minimizes the size of the storage containers and the amount of PCM used. A higher specific heat would increase the sensible energy portion of the storage, and a high thermal conductivity would reduce the charging and discharging times [149].

The small volume expansion during phase transition is necessary for designing simpler and more cost-effective containment or encapsulation methods. Low vapor pressures reduce the contamination and ease the encapsulation process. To prevent irreversible segregation, the PCMs must melt congruently.

Supercooling interferes with the extraction of energy and is very common in salt-hydrates. It is essential to minimize the supercooling effect as much as possible in thermal cyclic operations to get the best out of the discharge cycle [150]. The selected PCM should display a good chemical stability and corrosion resistance. PCMs can also degrade as a result of crystallization due to water loss, decomposition or chemical reactions with the containers. Toxicity and flammability must be considered for safety measures, and finally, the commercial availability and cost should be evaluated since the final TES system must be cost-effective and comparable with existing storage systems.

The operating temperature range considered for this research is above 500^{o}C. Chloride based salts are potential materials to meet the higher operating temperature requirements mainly because they are likely to have higher melting temperatures. Furthermore, many chloride salts are comparatively low cost compared to corresponding nitrates, carbonates and fluorides [114,151]. Table 3.1 shows some of the cost and thermophysical data for pure and eutectic chloride salts screened by Myers et al. [152]. The table includes only the salts that have melting temperatures higher than 500^{o}C and cost less than $0.10 per kilojoule (stored energy).

Table 3.1 Cost data and thermophysical properties for pure and eutectic salts [152]

Pure or eutectic salt	Cost (USD/kJ)	Cost (USD/kg)	$T_{melting}$ (°C)	ΔH_{fusion} (kJ/kg)
NaCl	0.01	4.76	801	482
KCl-NaCl	0.02	7.56	657	360
$MgCl_2$	0.02	8.00	714	453
$MgCl_2$-$NiCl_2$	0.03	11.18	692	443
KCl	0.03	9.80	771	353
$CaCl_2$-KCl	0.04	10.66	600	267
$CaCl_2$-NaCl	0.04	9.89	504	265
NaCl-$NiCl_2$	0.04	15.52	573	385
$CaCl_2$-KCl	0.05	11.88	641	237
CaCl2-$NiCl_2$	0.05	14.79	719	276
KCl-$NiCl_2$	0.05	16.41	513	303
LiCl-$MgCl_2$	0.05	21.56	571	418
$CaCl_2$	0.05	12.38	775	253
$BaCl_2$-KCl	0.06	10.92	656	181
$BaCl_2$-$MgCl_2$	0.06	10.49	559	176
$BaCl_2$-NaCl	0.06	9.85	651	163
$CrCl_3$-KCl	0.06	18.35	700	330
LiCl-$NiCl_2$	0.07	31.32	620	450
LiCl	0.07	34.00	610	467
$BaCl_2$-KCl	0.08	11.32	649	135
$CoCl_2$-$MgCl_2$	0.08	32.86	709	412
$CrCl_3$-NaCl	0.08	26.32	593	351
$BaCl_2$-$CaCl_2$	0.09	12.18	608	131
$CaCl_2$-$MnCl_2$	0.09	19.49	587	220
LiCl-$MnCl_2$	0.09	28.50	574	334

Considering the commercial availability, low cost, high enthalpy of fusion and melting temperature, three inorganic salts were selected as PCMs for this study (Table 3.2).

Table 3.2 Selected inorganic PCM with melting point above 500°C

Phase Change Material	Melting Point (°C)	Latent Heat of fusion (kJ/kg)
NaCl	801	482
NaCl-KCl	657	360
Na_2SO_4-KCl	515	197

*Measured in CERC, University of South Florida

The downside of these chloride salts is their corrosiveness in their molten state [153]. Therefore, containing these salts is a challenging task. One of the main objectives of this research was to identify materials and procedures to encapsulate these chloride based PCMs and overcome this difficulty.

3.2 Encapsulation Material Selection

When designing a LHTES system using EPCMs it is vital to ensure that the encapsulation of PCM should meet the requirements of strength, flexibility, thermal stability and corrosion resistance apart from its main feature of providing additional surface area for heat transfer. The best shell material for EPCMs should have the following properties[138]:

1. Adequate thermo-mechanical properties to withstand the phase change process and volume expansions of PCM
2. Consistent thermophysical properties
3. Leak-proof with the corresponding PCM
4. No reaction with the PCM or HTF
5. High thermal conductivity to enhance the heat transfer between the PCM and its surrounding.

In the literature, most common materials used for encapsulation are polymer-based materials. That is because the considered applications were low temperature based. Since our focus is on high-temperature applications and the PCM we selected are inorganic salts, these polymer-based encapsulation materials are not appropriate.

Depending on the operating range and PCM, following selections were made.

1. For temperatures over 600^{o}C, NaCl and NaCl-KCl eutectic were selected as PCMs and ceramic materials were selected as the encapsulation material.
2. For 500-600^{o}C temperature range applications, Na_2SO_4-KCl mixture as the PCM was selected as the PCM and Ni-coated carbon steel was selected as the encapsulation material.

These selections were based on their commercial availability and compatibility with fabrication. This selection of materials and encapsulation process are very interdependent processes.

3.3 Encapsulation Using Ceramic Materials

Ceramic materials can be adopted for both low and high-temperature applications, but are more effective in high-temperature applications as they are less prone to corrosion. Furthermore, ceramics have shown higher corrosion resistance with molten-salt conditions (hot corrosion) than metals and metal-alloys [21]. However, they are inherently porous in nature, which could be detrimental for encapsulation as molten salts normally seep through pores. Porosity also influences chemical and mechanical properties such as compressive strength, thermal diffusivity, and hardness of the ceramic materials [22]. For example, thermal diffusivity, which is important for the present application, decreases with an increase in porosity [23].

We have analyzed the influence of sintering temperature on the porosity and reactivity of the selected ceramic mixture comprising feldspar ($KAlSi_3O_8$), kaolin ($Al_2Si_2O_5(OH)_4$), ball clay (Al_2O_3. $2SiO_2.2H_2O$) and silica (SiO_2). This was done to find the right ceramic composition and sintering temperature for the ceramic capsules.

3.3.1 Material Preparation and Instruments for Testing

A mixture of feldspar, ball clay, kaolin, and silica was used for this study because of the easy availability and low cost of these ceramic components[154]. Feldspar lowers the sintering temperature of ceramics. However, a higher amount of feldspar in the ceramic mixture causes workability and molding issues while shaping a green body (ceramic body before the sintering process). An optimum ceramic composition, feldspar (50%), kaolin (16.67%), 16.67 ball clay (16.67%), silica (16.67%), was selected after several experiments. The composition was selected based on easy workability and molding of wet ceramic paste, lower rejection rate (cracks in the body) at the green and high-temperature sintering stages, and lower sintering temperature and duration when compared with other ceramic materials such as alumina.

Feldspar, Ball clay, Kaolin, Silica were obtained from Axner, USA. Sodium chloride and potassium chloride were obtained from Sigma-Aldrich, USA. Selected ceramic components were mixed in a requisite proportion by using a speed mixture machine (FlackTek). The differential scanning calorimetry (DSC) analysis was carried out using the SDT-Q 600 by TA instruments which can simultaneously perform DSC and thermogravimetric analysis (TGA). Based on metal melting standards, the heat flow, temperature and weight accuracy of this device are ±2%, ±1^oC and ±1%, respectively. All the DSC analyses were performed at a ramp rate of 20^oC/min under an argon (inert) atmosphere. The Fourier-transform infrared spectroscopy (FTIR) analysis of ceramic

samples were performed by using a JASCO 6300 FTIR instrument. Dye absorption by ceramic samples was analyzed with a Leitz Optical Microscope (5x to 100x). Scanning Electron Microscope (SEM) Imaging analysis of the fabricated ceramic samples was performed by using a Hitachi S-800 field emission scanning electron microscope (FE-SEM).

3.3.2 Making of a Workable Ceramic Slurry

Each ceramic component has a different solubility in water. Ball clay and kaolin have shown a higher degree of solubility, whereas feldspar and silica have shown lower solubility at room temperatures. A simple experiment was done to analyze the drying process of each component. This was done in an air-conditioned lab setup (Relative humidity of 65-70 % and temperature of 20 ^{o}C). Initial water amount needed for each material was different and was based on the mixing and workability of the slurry. Ball clay and kaolin showed good workability and needed a higher amount of water compared to feldspar and silica. As expected, evaporation rate (ER) reduced the time for all four cases.

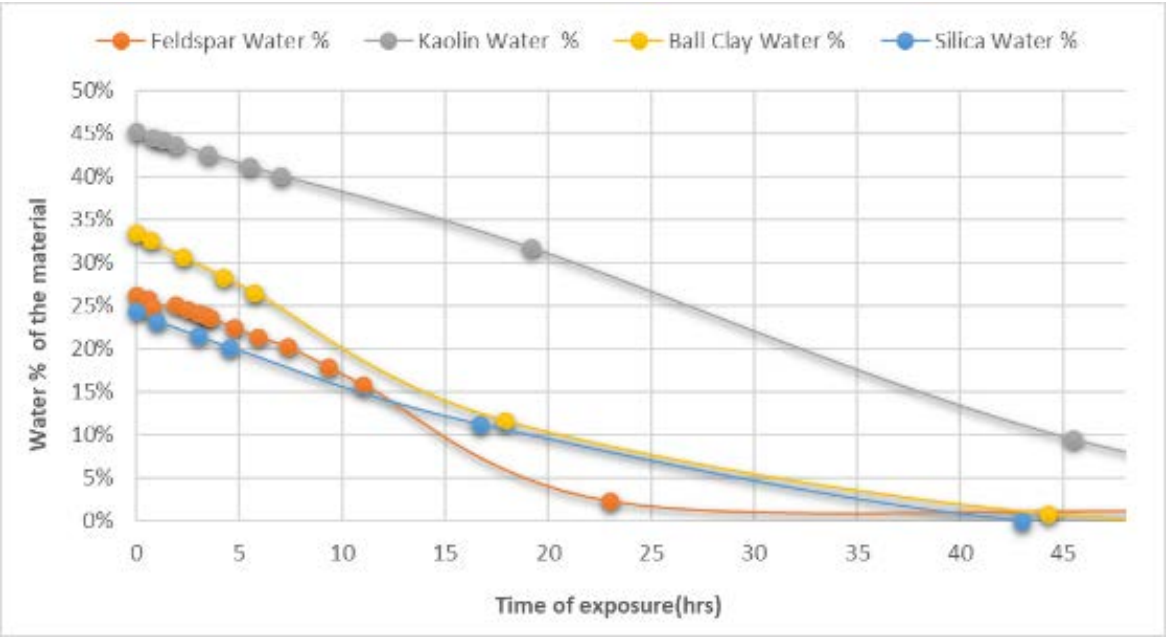

Figure 3.1 Water percentage of the material vs. time

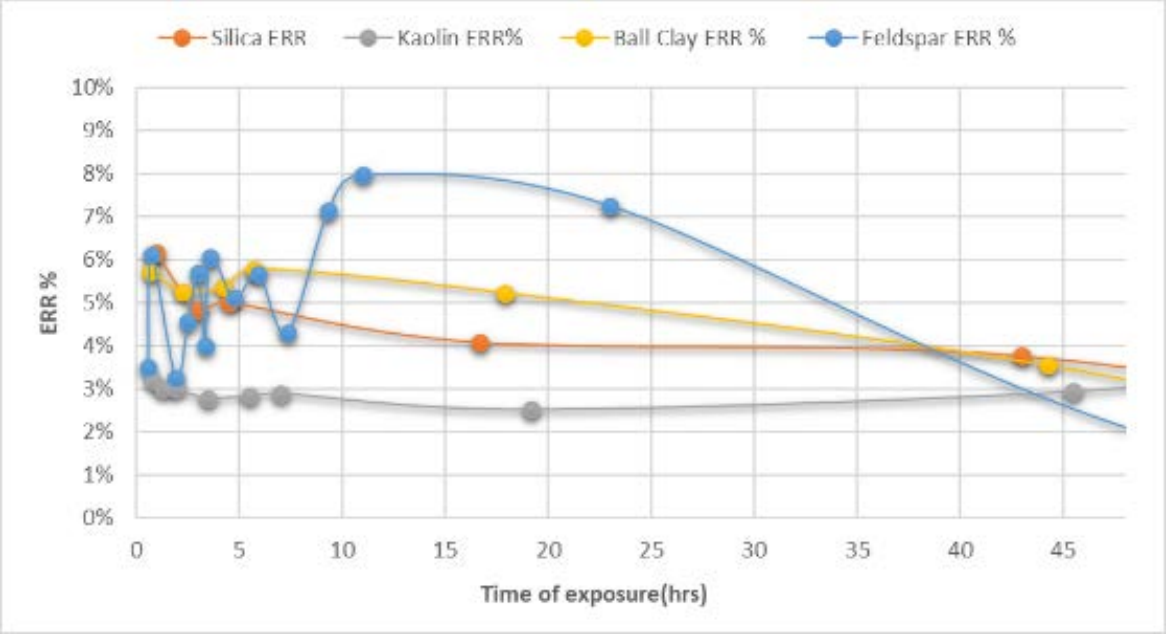

Figure 3.2 ERR percentage (%) vs. time

When further analyzing the data, it was found that the evaporation rate (ER) to the present remaining water amount ratio (ERR) had slightly constant values for the initial exposure period (Figure 3.2). Feldspar and silica both showed segregation and material deposition at the bottom with time. After a couple of hours, two layers were formed with the top being more of a liquid compared to the bottom high dense layer. This was visibly prominent in feldspar than silica. The ERR percentage of feldspar increased after a while, and that can be explained by the layer segregation. Once the layers were formed, the evaporation rate increased as the top layer became more of a liquid with high water content than the original feldspar-water mixture. Ball clay and kaolin did not show any segregation and remained homogeneous throughout the time. Initial water to the ceramic ratio for feldspar and silica was 25 % (weight of water to the weight of total water- ceramic mixture), and for ball clay and kaolin were close to 35% and 45% respectively.

After analyzing the individual drying curves, the right amount of water for the ceramic mixture, 50% of feldspar and 50% of rest of the materials contributing equally, was calculated to be close to 30%. Making several ceramic-water slurries for the combined mixture, it was experimentally found that the correct amount of water was the earlier predicted 30%. This was crucial as higher than the right amount of water content in the mixture increases the drying time and affects the stability of the green ceramic body. A lesser amount of water in the ceramic paste increases inhomogeneity and the rejection rate at the green stage due to cracking and chipping of fabricated parts.

3.3.3 Fabrication Procedure for the Flat Circular Ceramic Discs

A circular metal of one inch diameter mold was used (Figure 3.3 a) to optimize the capsule fabrication procedure, using a wet pressing technique. A ceramic slurry in water was poured onto a thin wooden board for drying purposes. After drying it for 2 hours, a workable ceramic dough was obtained. The workable ceramic dough was shaped into ceramic balls weighing approximately 9 g each. These clay balls were then shaped in a metallic mold by pressing with a 5 lb metal block. After 2 hours (hrs), the metal block was taken off and the molded flat circular green ceramic discs were dried in air for 24 hrs. A total of 24 samples were made, and eight samples were sintered at 800^{o}C (sample set-1). Another eight samples were sintered at 1000^{o}C (sample set-2), and the rest were sintered at 1190^{o}C (sample set-3). 1200^{0}C was the maximum limit of the furnace (Figure 3.3 c) and was not recommended to use it at 1200^{0}C for a length of time. The dwell time used on all three occasions was 6 hours.

Separate samples were sintered for different durations of 4 hrs, 6 hrs, and 8 hrs, to identify the right sintering duration. The best results were obtained with samples sintered for 6

hrs and 8 hrs. In the preliminary stage of development, we selected 6 hrs of sintering for the porosity and compatibility studies of the fabricated flat disk-shaped ceramic samples. For spherical bodies, due to their more complicated shape compared to a flat disc, the sintering duration was increased to 8 hrs.

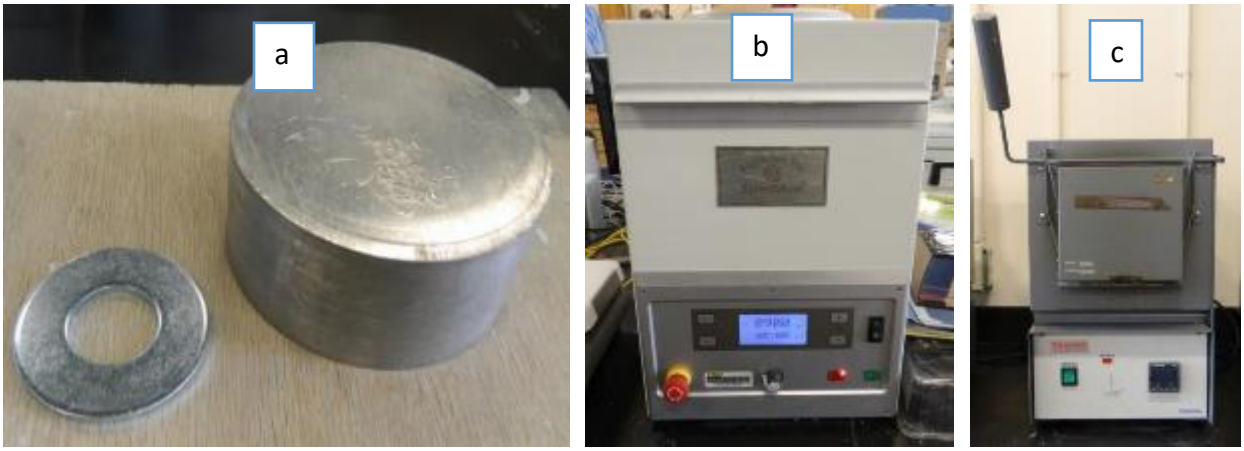

Figure 3.3 a) Ceramic mold & press weight b) FlackTek speed mixer c) Thermo scientific furnace (model: 2416)

Figure 3.4 Sintered ceramic disk

3.3.4 Water Absorption Test

Samples from all three different sintering temperatures were kept submerged in water for 24 hrs. After 24 hrs, the samples were taken out, and the surface water was removed using a water absorbing linen. As evident from Table 3.3, samples 1(sintered at 800°C) and 2(sintered at 100°C) absorbed a substantial amount of water, whereas sample 3(sintered at 1190°C) was found to be completely non-porous to water.

Table 3.3 Water absorption by ceramic samples

Sample No	Dry Weight (g)	Weight of the sample after water absorption (g)	% of water absorption
Sample 1 (Sintered at 800°C)	7.043	8.199	16.41%
Sample 2 (Sintered at 1000°C)	6.932	7.915	14.18%
Sample 3 (Sintered at 1190°C)	6.957	6.958	0.01%

3.3.5 Dye Absorption Test

Another set of ceramic samples was then subjected to a dye penetration test for the qualitative estimation of the extent of porosity and sintering in these samples. The samples were dipped into a 10% vol/vol solution of patent blue VF dye in water for 20 min and then kept in a vacuumed chamber (Figure 3.5) for an additional 1 hr to allow deep penetration of the dye into the sample matrix. The samples were removed from the solution, and their surfaces were cleaned with linen.

Figure 3.5 Vacuum furnace (Isotemp 280A)

The samples were analyzed, and it was found that the dye diffused deep into the matrix of samples 1 and 2 with no trace of the dye in the matrix of sample 3 (Figure 3.6). This illustrates that sample 3 is fully sintered and non-porous to the dye, whereas samples 1 and 2 are very porous. Sample 1 color intensity was high compared to the sample 2, which tells us that sample 1 has the highest porosity out of all three samples.

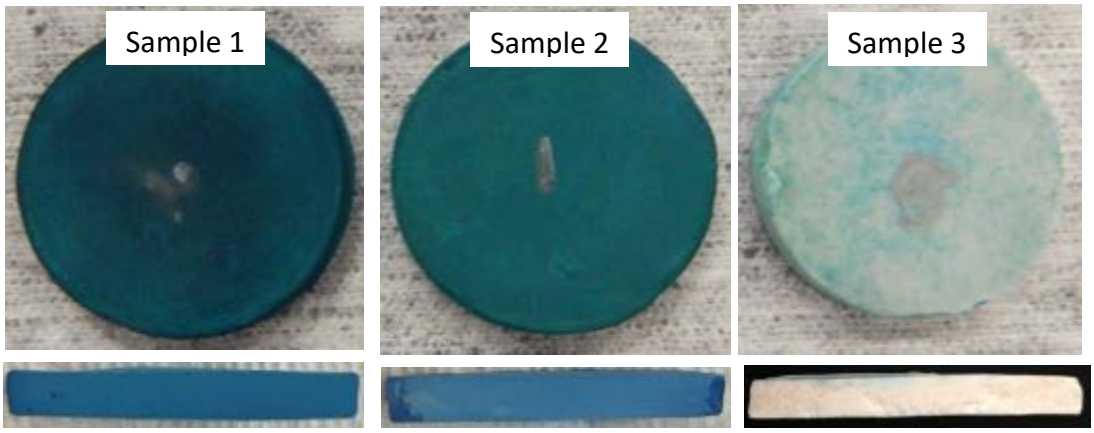

Figure 3.6 Dye absorption by ceramic samples, surface view (top) and cross-section view (below)

3.3.6 Scanning Electron Microscope (SEM) Imaging

Surface and cross sections of the samples were analyzed with a SEM for measuring pore size and microstructural details of the sintered ceramics. In the low-temperature sintered ceramic sample, large interconnected open pores are clearly visible, which may serve as channels for the seepage of molten salts in the fabricated capsules. Figure 3.7 shows the early intermediate stage of sintering (sample sintered at 800°C), as some sintering necks formed with neighboring particles are visible in the matrix (red circles).

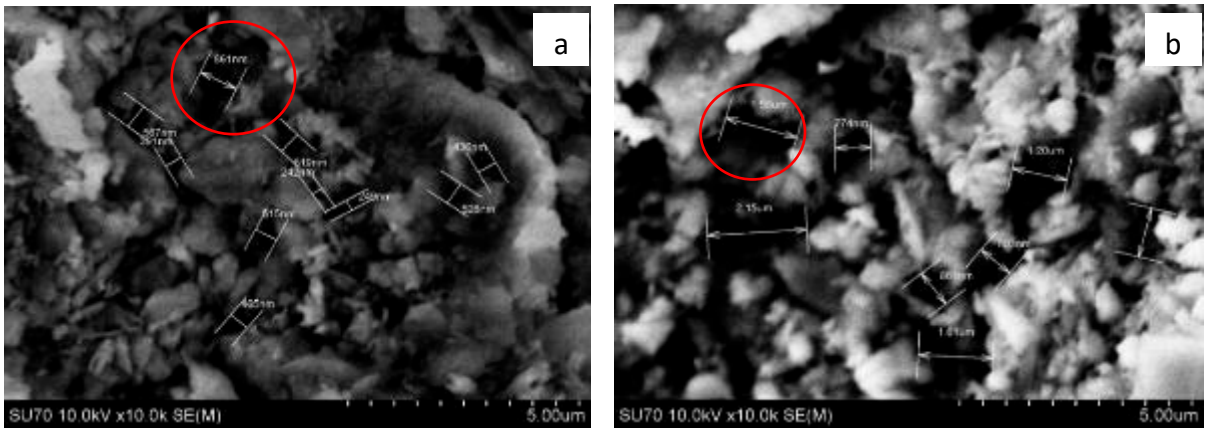

Figure 3.7 SEM of the ceramic samples sintered at 800°C a) surface and b)cross section

The pores were in the micrometer scale range, and the cross-sectional pores were as high as over 2 µm. Surface pores were slightly smaller and in the range of 0.3 – 0.9 µm.

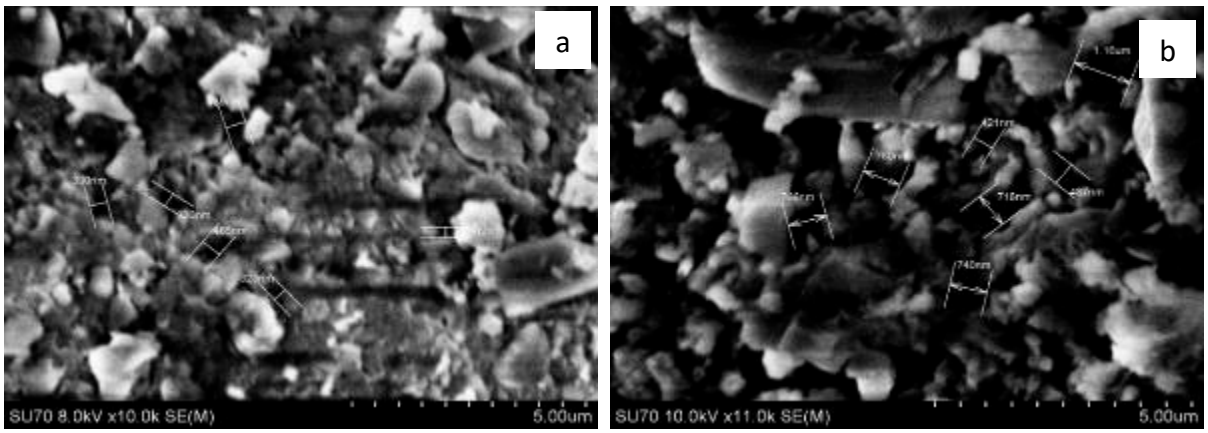

Figure 3.8 SEM of the ceramic sample sintered at 1000°C, a) surface and b) sample cross section

At 1000 ^{o}C, there is a significant decrease in the porosity, but still a few interconnected pores are visible which indicate an advanced intermediate stage of sintering (Figure 3.8). When the ceramic specimens were sintered at 1190^{o}C, the pores completely vanished from the surface (Figure 3.9), and only a few small isolated pores were visible in the cross-section of the sample. It appears that at this temperature a molten phase of the ceramic mixture has penetrated into the porous matrix, plugging interconnected pores completely. All this is indicative of a final stage of sintering of this ceramic composition.

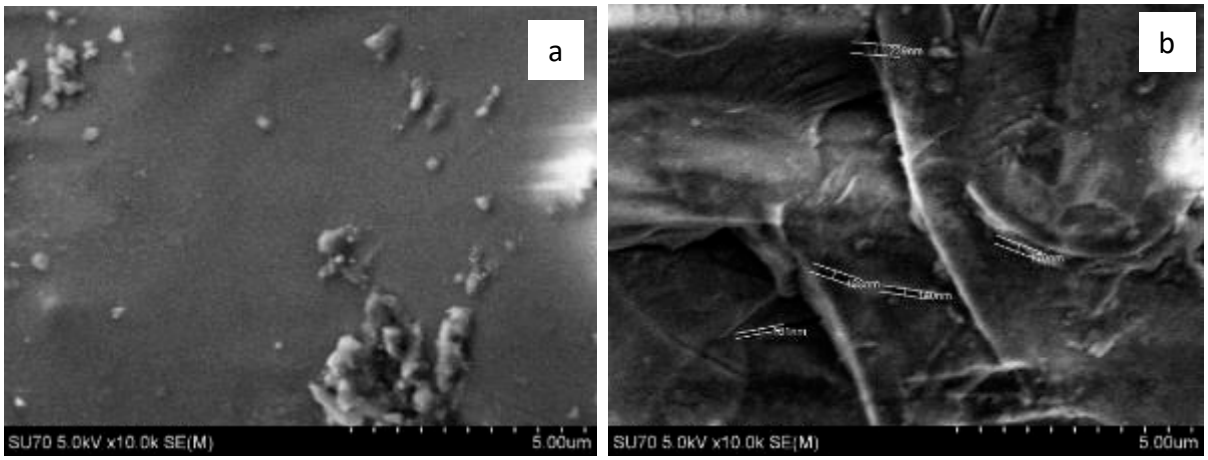

Figure 3.9 SEM of ceramic sample sintered at 1190^{o}C, a) surface and b) sample cross section

3.3.7 Material Compatibility (Hot Corrosion) Study

The compatibility of the encapsulating materials with molten chloride based inorganic PCMs is crucial for the present application. To the best of our knowledge, no such study has been reported in the literature. Ceramic samples of the aforementioned composition sintered at 800^{o}C and 1190^{o}C were tested for reactivity with molten NaCl.

The samples were cut into a small cylindrical shape to fit into the FTIR (JASCO 6300) sample chamber to collect reflectivity data. These samples were kept in separate crucibles and were exposed to the same amount of solid NaCl. As a control reference, two sets of samples

(sintered at 800°C and 1190°C) were placed in crucibles without any NaCl. These samples were then placed in a box furnace maintained at 850 °C for 24 hrs. After 24 hrs, the samples were removed from the furnace and subjected to visual and IR analysis.

The IR spectra of the ceramic samples sintered at 800°C; a) untreated, b) treated with molten NaCl, and c) heated at 850°C for 24 hrs are shown in Figure 3.10. The IR spectra of the untreated sample and the sample heated at 850°C for 24 hrs are nearly identical with respect to their band shapes, intensity, and positions indicating no significant change in the microstructure of the ceramic sample on heating. Interestingly, the IR spectrum of the ceramic sample subjected to a molten NaCl treatment displays significant variations in the intensity, bandwidth, and position of the bands. A comparatively narrower, symmetrical and high intensity band is observed at 3600-3350 cm^{-1}. The band in the untreated sample is much broader and centered at 3650-3270 cm^{-1}. This band is attributable to the surface and internal –SiOH and -AlOH groups. The broadening of the band is due to hydrogen bonding between the surface O-H group and the physisorbed H_2O which bonds to surface O-H groups via hydrogen bonds. Physisorption of water is a reversible process; desorption during heating and resorption on cooling in air. Therefore, we did not notice any change in the spectra of untreated and heated ceramic samples. However, in the presence of molten NaCl, there is a substantial decrease in the number of surface -OH groups due to the reaction shown below.

$$SiOH + Na^+ \longrightarrow SiONa + H^+$$

$$AlOH + Na^+ \longrightarrow AlONa + H^+$$

The decrease in the surface –OH group density is reflected in the decrease in the bandwidth and increase in the intensity of the band in the range 3600-3350 cm^{-1}. Further

evidence of ceramic-molten NaCl reactivity is reflected in the change in the position and appearance of new bands in the IR spectra (Figure 3.10).

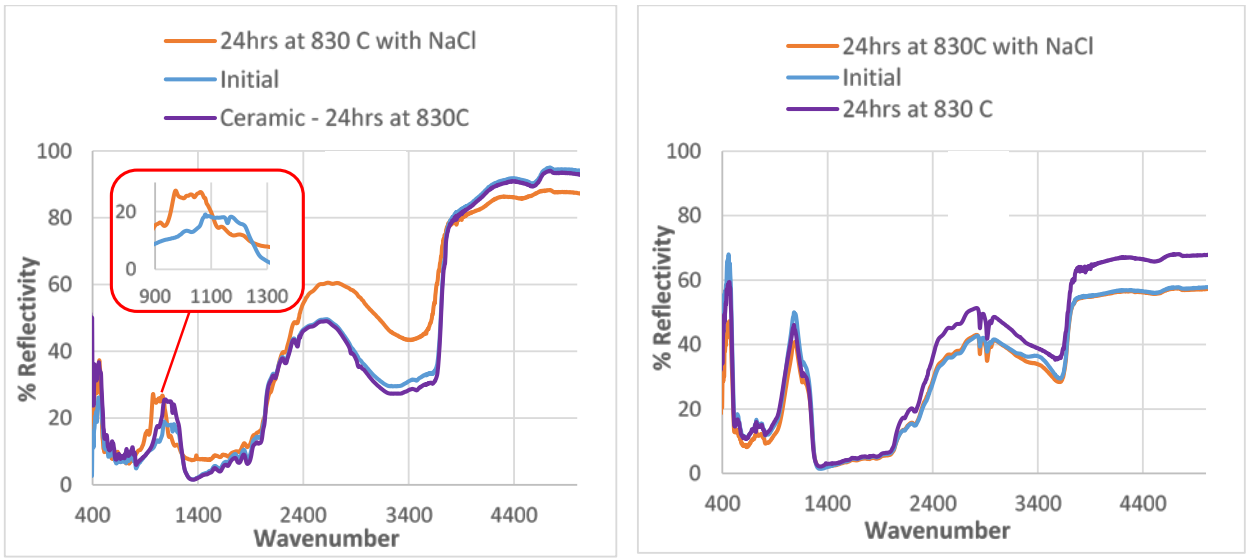

Figure 3.10 IR spectra of ceramic samples sintered at a) 800°C , and b)1190°C; before and after molten NaCl and heat treatment at 850°C for 24 hrs

The IR spectra of the ceramic sample sintered at 1190°C is significantly different from that sintered at 800°C. A very sharp, symmetrical and high intensity band centered at 3616 cm^{-1} is observed which suggest a high degree of dihydroxylation of the surface –SiOH and -AlOH groups. This is evident from the hydrophobic surface of the ceramic sample sintered at 1190 °C (Figure 3.11). The reaction of this sample with molten NaCl did not show any significant change in the IR spectrum (Figure 3.10). Therefore, it can be inferred that molten NaCl reacts with ceramic samples sintered at 800°C, but has no impact on ceramic samples sintered at 1190°C. This was also confirmed from the color change observation after treatment with molten sodium chloride (Figure 3.12). The ceramic samples sintered at 800°C changed color on reaction with molten NaCl, whereas the ceramic samples sintered at 1190°C did not show any change in color after 24 hrs of

treatment with molten NaCl (Figure 3.13). An Energy Dispersive X-ray Spectroscopy (EDS) analysis of these samples displayed an increase in chloride content from 0 to 31% in the 800°C sample and only 2.6% increase in the 1190°C sintered ceramic sample (Figure 3.14).

Figure 3.11 a) Hydrophilic, sintered at 800°C b) hydrophobic, sintered at 1190°C

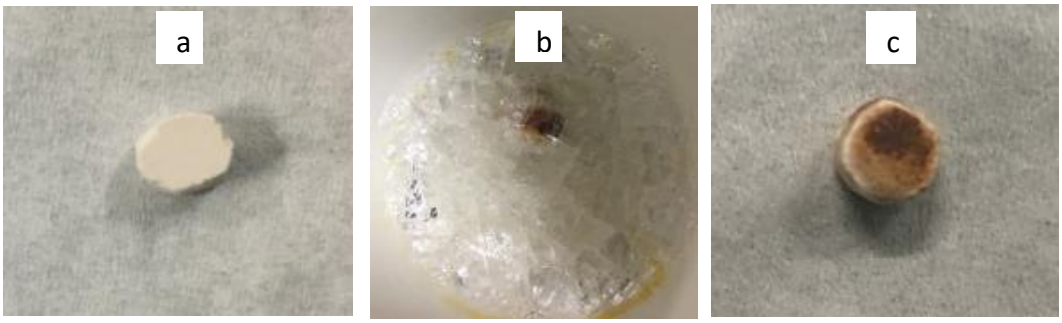

Figure 3.12 Ceramic disc sintered at 800°C; a) before testing, b) and c) after treatment with molten sodium chloride at 850°C for 24 hrs

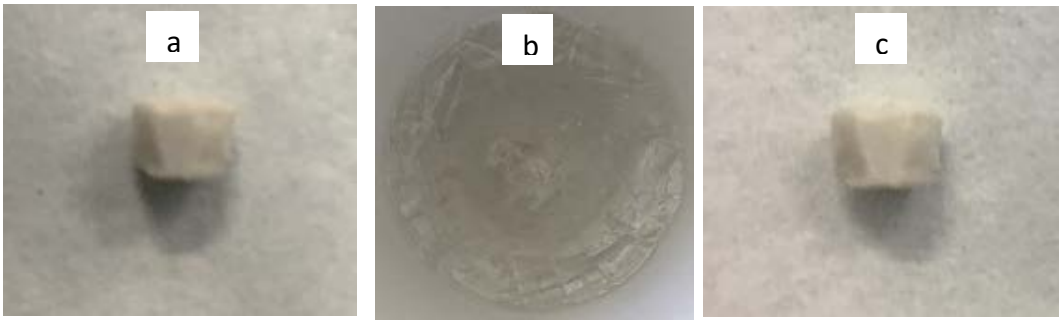

Figure 3.13 Ceramic disc sintered at 1190°C; a) before testing, b) and c) after treatment with molten sodium chloride at 850°C for 24 hrs

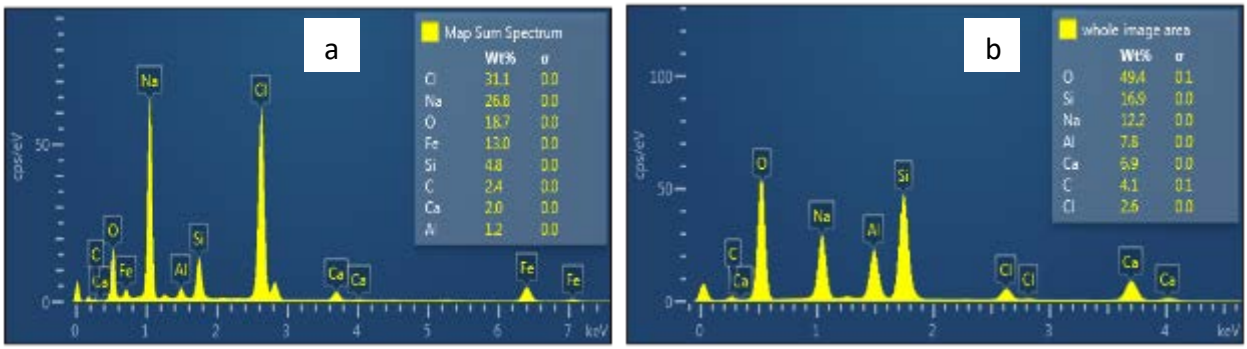

Figure 3.14 EDS of molten NaCl treated ceramic samples sintered at a) 800°C and b) 1190°C

We also subjected individual components of the ceramic mixture, sintered at 800°C and 1190°C, to molten NaCl treatment in order to identify the reactive component in the mixture. The individual components included ball clay, feldspar, kaolin, and silica. Figure 11 displays sintered samples (at 800 °C) before and after treatment with molten NaCl for 24 h at 850 °C. As evident from the color intensity (Figure 3.15), ball clay and kaolin showed the strongest reactivity with molten NaCl. This was confirmed by the reflectance IR spectroscopy of kaolin and feldspar. The spectra of kaolin in Figure 3.16 displayed significant shifting of peaks in the region 370-1034 cm^{-1} and also showed two additional peaks at 637 and 581 cm^{-1}, which suggested significant changes in the internal structure of kaolin after treatment with molten NaCl.

Figure 3.15 Components of ceramic mixture sintered at 800°C (top) and subsequent treatment of the sintered components with molten sodium chloride at 850°C for 24 hrs (bottom)

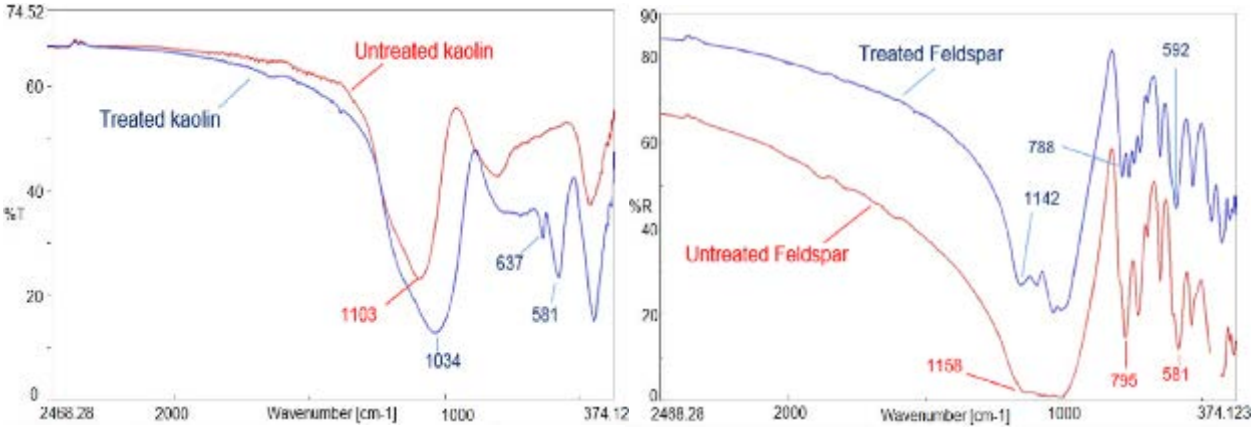

Figure 3.16 IR spectra of kaolin(a) and feldspar(b) before and after treatment with molten NaCl

Interestingly, the samples sintered at 1190 °C showed little or no reactivity with NaCl (Figure 3.17). Only a small variation in the color of the ball clay and kaolin was noticed after treatment with molten NaCl. Clearly, even highly reactive ceramic components, kaolin, and ball clay, become unreactive when sintered at 1190 °C. All this indicate that sintering at 1190 °C is essential to prevent reaction of ceramics with molten salts. It appears that high-temperature

sintering causes dehydroxylation and ceramic densification leading to a reduction in free energy which may be responsible for the decline in material reactivity.

Figure 3.17 Sintered (1190 ^{o}C) ceramics after treatment with molten NaCl at 850 ^{o}C for 24 hrs

3.4 Fabrication of Ceramic Capsules

Once we identified the ceramic composition (50% feldspar, 16.67% kaolin, 16.67 ball clay, and 16.67% silica), sintering temperature and duration, we focused our attention on optimizing the fabrication procedure of the ceramic capsules. We found clear evidence that any partially sintered part of the ceramic capsule could cause sample failure during thermal cycling. We observed that a partially sintered porous ceramic parts react together with molten alkali metal chlorides. This can cause critical structural changes at the grain boundary of the incompletely sintered ceramic body resulting in the development of micro-cracks that subsequently grow in size during thermal cycling, thus leading to leakage of the molten PCM. To ensure complete sintering of the ceramic capsule, the sintering time was increased from 6 to 8 hrs.

Apart from heat transfer benefits of the spherical shape, the stress calculation based on the thin wall equations indicated that the hoop stress generated in a spherical body is half of that of generated in a cylindrical body with the same radius. Therefore, attention was focused on the fabrication of spherical capsules for this application with ceramic.

A mixture of 50% feldspar, 16.67% kaolin, 16.67 ball clay, and 16.67% silica was taken in a container and mixed thoroughly by using a speed mixture machine (FlackTek). Water (30% w/w) was added to the ceramic mixture and mixed to form a ceramic dough or paste. The paste was molded into hemispherical cups by pressing the paste into a hemispherical dye. Two hemispherical cups were then joined by using water and applying some pressure with hands, and a hole was created at the top of the capsules. The green ceramic capsule with a hole at the top was air dried for 24 hrs. After air drying, the capsules were sintered in a controlled temperature environment. The green ceramic capsules were heated to a temperature of 100^{o}C (2^{o}C/min) and dwelled for one hour at this temperature. After this step, the ceramic capsules were heated to a temperature of 1190^{o}C (at 3 ^{o}C/min) and dwelled for approximately 8 hrs. The Figure 3.18 shows the fabrication process flow chart.

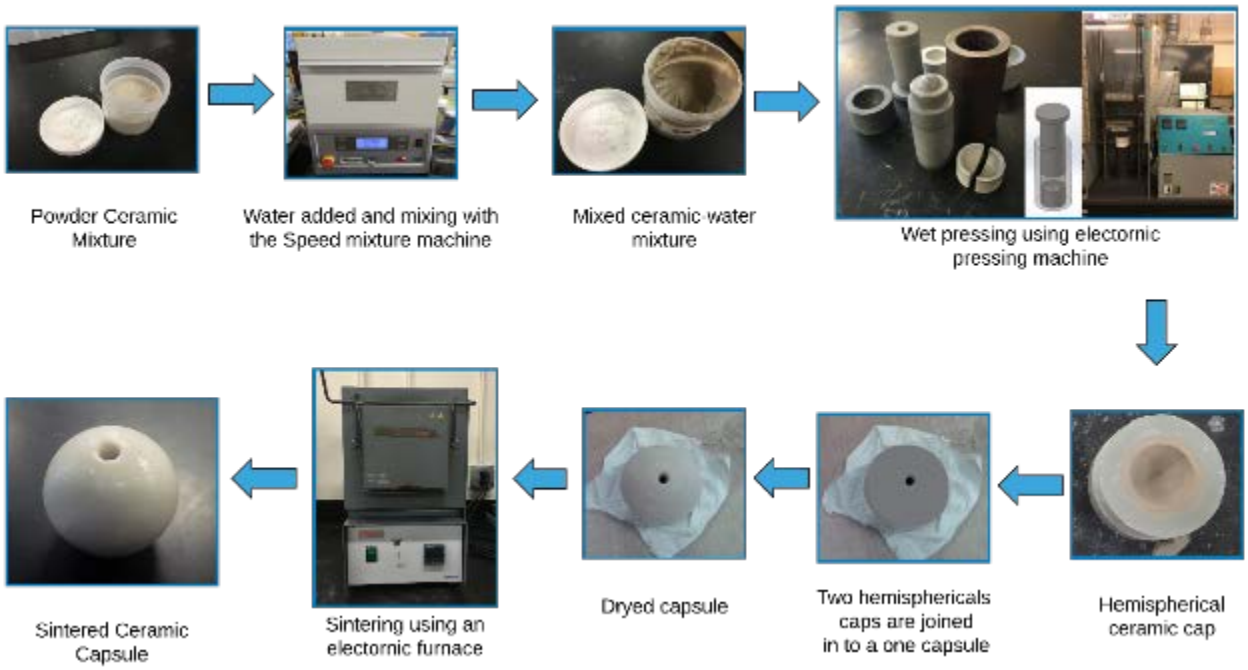

Figure 3.18 Flow chart of the fabrication procedure of the spherical capsule

3.5 Sealing the Capsule

Sealing is one of the major challenges in the encapsulation process. The sealing temperature is restricted because of the phase change temperature and the molten PCM vapor pressure. The contamination happening with PCM vapor can cause damage to the seal making the whole capsule vulnerable to the outside conditions. The post-formed and pre-formed approaches were initially adopted to tackle this problem.

3.5.1 Post-formed Approach

In the post-formed approach, a slurry of ceramic materials was directly applied over spherical salt pellets. Ceramic materials are not flexible and have a low coefficient of thermal expansion compared to inorganic salts. The expansion of salt at elevated temperatures can cause cracks in the ceramic coating. Therefore, provisions were made to allow expansion of the salt in its solid state without cracking the overlying ceramic coating. A temporary intermediate layer was used, which melts on heating and flows out of the porous ceramic layer leaving a space in-between the salt pellet and the ceramic layer. Palmitic acid was used as this intermediate layer. Even after fixing the issue with thermal expansion mismatch, finding a reliable nonporous encapsulation was not easy with the temperature restriction. Combination of Tetraethyl ortho-silicate (TEOS), Carbon fiber and several other chemicals were used with the ceramic mixture (50% feldspar, 50% - Ball clay, Kaolin, Silica) without much success.

Figure 3.19 Ceramic coated sodium chloride salt pellets

Figure 3.20 shows a capsule that was subjected to thermal testing and then cut open to check for reactivity and leakage of salt into the pores of the ceramic layer. The maximum number of thermal cycles that survived post-formed capsule approach did not exceed ten. Therefore, we shifted our attention towards the pre-formed approach.

Figure 3.20 Salt pellet after thermal testing (left)- cut portion of pellet(right)

3.5.2 Pre-formed Approach

The procedure involved the use of a workable slurry of ceramic materials obtained by mixing of ceramic materials which we already discussed in section 3.3.2 & 3.3.3. Two types of dies, spherical and rectangular dies, were used initially to test the sample compatibility.

Figure 3.21 Pre-formed capsules

Sealing materials were chosen considering the PCM melting temperature. Commercially available alumina adhesive (Alumina and latex material) was used initially as the sealing material. This alumina adhesive was for high-temperature applications and had a lower curing temperature than PCM melting temperature. Even with this technique, highest number of cycles achieved from EPCM was around 20 thermal cycles. Again the main issues lied with the sealing. First, the sealing area was not enough, and then the sealing material was porous.

Certain strategies were developed to encounter the issue of the sealing area. Capsules such as Figure 3.22 were able to hold a high amount of sealing materials, but material porosity was still an issue that needed more attention.

Figure 3.22 Techniques of increasing the sealing area

3.5.3 Making Nonporous Seals

Porosity was addressed in two different approaches for two different PCMs because of its melting temperature. For NaCl, which melts at 801°C, a combination of sodium silicate (Na_2SiO_3) and alumina adhesive was used. A small amount of alumina adhesive was initially used, and it was cured at 200°C. On top of the alumina, Na_2SiO_3 powder was added. The softening point of Na_2SiO_3 is around 1000 °C. The localized heating method was adopted to prolong the melting and avoid NaCl vapor as much as possible. Figure 3.23 shows the localized heating block that was used. The sealing area was the only exposed area while the rest were well insulated. The capsules were successful for over 100 cycles but showed small weight reduction after some thermal cycles. For the PCM of NaCl-KCl eutectic, a different approach was used.

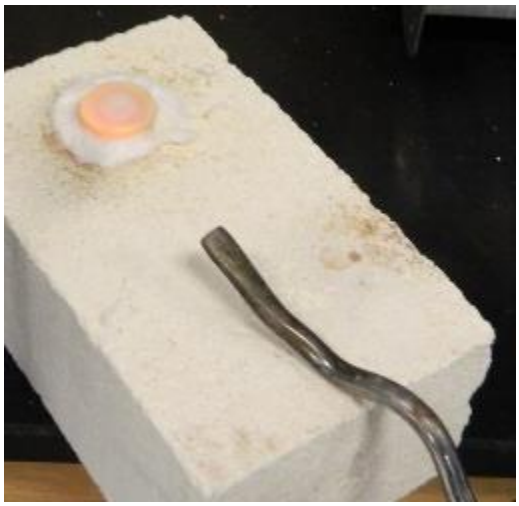

Figure 3.23 Ceramic block for localized heating

3.5.3.1 Novel Concept for Sealing Eutectic Mixtures

This is an innovative novel approach and can be adopted for any eutectic mixture. However, it is more effective if the individual melting points of the pure components are considerably higher than the combined eutectic melting temperature. This was experimentally investigated for the PCM of NaCl-KCl, which was one of our selected PCMs.

Fifty grams of NaCl-KCl eutectic with a melting point of 657^{o}C was used for the experiment. The initial furnace temperature was varied and the time of melting was recorded. This experiment relied on visual inspection, so the status was checked every 15 minutes by opening the furnace (Figure 3.24).

Table 3.4 Melting time comparison of layered and mixed eutectic

Furnace temperature	Time of melting for layered arrangement of eutectic (minutes)	Time of melting for mixed eutectic (minutes)
760 °C	30-45	15-30
750 °C	30-45	15-30
740 °C	30-45	15-30
730 °C	30-45	30-45
720 °C	30-45	30-45
710 °C	45-60	30-45
700 °C	45-60	30-45
690 °C	180 (3hrs)	45-60
680 °C	No melting even after 16 hrs	45-60

Figure 3.24 Molten eutectic of NaCl-KCl

A more accurate quantitative experiment was planned with several thermocouples inside the NaCl-KCl eutectic mixture. Unfortunately, the results were inconclusive. Thermocouples failed due to the corrosion of thermocouple body in the presence of molten salt (Figure 3.25).

Figure 3.25 Corrosion of thermocouples (investigation of melting for an enclosed spherical capsule)

Since we already established some proof with the earlier visual inspection of NaCl-KCl eutectic, we tested the concept with a low-temperature eutectic salt. Melting points of the pure materials and the eutectic used here are as follows;

- $NaNO_3$ – melts at 308^oC
- KNO_3 – melts at 334 ^oC
- $NaNO_3/KNO_3$ eutectic - melts at 221 ^oC

45.7 % wt (50% mol) of $NaNO_3$ and 54.3 % (50% mol) of KNO_3 were used for the eutectic mixture[155]. Three separate samples were made.

- Sample 1 - Mixed the whole eutectic with a speed mixture machine
- Sample 2 - First $NaNO_3$ layer was melted and solidified, and then KNO_3 was added
- Sample 3 - Separate NaNO3 and KNO3 powder layers

Same size alumina crucibles were used for the experiment. The first sample was made by adding 45.7g of NaNO3 and 54.3g of KNO3. This sample was mixed thoroughly using a speed mixture machine (Figure 3.3 b). The second sample was made by adding 45.7g of NaNO3 and melting and solidifying it while in contact with a thermocouple (Figure 3.26). The rest of the KNO3 of 54.3g were added later on to complete the eutectic composition. The third sample was made by carefully adding first, a layer of $NaNO_3$, and then a layer of KNO_3. The particle size of these layers was fairly large, close to 1000µm (1mm).

Figure 3.26 Solidified bottom layer with the attached thermocouple

a b c

Figure 3.27 a) Three thermocouples with different heights, b) All 3 samples with thermocouples, c) Data gathering

The temperature profile of each sample was recorded using three thermocouples at three different heights (Figure 3.27 (a)). The thermocouple distance was calculated based on the layer heights and intersection plane. The bottom thermocouple was placed close to the middle of the bottom layer, and the middle thermocouple was in the range of the intersection plane. A third thermocouple was positioned close to the middle of the top layer (Figure 3.27).

After analyzing the collected data, it was evident that the sample one with the mixed eutectic showed a melting phase during the first run. The mixture started melting after 30 minute mark (Figure 3.28). Melting was evident from 30 to 60 minute period. In the second run, thermocouple relevant to the inside furnace temperature, placed right above the crucible, increased to a slightly higher temperature even though the furnace set temperature of 280 ^{o}C was kept intact for both the experiments. These small variations are common with furnaces when there is more than one sample of phase change happening (with different temperatures). Most of the furnaces take the feedback from one inbuilt thermocouple and thus, small variation inside the furnace is normally common. To address this, reference thermocouples were placed (labeled as furnace inside) above each of the crucibles, therefore not relying completely on furnace temperature for the analysis. Figure 3.29 shows that the solidification happened around 220^{o}C, which is very close to the literature value of melting for this eutectic (221^{o}C).

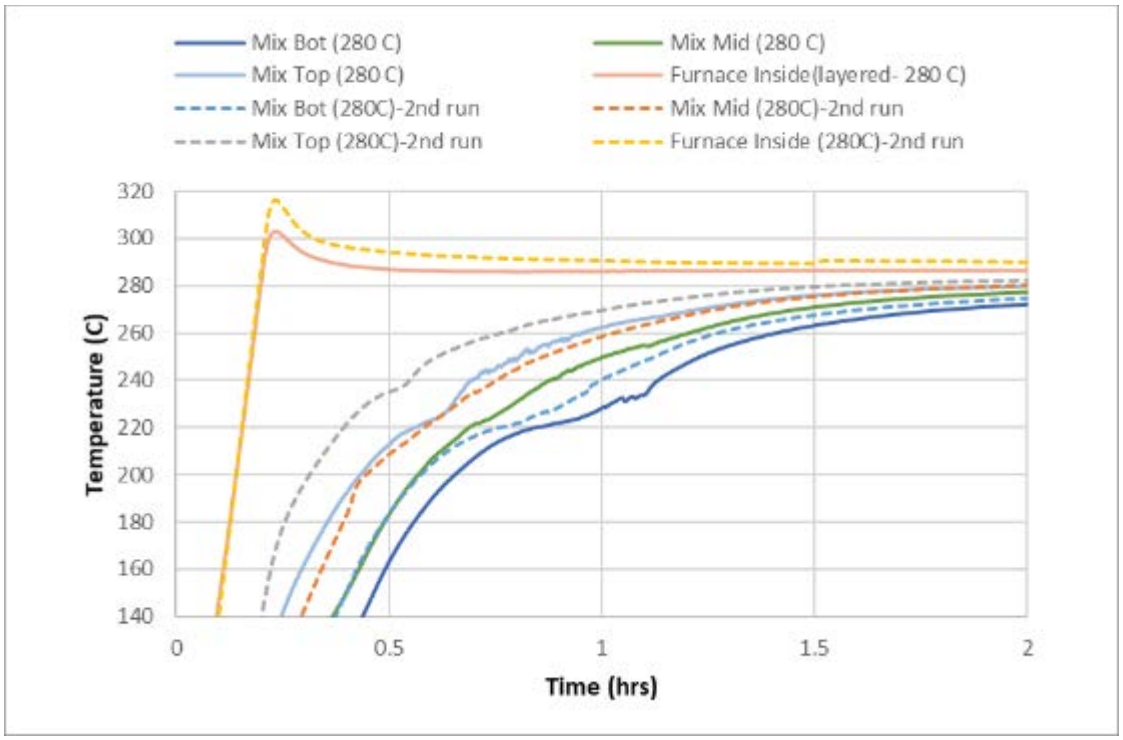

Figure 3.28 Heating comparison of 1st and 2nd run of the initially mixed eutectic

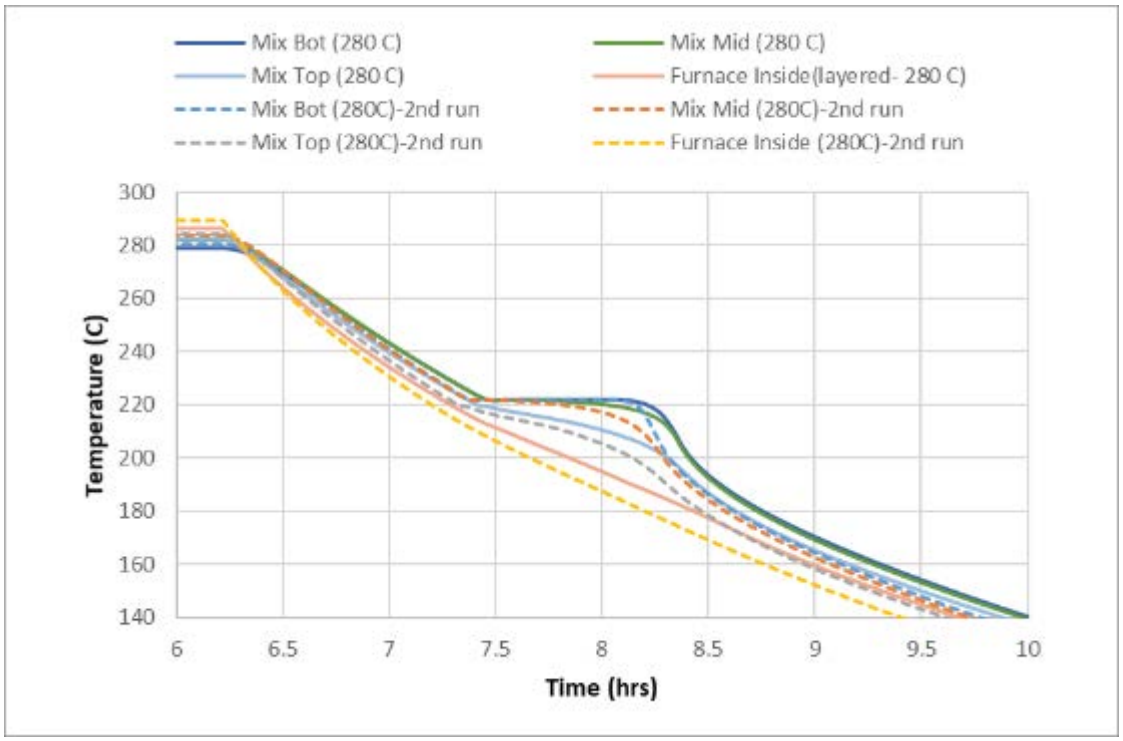

Figure 3.29 Cooling comparison of 1st and 2nd run of the initially mixed eutectic

The mixture with the initial solidified layer (Sample 2) showed no melting in the first run for the set furnace temperature of 280°C (Figure 3.30). However, it clearly showed a solidification phase during the cooling (same run) and also during the second time of heating for the same furnace temperature. Clearly, it was melted during the middle period. This phenomenon is not a common occurrence in the phase transition. The furnace was kept at 280°C for close to 6 hrs. According to the data, it was noticeable that some activity happened during the 3 - 6 hr period (Figure 3.31). The temperature reduction in that period was only seen in the first run. It was evident that some sort of phase transition happened during this period and it happened way above its eutectic melting point of 221°C (Figure 3.31).

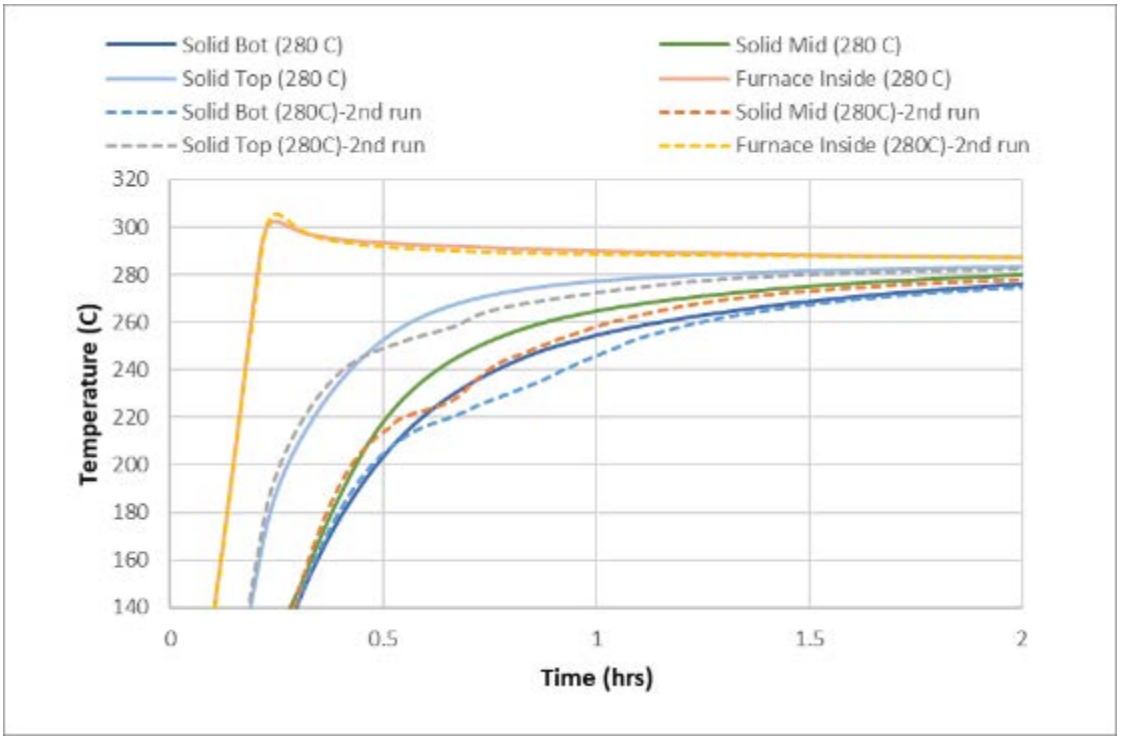

Figure 3.30 Heating comparison of the 1st and 2nd run of the mixture with the initial solidified layer

Figure 3.32 shows the cooling comparison of the first and second run. Solidification was much prominent in the second run indicating that the melting happened during the first run could be partial and needed more time (or higher temperature) for complete melting.

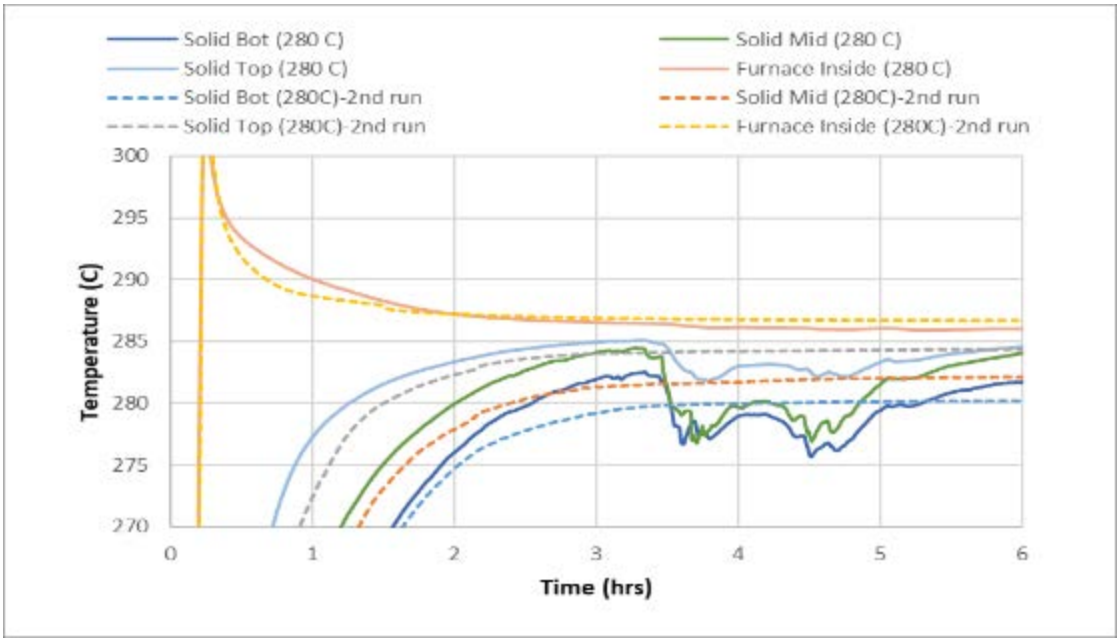

Figure 3.31 Comparison in the middle period of the 1st and 2nd run of the mixture with the initial solidified layer

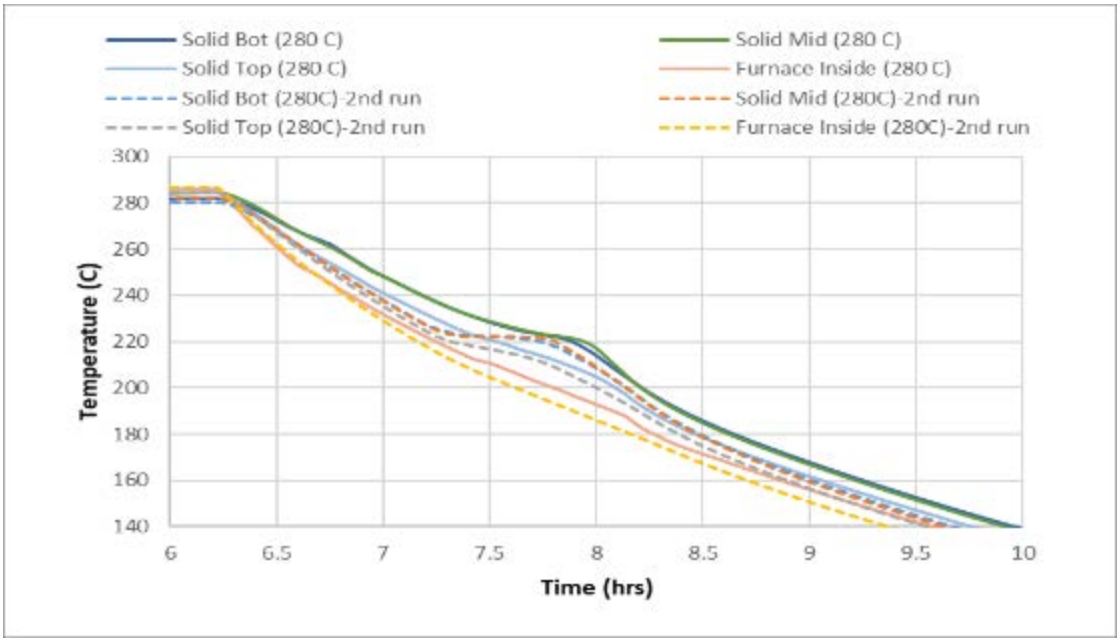

Figure 3.32 Cooling comparison of 1st and 2nd run of the mixture with the initial solidified layer

The third sample of layered arrangement showed no sign of melting or solidification for the set furnace temperature of 280°C (Figure 3.33 & Figure 3.34). Several experiments were carried out with increasing furnace temperature to find the point of melting. The melting was finally visible for the set furnace temperature of 340°C (Figure 3.35). The melting occurred way above 300°C temperature. To check the consistency of the eutectic mixture, second time melting was carried out and then compared with the initial run. Figure 3.36 & Figure 3.37 show the melting and solidification curves. It was noticeable that second time melting happened close to the 220°C temperature and therefore we can conclude the composition was same throughout the experiment.

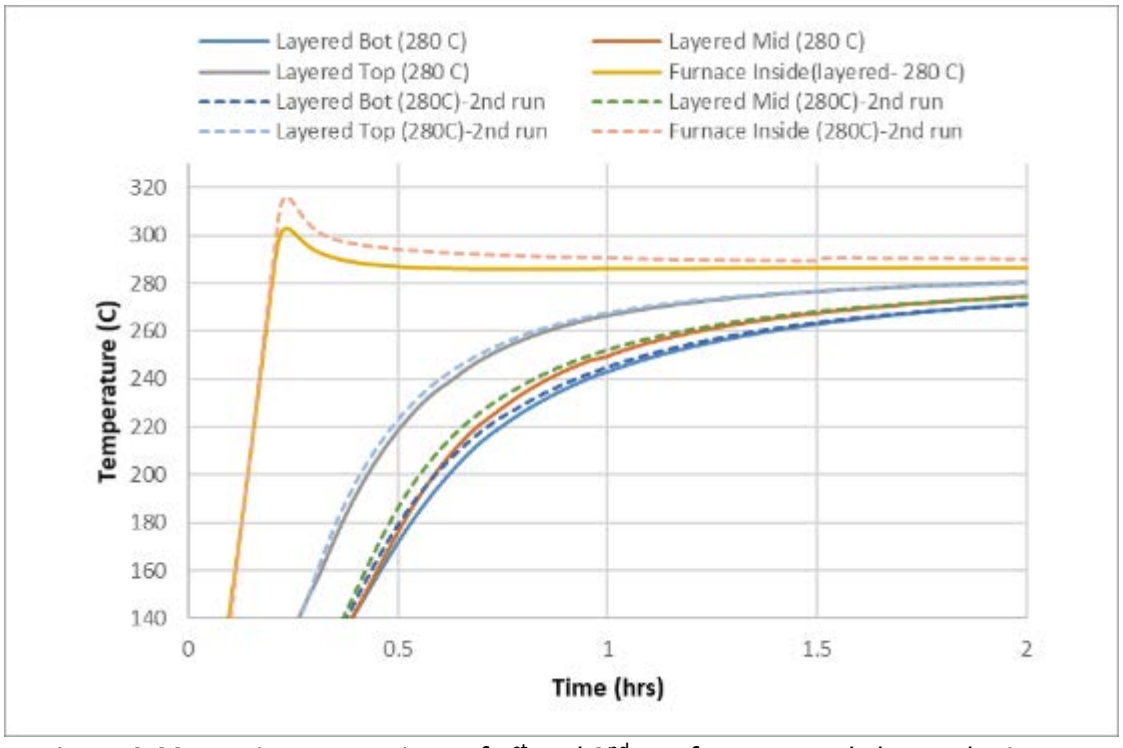

Figure 3.33 Heating comparison of 1st and 2nd run for separately layered mixture

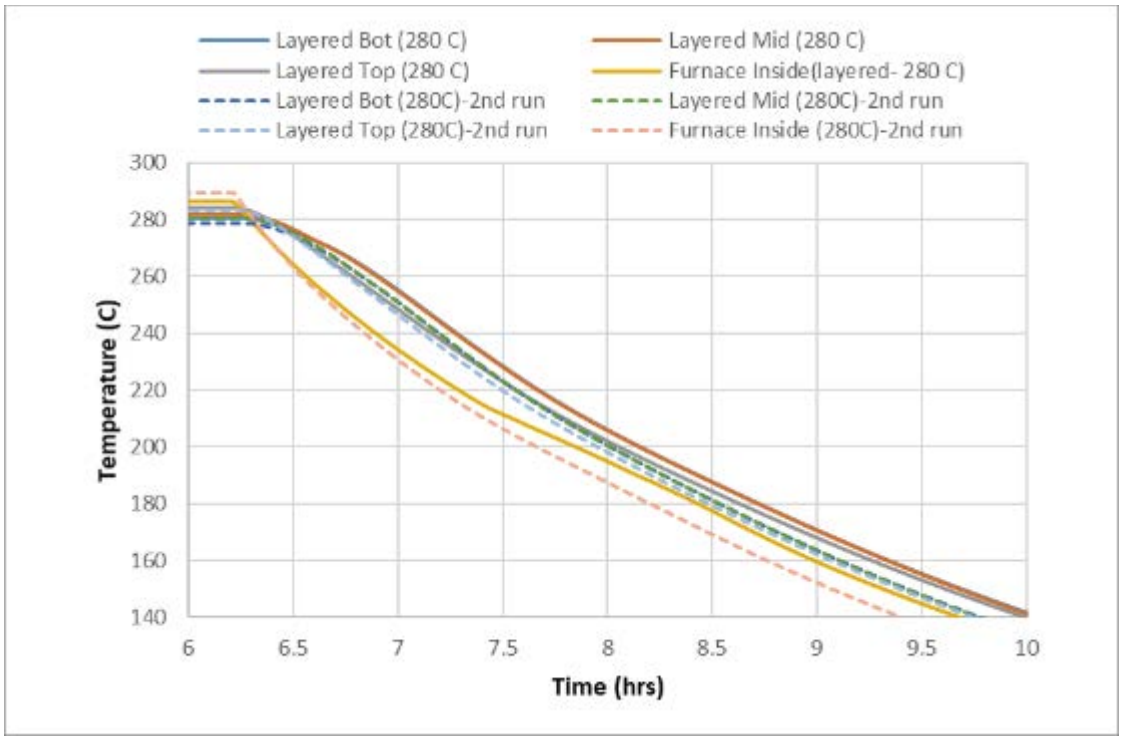

Figure 3.34 Cooling comparison of 1st and 2nd run for separately layered mixture

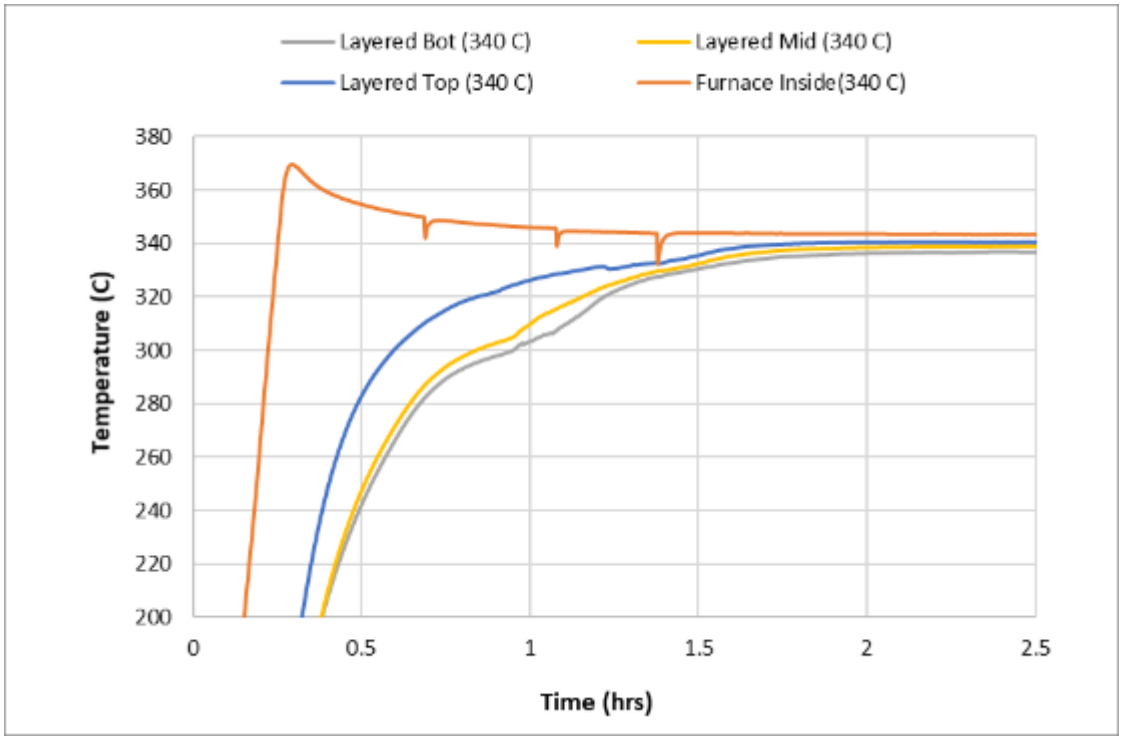

Figure 3.35 Heating of separately layered mixture with the furnace temperature of 340°C

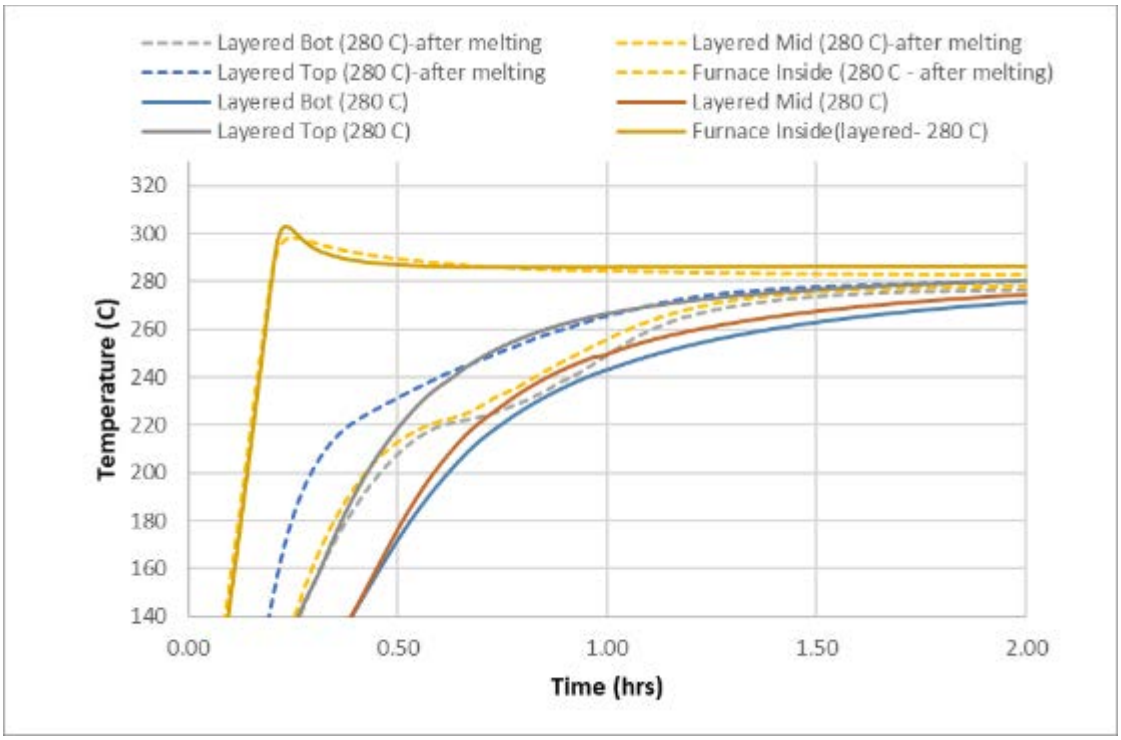

Figure 3.36 Heating comparison of second time melting with the first run

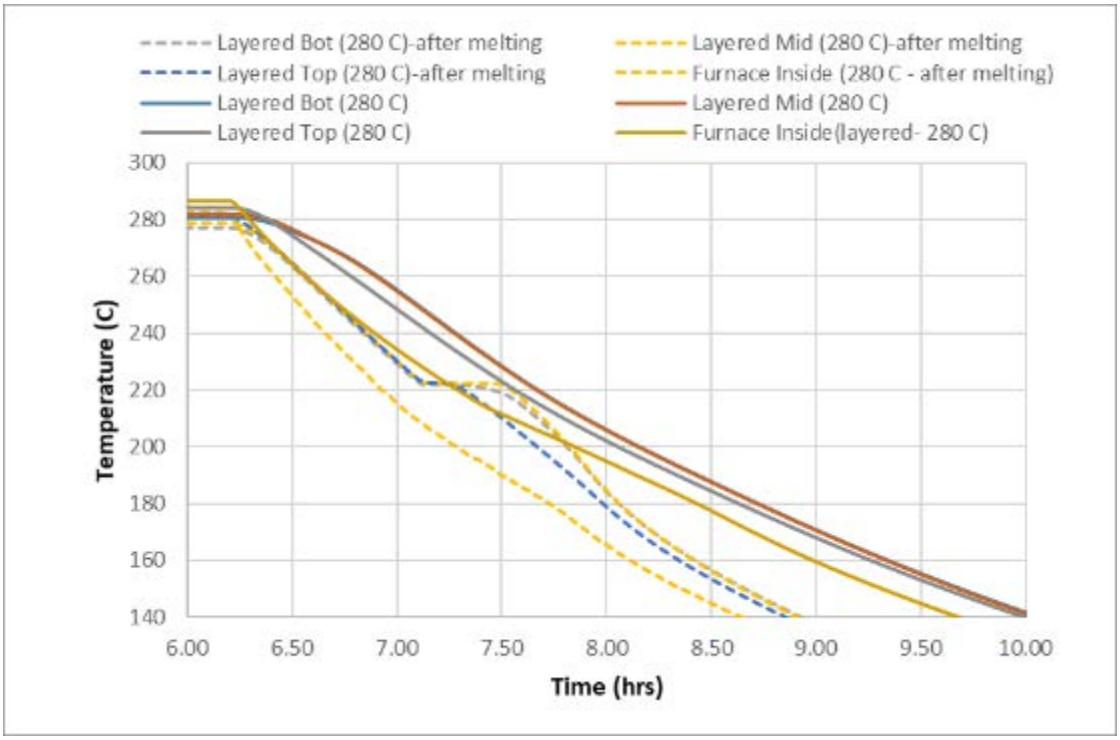

Figure 3.37 Cooling comparison of second time with the first run

These results clearly demonstrate that having layers (powder or solid), instead of a mixture can prolong the melting time and even go close to the individual melting temperatures without going through the phase transition. This technique was effectively adopted for the sealing process as most of the sealing materials get contaminated by the PCM vapor, if the sealing happens close to the melting or above the eutectic melting temperature.

3.5.3.2 Sealing the Capsule of NaCl-KCl Eutectic Mixture

For the case of NaCl-KCl eutectic preparation, the right amount of KCl is added to the sintered capsule which is first melted (at 770^{o}C) and later solidified by cooling. This was followed by the addition of a requisite amount of NaCl powder to make a NaCl-KCl eutectic. A mixture of sintered ceramic powder and sodium tetraborate was used as a sealing agent to plug the hole as indicated in the Figure 3.38. The capsule was then heated up to 760^{o}C and cooled quickly. Sodium tetraborate melted at this temperature and formed a non-porous plug at the hole and simultaneously, NaCl and KCl grains diffused into each other leading to the formation of eutectic with a melting point of 657^{o}C.

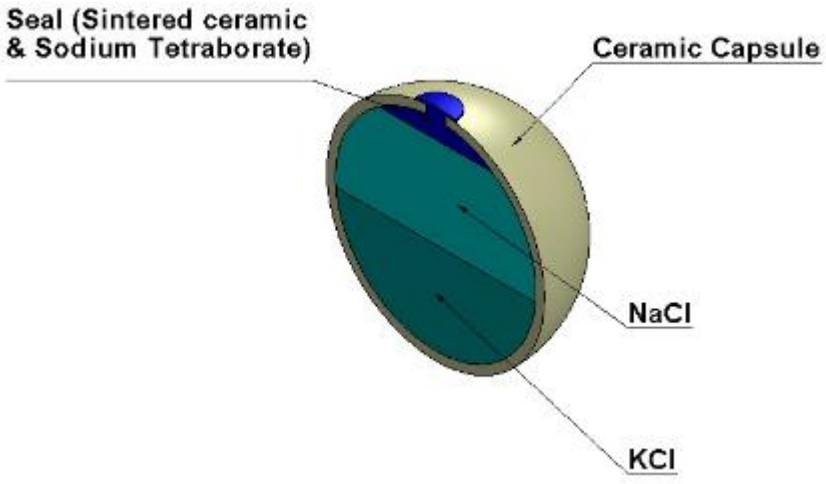

Figure 3.38 Cross-section view of the sealed alumina capsule containing NaCl-KCl eutectic

Capsules made earlier, before introducing this sealing technique, survived only up to 65 thermal cycles. Capsules made with this sealing technique survived many thermal cycles, and one capsule survived 510 (Figure 3.39) thermal cycles. This capsule also had a thin alumina paste layer for additional protection. The weight loss after 510 thermal cycles (over 1000 hrs) was in the range of 15-20 %.

Figure 3.39 Capsule that survived 510 thermal cycles

3.5.4 Alumina Capsules

As a material, alumina (Al_2O_3) was found to be one of the most suitable candidates for encapsulation. It is fairly inexpensive and non-reactive with the molten chloride salts. The downside of alumina is with the encapsulation process, as Al_2O_3 has a high sintering temperature (1400 - 1600^oC). A collaborative effort with Kyocera, USA, was initiated to fabricate alumina capsules as in-house furnaces had a limitation of 1200^oC. Many different capsules were made with slip casting and dry pressing techniques using 99% pure Al_2O_3.

Figure 3.40 Different types of alumina capsules by Kyocera

After carrying out several experiments, the best results were achieved for the PCM of NaCl-KCl. This is accomplished with a slight modification to the sealing materials. The new material was a mixture of Feldspar 50% and sodium tetraborate 50% composition. Sealing was again done at 760^{o}C (Figure 3.41).

Figure 3.41 Tested alumina capsule

3.6 Testing and Thermal Cycling

The durability of the fabricated capsules was evaluated by thermal cyclic tests performed by repeating melt and freeze cycles. The ceramic capsules containing NaCl-KCl eutectic were thermally cycled between 580^{o}C to 680^{o}C, dwelling for one hour at each temperature (Figure 3.42). The capsules filled with NaCl were tested from 780^{o}C and 850^{o}C. Post-formed capsules and

initial pre-formed capsules showed cracks and sudden dramatic weight losses during the thermal cycling tests. In the latter part of the study, the tested ceramic capsules did not fail during thermal cycling due to cracks in the capsules. However, these capsules showed small continuous weight losses with time. The ceramic capsules sealed with 50-50 feldspar-sodium tetraborate mixture did not show any significant weight loss compared to all other sealant materials. It appears that the 50-50 feldspar-sodium tetraborate is significantly non-porous to liquid PCM. Due to the innovative sealing technique used (section 3.5.3.1), the eutectic of NaCl-KCl capsule showed a lot of promise compared to the NaCl capsules.

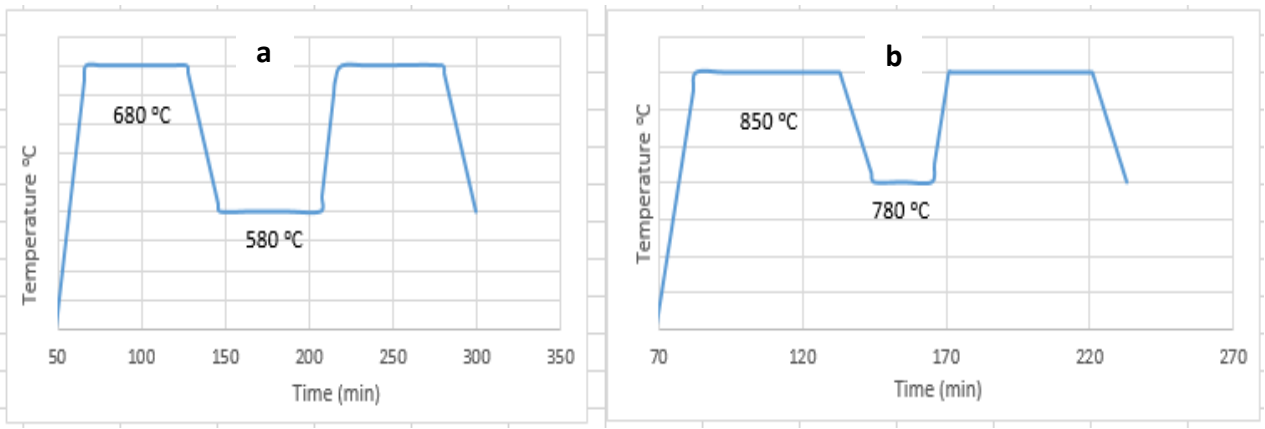

Figure 3.42 Temperature profile of the thermal cycling test for a) NaCl-KCl eutectic and b) NaCl containing capsules

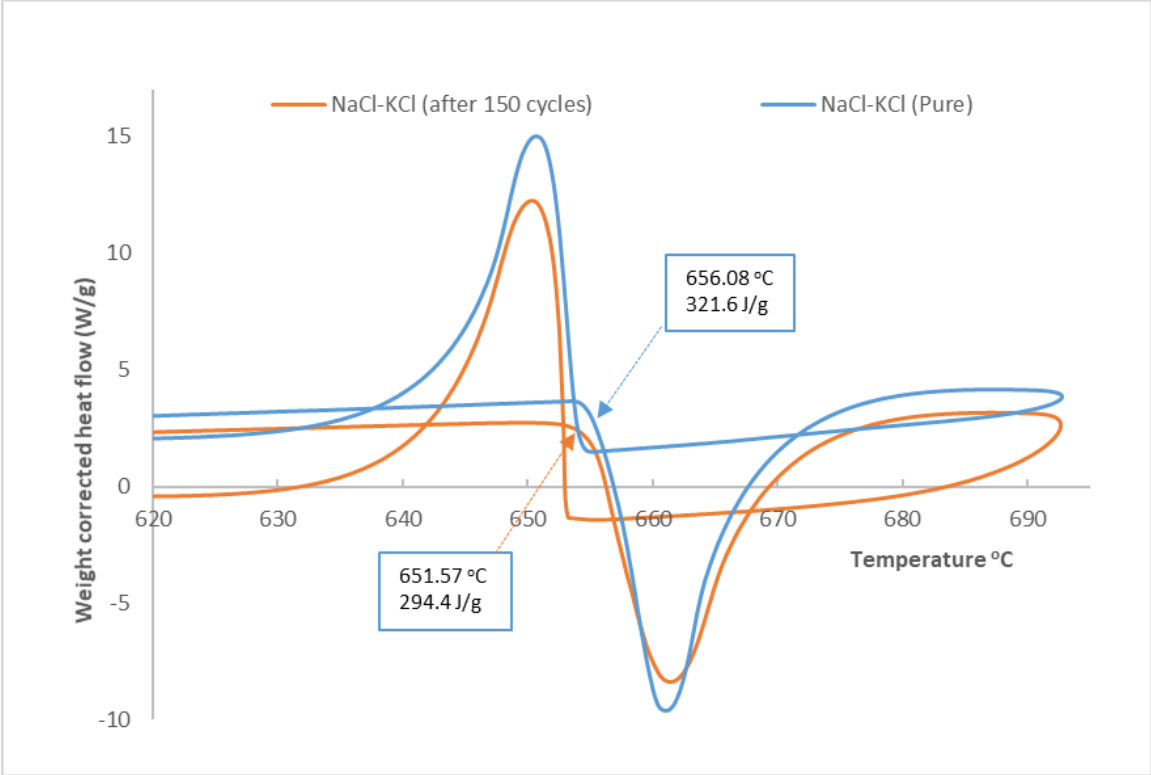

Figure 3.43 DSC analysis of NaCl-KCl eutectic salt

At different stages of thermal cycling process, capsules were dissected to analyze their thermophysical properties. DSC analysis of the thermally cycled capsules of NaCl and NaCl-KCl eutectic showed no significant change in their thermophysical properties (Figure 3.43).

In a previous experiment, weight loss of 15% - 20 % was observed after 500 thermal cycles. A capsule made of Alumina, with NaCl/KCl eutectic as the PCM, had successfully undergone 1000 thermal cycles. This capsule was thermally cycled at 580°C and 680°C, with a dwelling time of one hour at each temperature.

Table 3.5 Alumina capsule configuration

Empty capsule weight	66.06 g
PCM (NaCl/KCl eutect) weight	73.99 g
Total Weight with Sealant mixture	140.63 g
*After curing	140.44 g

*Curing sequence- 760 °C at the rate of 3 °C/min & dwell for 10 minutes.

Table 3.6 Weight loss of alumina capsule which completed 1000 thermal cycles

No of thermal cycles (580 °C - 680 °C)	Weight of the PCM	PCM weight loss	% PCM loss - new capsule(1000)
0	140.44	0.00	0.00%
20	140.44	0.00	0.00%
50	140.42	0.02	0.03%
80	140.37	0.07	0.10%
110	140.25	0.19	0.26%
150	140.09	0.35	0.47%
200	139.78	0.66	0.89%
300	139.10	1.34	1.81%
400	138.86	1.58	2.14%
500	138.55	1.89	2.55%
600	138.34	2.10	2.84%
800	137.33	3.11	4.21%
1000	136.78	3.66	4.93%

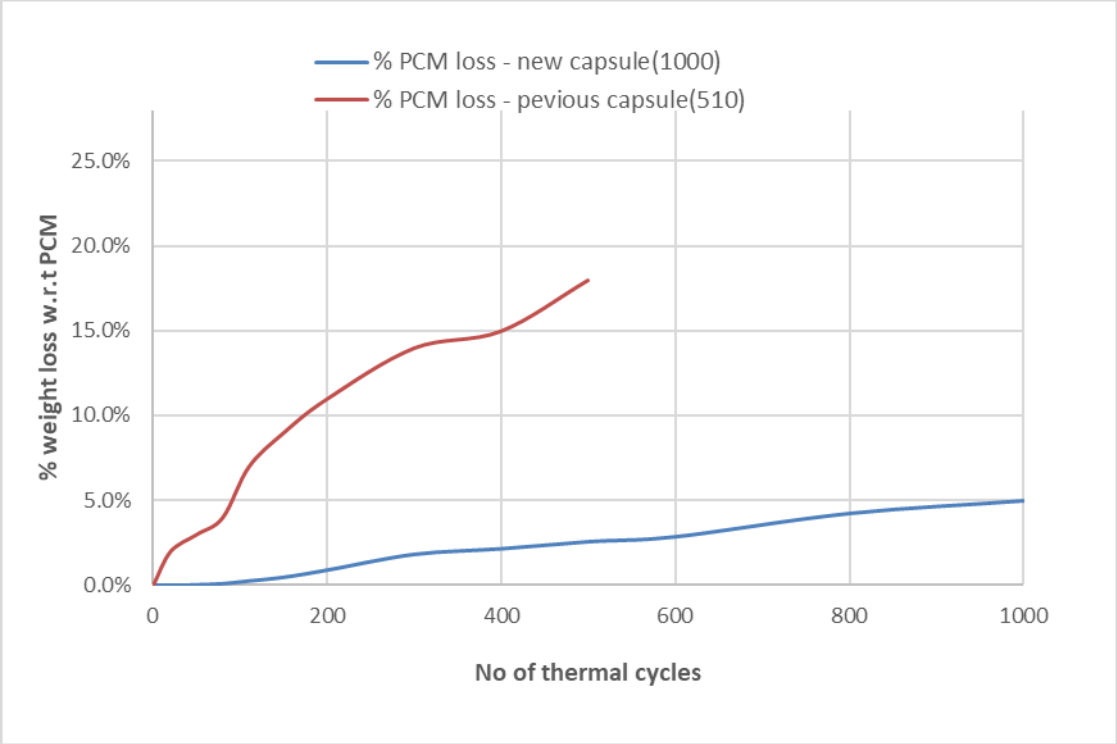

Figure 3.44 Comparison of PCM weight loss percentage

Table 3.6 and Figure 3.44 show the weight loss and weight loss percentage comparison with the previous sample which ran for 510 thermal cycles. Even though there is a small continuous weight loss, the rate of weight change has decreased in the latter stages of thermal cycling. These results are still a significant improvement compared to previous capsules tested. Due to fatigue induced by the thermal cyclic load, almost all prior capsules began to show some sort of surface cracks long before failing. The new capsule showed no sign of cracks even after enduring 1000 thermal cycles demonstrating high dimensional stability.

3.6.1 Pressure Build-up

In the initial stages of the study, we established that the pressure build-up inside the capsule due to the expansion of air during charging of the LHTES system is one of the major causes of failure. The sealing temperature of the capsule is crucial as it directly influences the final pressure inside the capsule. The sealing of a NaCl containing capsule at around room temperature causes the pressure to increase by 25 times the initial pressure when heated to 830^{o}C. We considered a 30% void fraction and 28% volume expansion of NaCl on melting for this calculation (Table 3.7). One would need a thick capsule wall to accommodate this pressure. However, this would decrease the fraction of PCM and in turn the total energy storage density of the system. On the other hand, sealing at elevated temperatures diminishes the pressure and the need to have a thick encapsulation wall. Therefore, to minimize the wall thickness, the capsule was sealed just above the melting point of the contained PCM.

Sealing at high temperature is essential to reduce internal pressures and tensile stresses on the body of the capsule. Ceramic is not a good material to handle tensile loads and therefore, it is essential to minimize the pressure build-up.

Table 3.7 Pressure calculations based on sealing temperature

Diameter Of the Capsule(Inch)	Void Fraction(%)	Sealing Temperature (C)	NaCl amount(g)	Final Pressure @ 830 C (in atm)
1	30	25	12.97	25.6
		400	12.97	10.04
		790	12.97	5.37
	40	25	11.12	8.22
		400	11.12	3.37
		790	11.12	1.93

A ceramic cap, made from a 50-50 feldspar-sodium tetraborate mixture or even pure sodium tetraborate was used for sealing as explained earlier. At the initial stage of heating before 760 ^{o}C , the sealing cap is porous, allowing the diffusion of air out of the capsule that could otherwise expand during phase change and cause the capsule to rupture. In the final stage, the materials in the sealing cap melt and turn into a very viscous liquid, which when cooled turn into a non-porous plug. With the layered eutectic arrangement, pressure build-up was further reduced as the initial sealing temperature exceeds the maximum limit of the operating range.

3.7 Encapsulation Using Metals

Finding cost-effective yet reliable encapsulation techniques becomes difficult with the increase of operating temperature. Ceramics provide high corrosive resistance but are not as economical in comparison to metallic encapsulation [37–40]. For a temperature range of 500-600˚C, if certain preventive measures were taken to control the surface oxidation, metallic encapsulation was found to be reliable and cost-effective [40,41]. For metallic encapsulation, cylindrical type encapsulation was the cost-effective and more practical technique at the moment, considering the availability of steel tubes in the market [40].

There has been some research on thermal storage with cylindrical capsules [24,27,66,69,156–170]. Regin et al. [160] used paraffin wax as the PCM and analyzed the melting behavior experimentally. Wang et al. [158] examined the enhancement of charging rate by the use of multiple phase change materials in a cylindrical capsule. Heat transfer characteristics of the liquid region in a horizontal cylindrical capsule were studied experimentally by Saitoh et al. [157]. Shmueli et al. [165] numerically investigated the PCM melting procedure in a vertical cylindrical tube. Farid et al. [170] discussed the role of natural convection during melting and solidification. Bhardwaj [40] tested the compatibility of Metal and metal coating with chloride salts under temperatures above 600 ^{o}C. PCM of NaCl-KCl eutectic was contained in a Ni coated (200 µm) carbon steel cylindrical capsule. It survived for 1700 thermal cycles with no weight loss.

The objective of selecting a PCM in the range of 500^{o}C -550^{o}C was aligned with the operating temperature range of high-pressure steam power plants. A eutectic mixture of sodium sulfate (Na_2SO_4) and potassium chloride (KCl), relatively cheap salts, was selected for its melting temperature of 515˚C and low reactivity. The eutectic mixture was tested for several thermal cycles continuously and with differential scanning calorimetry (DSC) & thermogravimetric analysis (TGA). Figure 3.45 shows the repeatable results achieved for five continuous cycles.

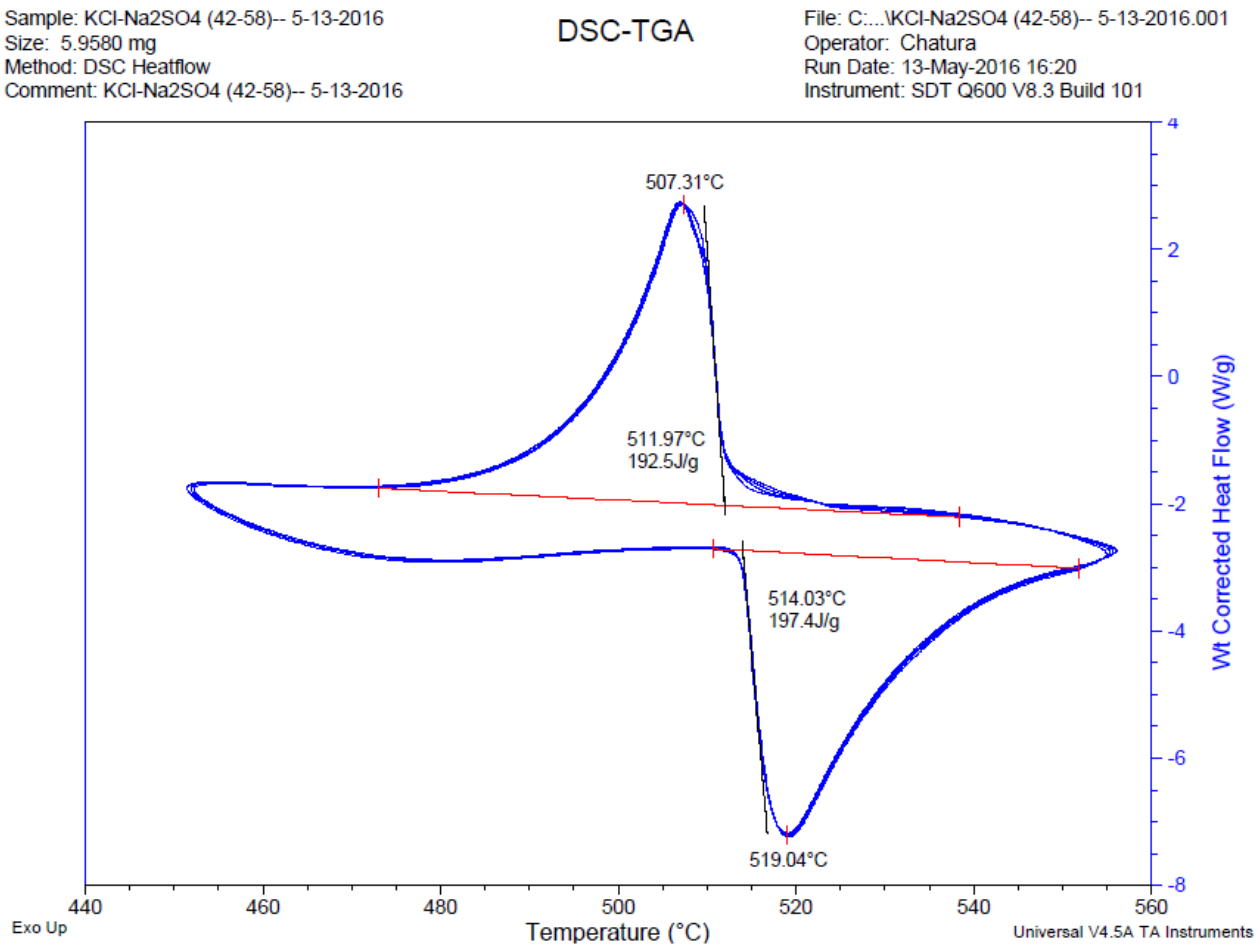

Figure 3.45 DSC & TGA results for Na_2SO_4-KCl mixture

3.7.1 Encapsulation Criteria

Carbon steel, though inexpensive, does not fare well in aerobic conditions at high temperatures. On the other hand, high corrosion resistant metals are expensive. For example, Ni shows excellent corrosion resistance but is very expensive to use as a base material. An effective solution to tackle both the corrosion and cost issue was to have a thin coating of Ni on Carbon steel.

The outside surface of the encapsulation would be exposed to the heat transfer fluid, therefore requires a corrosion resistant exterior surface. The inside surface of the encapsulation

would be in contact with PCM at high temperatures. This would be an extremely corrosive environment under aerobic conditions. However, in anaerobic conditions, the interior of the encapsulation would not require corrosive resistant surface. A successful approach was proposed for sealing under inert conditions by Bhardwaj [40]. The same method was adopted for this application as well, and as a result, Ni coating was done only on the exterior surface.

Figure 3.46 Ni coated carbon steel capsule

3.7.2 Fabrication Procedure

Different sized capsules were made and tested, but the capsule with 10" in height and 2" in diameter was the one used for the lab-scale LHTES setup, which will be discussed further in the next chapter. This capsule was filled with 0.95 kg of powdered PCM through a narrow opening. Before sealing, inert conditions were maintained while the PCM was melted to reduce the amount of air present inside the capsules. This is to prevent the carbon steel from corrosion. While the PCM was molten, a cap was welded to the narrow opening. TIG welding provided a smooth joint appropriate for a uniform nickel coating. The sealed capsules were electroplated with 200 µm of nickel and coated with Rust-oleum® corrosion paint for added protection. A

similar capsule was tested with NaCl-KCl eutectic and tested for more than 1000 thermal cycles (580-680C) [40]. The recorded weight loss was insignificant, and the thermochemical properties were consistent throughout testing. Thus, refilling or changing PCM is not required and should also be avoided considering the economic feasibility of fabricating these capsules. The final capsule is shown in Figure 3.47.

Figure 3.47 Metalic capsule of 2" diameter and 10" height (with Rust-Oleum coating)

3.7.3 Improvement of Heat Transfer Rate by Radiation Absorbing Particles

As a step to further improve the heat transfer between the PCM and capsule boundary, radiation absorbing particles were added to the eutectic mixture. The presence of transition metal chloride additives shows a distinct increase in absorption in the infrared radiation(IR) spectrum, with very minimal impacts on melting temperature and latent heat of fusion [171]. Myers et al. [171,172] experimentally analyzed the effect of additives on radiation heat transfer in high-temperature applications. This approach is an effective enhancement for temperatures above 500^{o}C. This technique of enhancement can be categorized as combined heat transfer enhancement due to the encapsulation as well as radiation absorbing particles. The additives selected for this case are cuprous chloride (0.2% wt.) and ferrous chloride (0.1% wt.) [172].

Use of metal capsules is further discussed in the next chapter, in the design of a lab-scale LHTES system.

CHAPTER 4: TESTING OF A LAB-SCALE THERMAL ENERGY STORAGE WITH PCM CAPSULES[1]

As mentioned earlier, most of the experimental research on thermal energy storage has been done at low temperatures, even though there is considerable focus on high-temperature range applications. There is a lack of experimental data for performance analysis of high-temperature LHTES systems in the literature. This study focused on the design and performance analysis of a lab-scale high-temperature LHTES unit [60].

A temperature range of 500°C-600°C was selected because it represents the operating temperature range of high-pressure steam power plants. The experiment could be used for temperatures below 650°C, and in fact the system was also used earlier for a temperature range of 280-350°C [173].

4.1 PCM Selection and Capsule Fabrication for the Lab-scale LHTES System

A eutectic mixture of sodium sulfate (Na_2SO_4) and potassium chloride (KCl) was selected as the PCM. The fabrication of the metal capsules is explained in the section 3.7.2. Radiation absorbing particles were also added to further enhance the heat transfer (section 3.7.3). To measure the temperature inside the capsules, thermocouples were placed in direct contact with the PCM. However, these thermocouples degraded and corroded after multiple runs, which affected the accuracy of the temperature measurements.

[1] The content of 4.1 to 4.6 was published in Wickramaratne C, Moloney F, Pirasaci T, Kamal R, Goswami DY, et al. "Experimental Study on Thermal Storage Performance of Cylindrically Encapsulated PCM in a Cylindrical Storage Tank With Axial Flow", ASME 2016 Power Conf., ASME; 2016, p. V001T08A014. doi:10.1115/POWER2016-59427. Permission is included in Appendix C.

To allow temperature measurement inside the capsules and to protect the thermocouples, an inner tube composed of carbon steel was welded inside the cylindrical capsule, as shown in Figure 4.1.

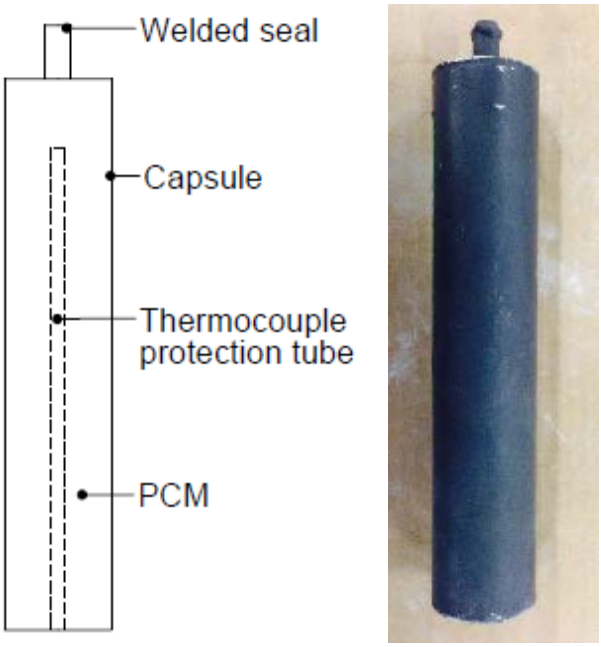

Figure 4.1 Capsule schematic with the inner tube and the actual photograph

4.2 System Components

System components were selected considering the operating conditions of temperature, flow rate and pressure, compatibility with each other, reliability and cost.

4.2.1 Storage Tank

A preexisting lab-scale packed bed system was retrofitted and used as a thermal storage tank. The cylindrical carbon steel tank had both a diameter and height measuring 0.254 m. The storage tank housed 14 cylindrical capsules (Figure 4.2), which gave the porosity of the tank to be around 0.37. A perforated plate was used to support the cylinders in an upright position while

still allowing for the HTF to flow through the tank. Only four capsules, A through D (Figure 4.2), were prepared to have internal temperature measurement recordings, as shown in Figure 4.3.

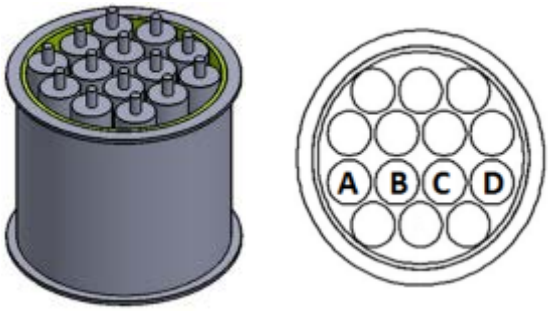

Figure 4.2 Storage tank schematic

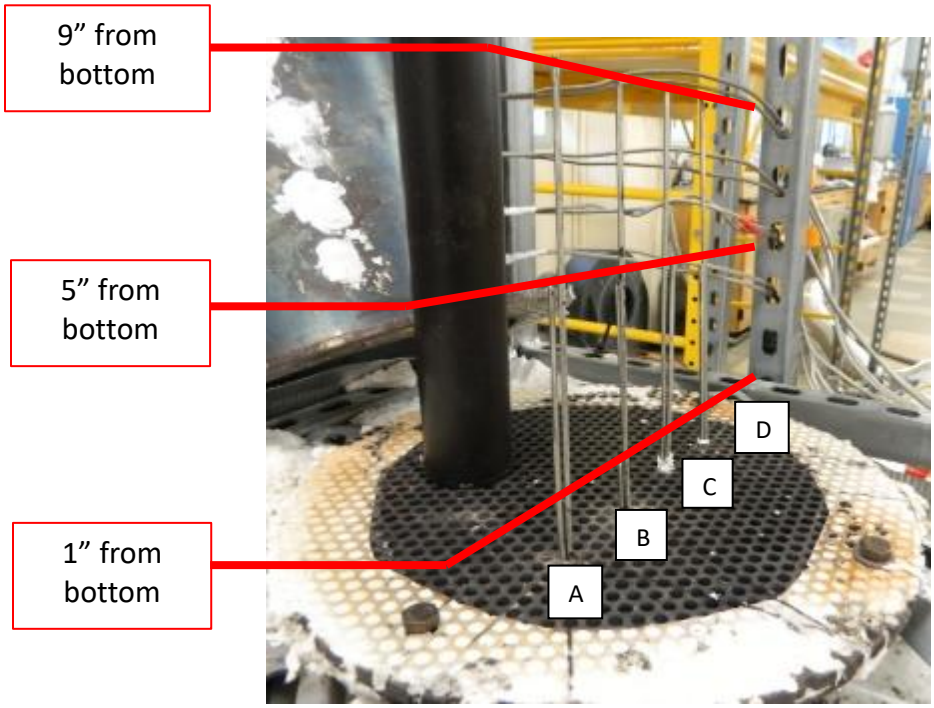

Figure 4.3 Inside thermocouple arrangement for capsule A, B, C, and D

Figure 4.4 Capsule arrangement inside the storage tank

Figure 4.5 Storage tank with the thermocouples(without the insulation)

4.2.2 Heater

Air was used as the heat transfer fluid in this experiment, and 6kW Sylvania air heaters were used to heat the air to maintain required temperatures. Two separate heater systems were used for charging and discharging processes. The charging and discharging heater units consisted of six and four air heaters respectively. The target operating temperatures were 20˚C above and below the melting temperature of PCM of 515˚C. However, at first, the discharge heaters could not support a temperature greater than 380˚C, limiting the operating range between 380˚C and 535˚C. But later on, with the addition of new heat to the discharge side, the expected 495ºC was achieved.

4.2.3 Blower

A square Dayton 115V, 2860 RPM capacity blower was selected to pass air through the system. It was adapted to have a 4" diameter round outlet to match the pipe entering the heaters. A variable switch allowed for the flow rate to be adjusted. Flow rates between 120 and 140 m^3/h were chosen considering the heater capacity and its limitations. The flow direction was reversed for charging and discharging. During charging, the flow entered through the top set of heaters and down through the tank; while for discharging, the flow direction was reversed, allowing the cooler air to flow up through the tank. The setup of the system was symmetrical through the middle of the storage tank (Figure 4.7).

4.2.4 Data Acquisition System

K-type thermocouples were employed for temperature measurement at various axial and radial positions. Four capsules with thermocouples inserted inside for PCM temperature measurements were installed across the diameter of the bed. Inside capsule temperatures were measured 1" from the top, 1" from the bottom, and at the center of the capsule. To measure the amount of energy absorbed by the storage tank, thermocouples were installed above and below the tank. Additionally, four rows of thermocouples spaced 2" apart, were installed across the tank diameter to measure the axial temperature profile. Five probes per row were placed to analyze the radial temperature variation of the HTF as shown in Figure 4.6.

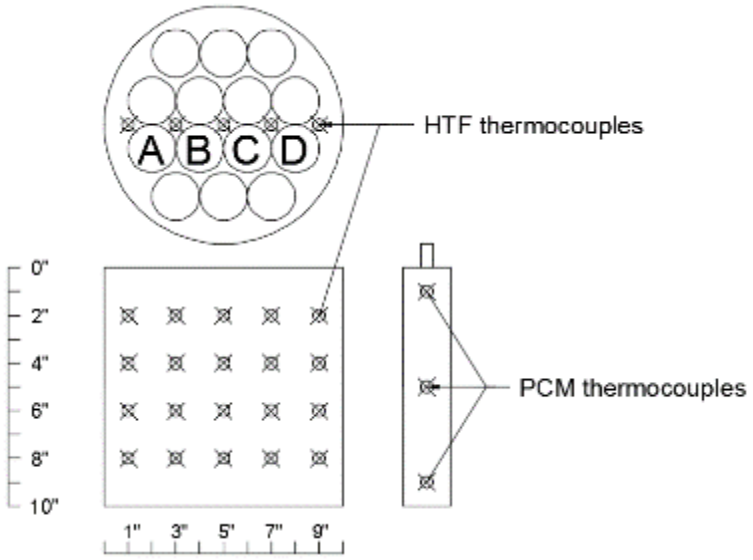

Figure 4.6 Thermocouple placement inside the tank & tubes

4.2.5 Connecting Components

The air enters the system through the blower to a pipe of 4 inch diameter and 5 feet length. The horizontal pipes between the heaters and the tank were 6 inch in diameter. Carbon steel diffuser cones, 19 inch in length, were installed to increase the diameter to 10 inch in the storage tank. To reduce heat losses, fiberglass insulation was installed around the whole system. The insulation placed around the storage tank was 6 inch thick. Figure 4.7 shows the final arrangement of the LHTES lab-scale setup.

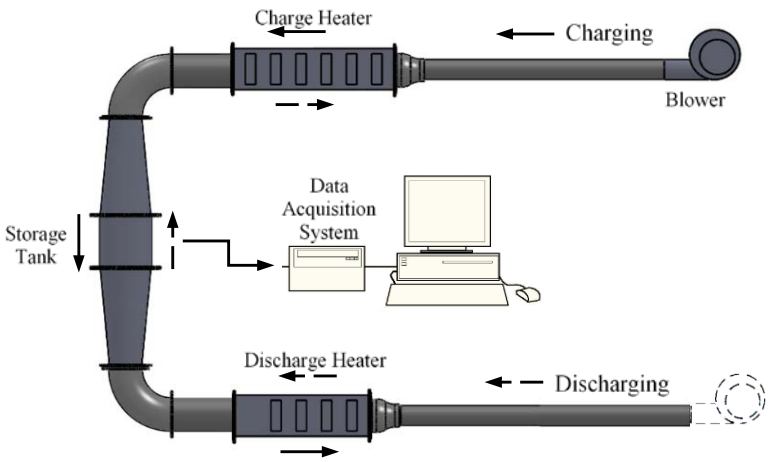

Figure 4.7 Schematic (top) and the actual (bottom) lab-scale setup

4.3 Experimental Procedure

Before each run, the system was first stabilized at 380°C (later on 495°C). To begin the cycle, the inlet flow was set to 535°C, which was 20°C above the melting temperature of the PCM, and the system was allowed to stabilize. The system was considered stable when there was no significant change in the outlet temperature. To start the discharge cycle, the flow was then reversed and the discharge inlet air was heated to 380°C. One cycle is defined as one charging

cycle followed by a discharging cycle. Seven cycles were tested at two flow rates each: 122 m^3/h and 138 m^3/h.

4.4 Uncertainty Analysis

To check the repeatability of the whole setup, several trials were carried out with the same operating conditions. Observed data showed minimal deviation. The uncertainty of a measurement is defined as the root sum square of the instrumental error, and the random error observed in repeated measurements [174]. Temperature uncertainty was found to be ±4.0°C for an operating temperature of 535°C. According to the manufacturer, the digital anemometer had an uncertainty of 0.14 ms^{-1} for 4.8 ms^{-1}.

4.5 Results and Discussion

The temperature readings of the tank were mainly used to calculate the energy and exergy efficiencies of the lab-scale LHTES system. The HTF temperatures for one run at the higher flow rate tested are shown in Figure 4.8 and Figure 4.9. Figure 4.8 shows the axial temperature profile of the system. During charging, the capsules absorb the heat from the HTF, thereby cooling the HTF as it passes through the tank. While during discharging, the heat transfer happens in the reverse direction. Figure 4.9 shows the average radial temperature profile, indicating a decrease in temperature from the outer bend to the inner bend side. The reason for this difference in temperature was that the diffuser cone before the storage tank was not long enough to provide a developed flow after the bend in the system (Figure 4.7). Due to this setup, the air velocity was uneven in the system; the air was faster on the outside, near capsule A, and slower on the inside of the system, near capsule D (Figure 4.10). Subsequently, the heat transfer was faster where the velocity was faster, causing capsule A to melt before capsule D (Figure 4.11).

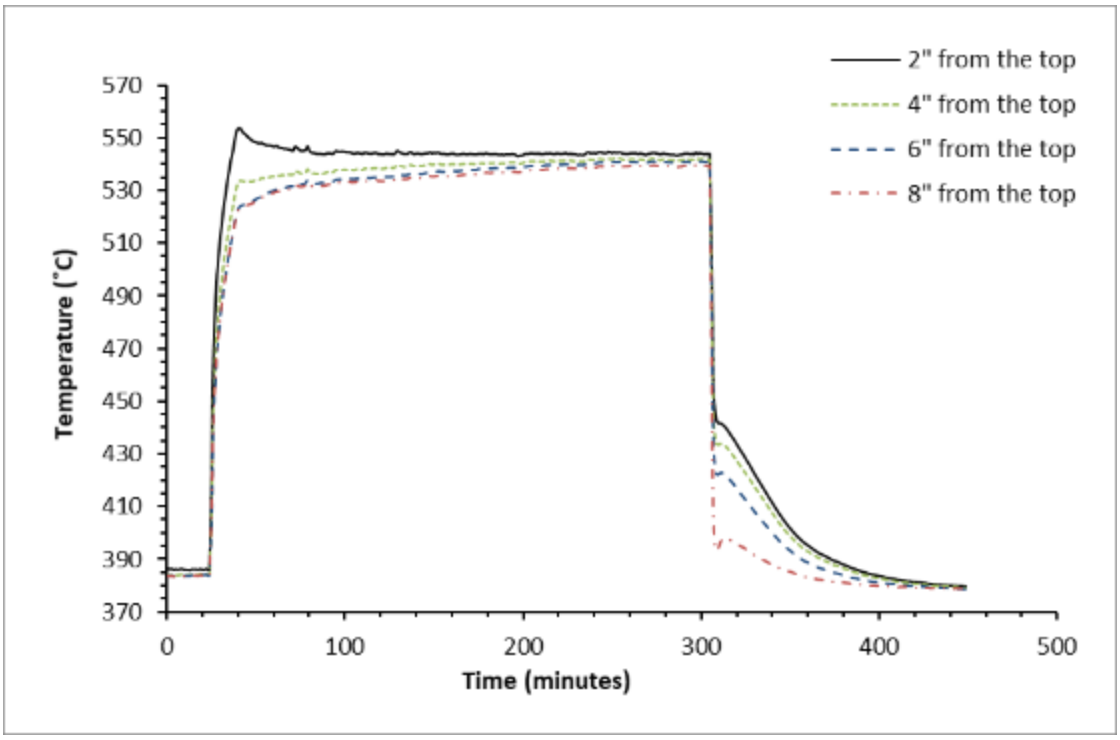

Figure 4.8 Average axial air temperatures for one run at 138m^3/h

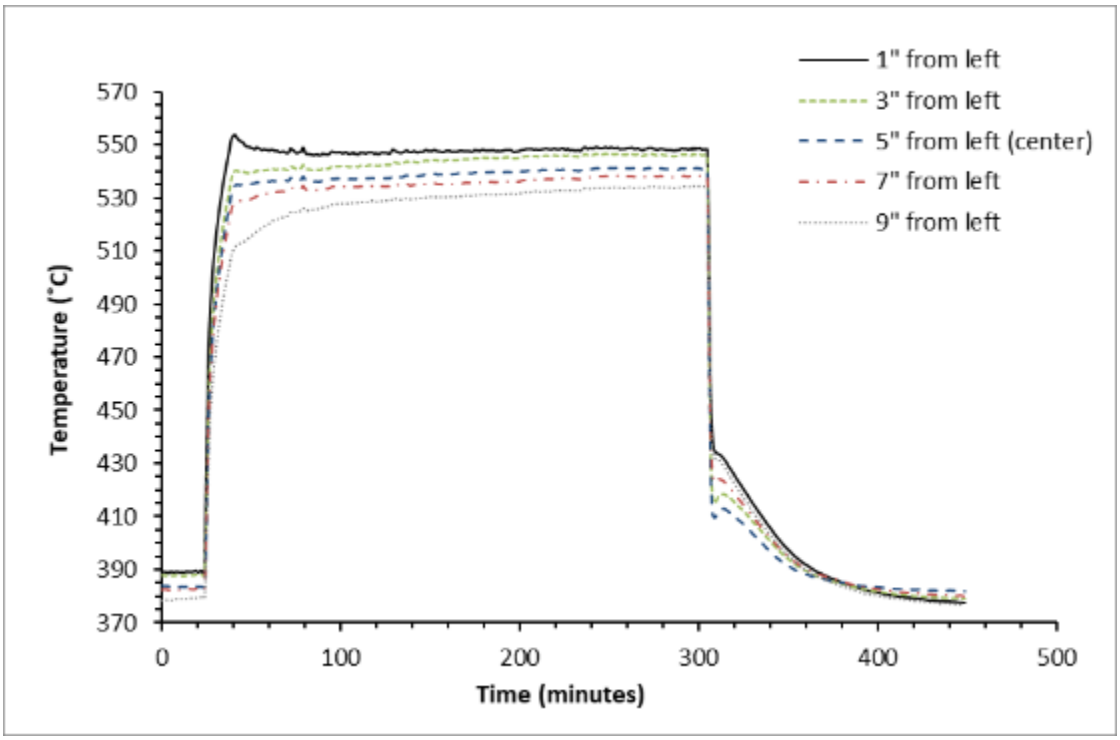

Figure 4.9 Average radial air temperatures for one run at 138m^3/h

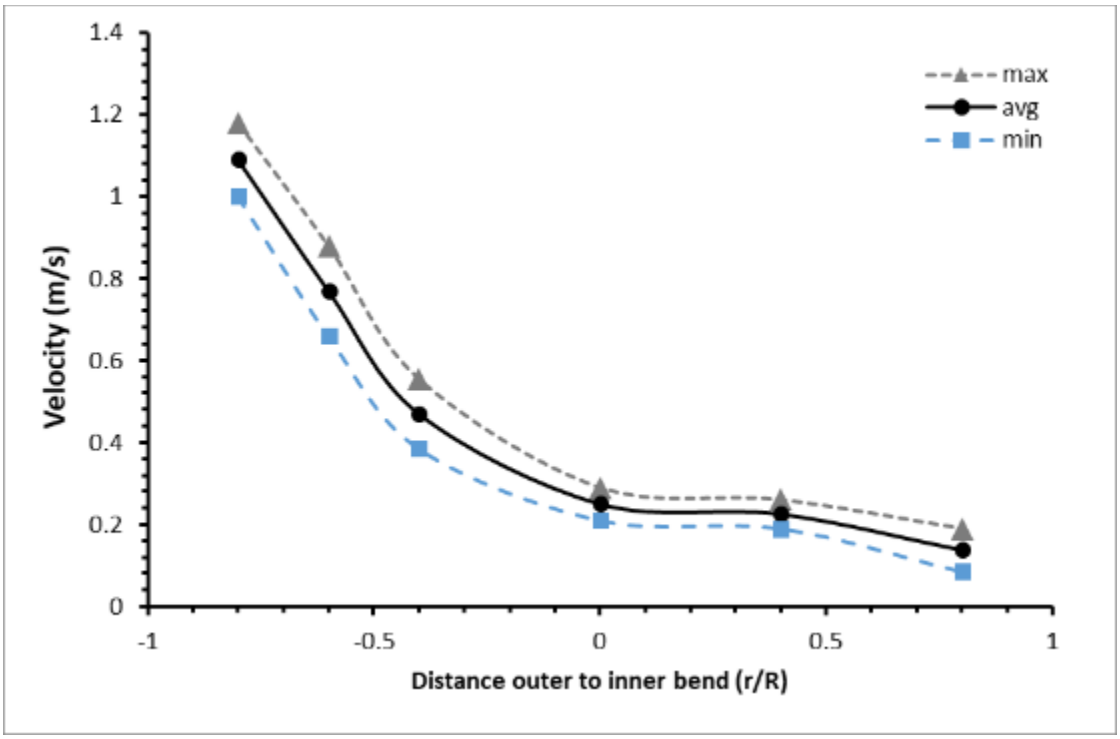

Figure 4.10 Tank velocity from outer bend to inner bend

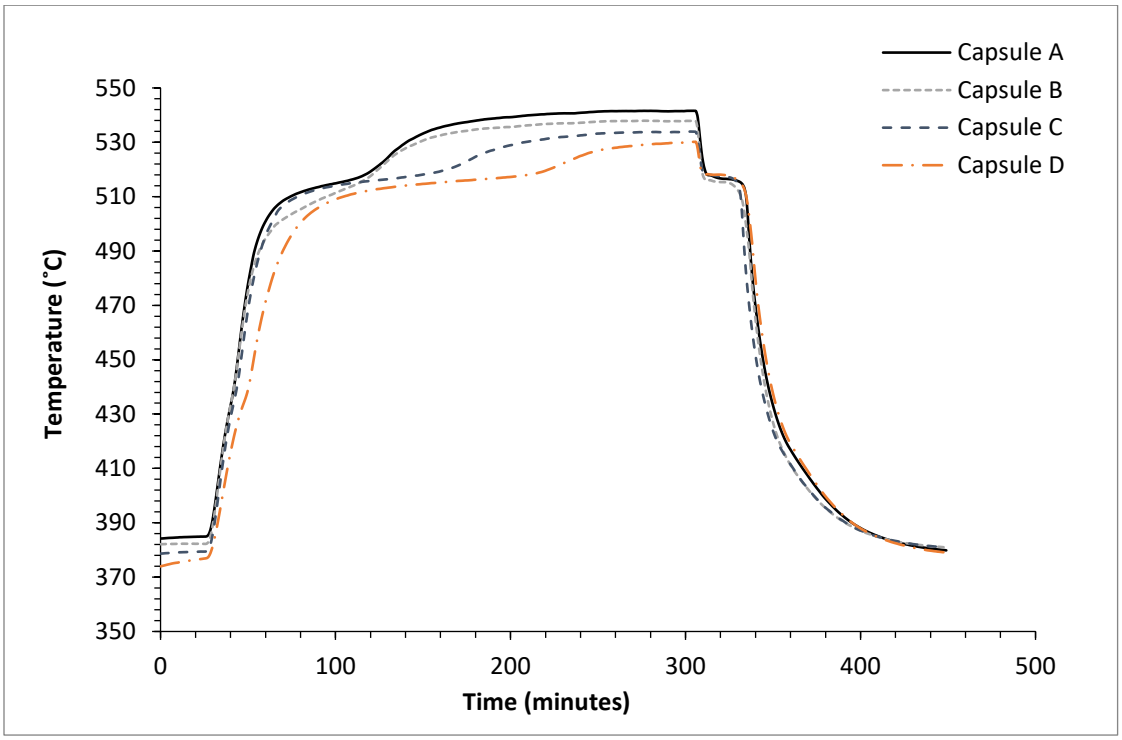

Figure 4.11 Capsule center temperatures for one run at 138m^3/h

Figure 4.11 illustrates the temperature measurements at the center of four measured capsules for one cycle at 138 m^3/h. The temperature distribution in capsule A for the same cycle is shown in Figure 4.12. Capsule A took a total of 120 minutes to melt and 30 minutes to solidify. The melting time was much longer than the solidification time due to the operating temperatures. If the operating temperatures were centered on the melting point, the solidification time would be longer than the melting time for the same HTF flowrates. This is because solidification is a conduction dominant process while melting is a convection dominant process. However, due to the setup limitations, the charging HTF temperature was supplied 20°C above the melting point while the discharging HTF was supplied 135°C below the melting point, resulting in higher heat transfer rate during the discharge process. This caused the solidification process in the discharge cycle to occur significantly faster than the melting process in the charging cycle. Analysis with the modified discharge heater is discussed later in this chapter.

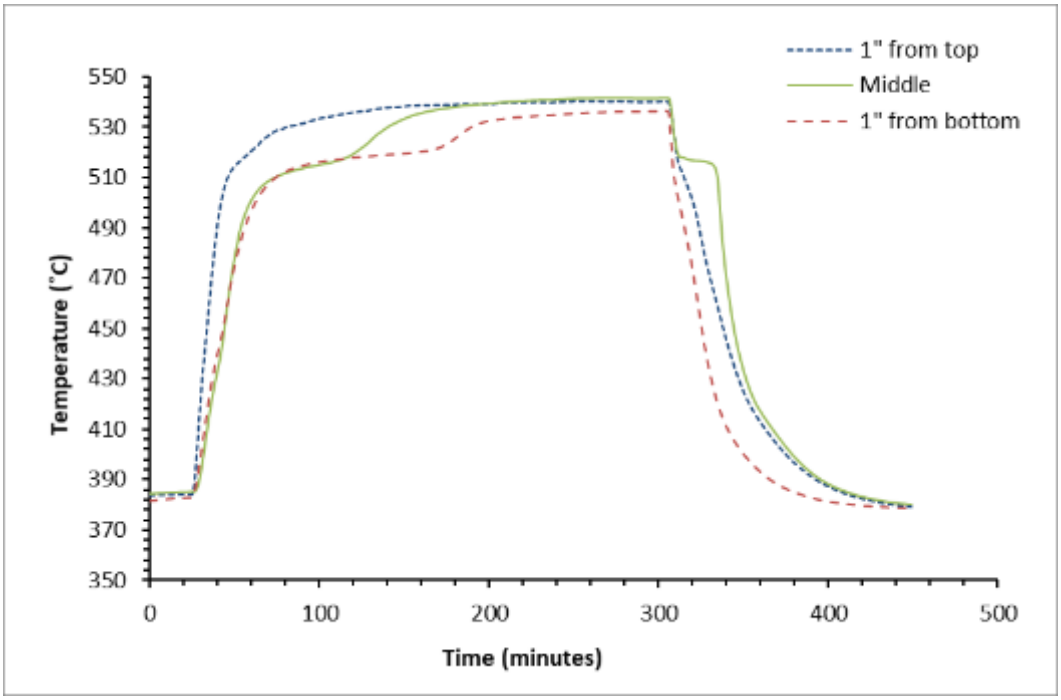

Figure 4.12 Capsule 'A' temperatures for one run at 138m^3/h

The temperature profile at the top of the capsule did not represent the melting or solidification due to the void space around the top thermocouple. The bottom of the capsule A took longer to melt than the center since it was located near the outlet of the tank during charging where the HTF has already transferred heat to the upper portions of the tank. During discharge, when the flow is reversed, the bottom of the capsule is the first region to come into contact with the cold HTF, causing it to solidify significantly faster than the center of the capsule, as shown in Figure 4.12. Another reason was the bottom of the capsules were in contact with the perforated plate, and the perforated plate was in contact with the whole structure. So it was evident that heat was being lost through the perforated plate.

The exergy and energy were calculated using the charging and discharging inlet and outlet temperature data. Equations (1) and (2) were used to calculate the energy efficiency while eq. (3) through (5) were used to calculate the exergy efficiency.

$$\eta_{I} = \frac{E_{DCh,HTF,Net}}{E_{Ch,HTF,Net}} \tag{1}$$

$$E_{HTF,NET} = \int \dot{m} C_{p,HTF} \Delta T dt \tag{2}$$

$$\eta_{II} = \frac{Ex_{DCh,HTF,Net}}{Ex_{Ch,HTF,Net}} \tag{3}$$

$$Ex_{DCh,HTF,NET} = \int_{t_{i,d}}^{t_{f,d}} \left[\dot{m}_{HTF} C_p \left(T_{HTF,out} - T_{HTF,in} - T_o \ln\left(\frac{T_{HTF,out}}{T_{HTF,in}} \right) \right) \right] dt \tag{4}$$

$$Ex_{Ch,HTF,NET} = \int_{t_{i,c}}^{t_{f,c}} \left[\dot{m}_{HTF} C_p \left(T_{HTF,in} - T_{HTF,out} - T_o \ln\left(\frac{T_{HTF,in}}{T_{HTF,out}} \right) \right) \right] dt \tag{5}$$

The standard deviation was calculated by measuring six trials at the flow rate of 122 m^3/h and seven trials at 138 m^3/h. The two different flow rates had similar heat transfer rates as shown in Figure 4.13. The resulting efficiencies of energy and exergy are shown in Table 4.1. The exergy to energy ratio was calculated at 89% for both flow rates. This matches the theoretical exergy efficiency for this temperature range. The low exergy efficiency of this system of 55% is also a result of the losses, in the range of 35-40%. A larger system would have considerably smaller losses in respect to its storage size.

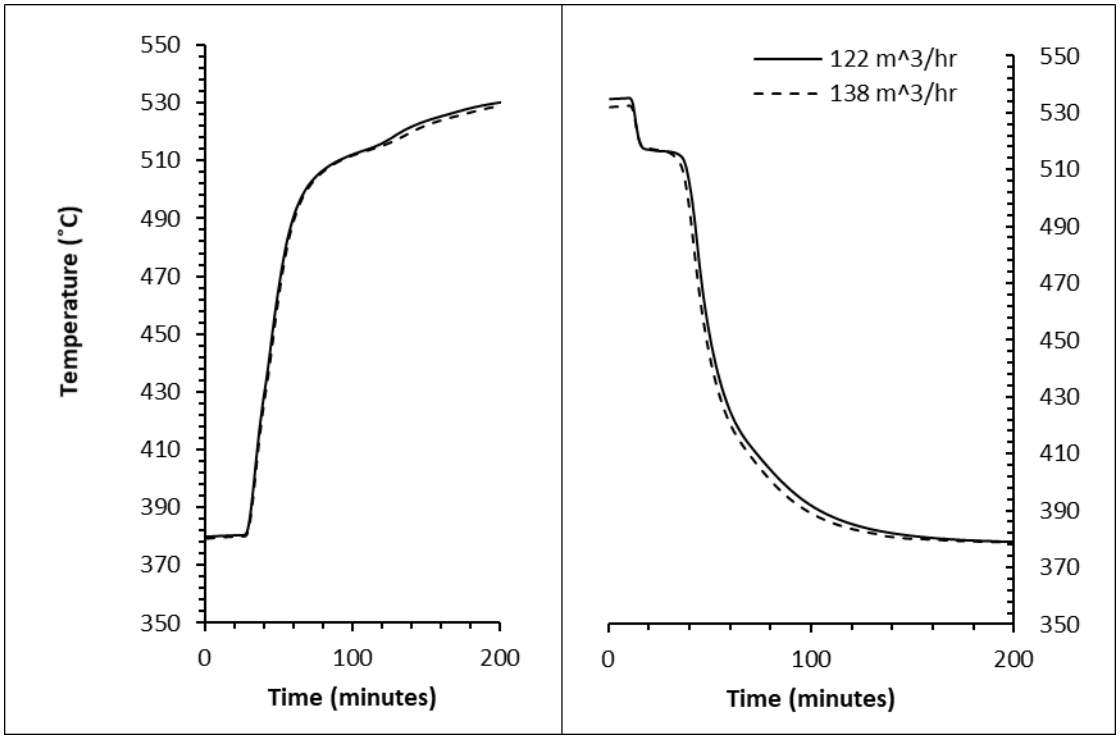

Figure 4.13 Average temperatures at the center of all capsules from all tests: charging (left); Discharging (right)

Table 4.1 TES unit performance

Flowrates	122 m^3/hr		138 m^3/hr	
	Avg.	St. Dev	Avg.	St. Dev
Energy Efficiency	62%	1.8%	61%	2.7%
Exergy Efficiency	55%	1.6%	55%	2.3%
Exergy to Energy Ratio	89%	0.06%	89%	0.11%
Charge Energy (kWh)	2.8	0.08	3.0	0.14
Discharge Energy (kWh)	1.7	0.06	1.8	0.06
Charge Exergy (kWh)	1.7	0.05	1.9	0.09
Discharge Exergy (kWh)	1.0	0.04	1.0	0.03
Charge Losses (kWh)	0.4	0.02	0.4	0.05
Discharge Losses (kWh)	0.1	0.01	0.1	0.01

4.6 Model Validation

A numerical model was developed using the methods from Pirasaci et al. [175] and validated against the experimental data using MATLAB after extracting the heat transfer properties from an ANSYS Fluent model. The enthalpy-porosity approach was used for the solidification and melting regions. The following assumptions were made for the analysis:

- All the PCM and HTF thermophysical properties except thermal conductivity(PCM) are constant.
- Heat capacity effects of the tubes are negligible.
- The outer wall temperature of the tube is constant.
- Flow through the tank is uniform.

The following boundary conditions were applied to the model:

- The system and the capsules are axisymmetric.

- The walls of the tank are adiabatic.
- The temperature of the heat transfer fluid does not vary across the radius of the tank.

The model shows good agreement with the data as shown in Figs. 12 and 13. Small inconsistencies between the model and experimental data were caused by the thermocouple uncertainty and the assumptions that the flow was uniform through the tank and the tank walls were adiabatic.

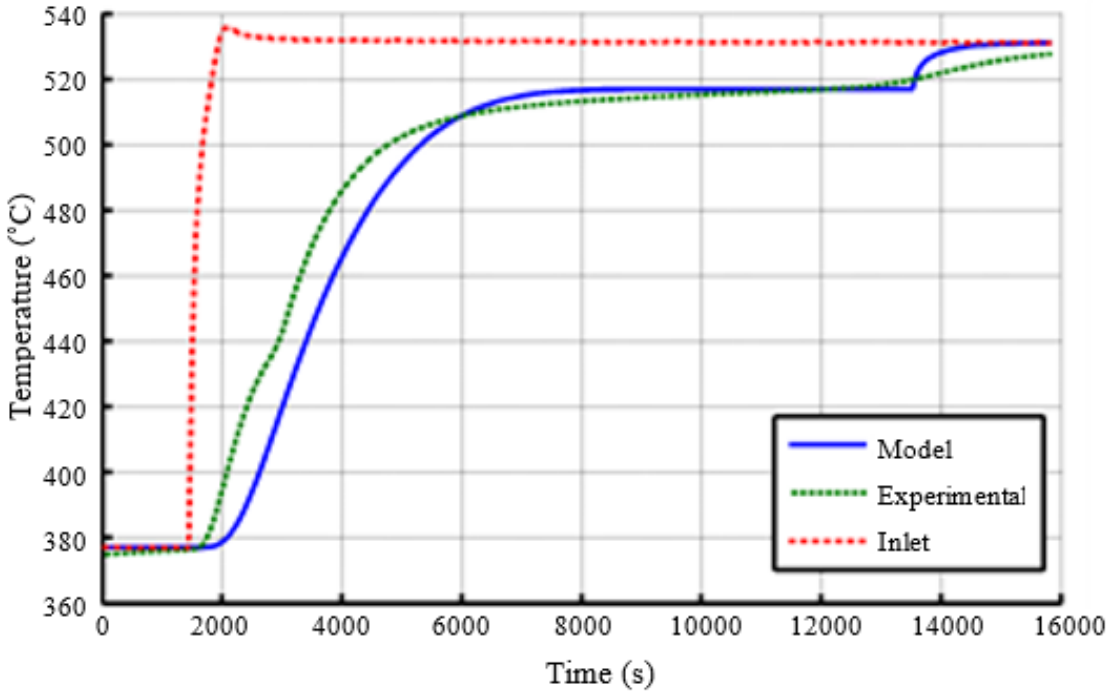

Figure 4.14 Modeled and experimental temperatures at the center of capsule during charging

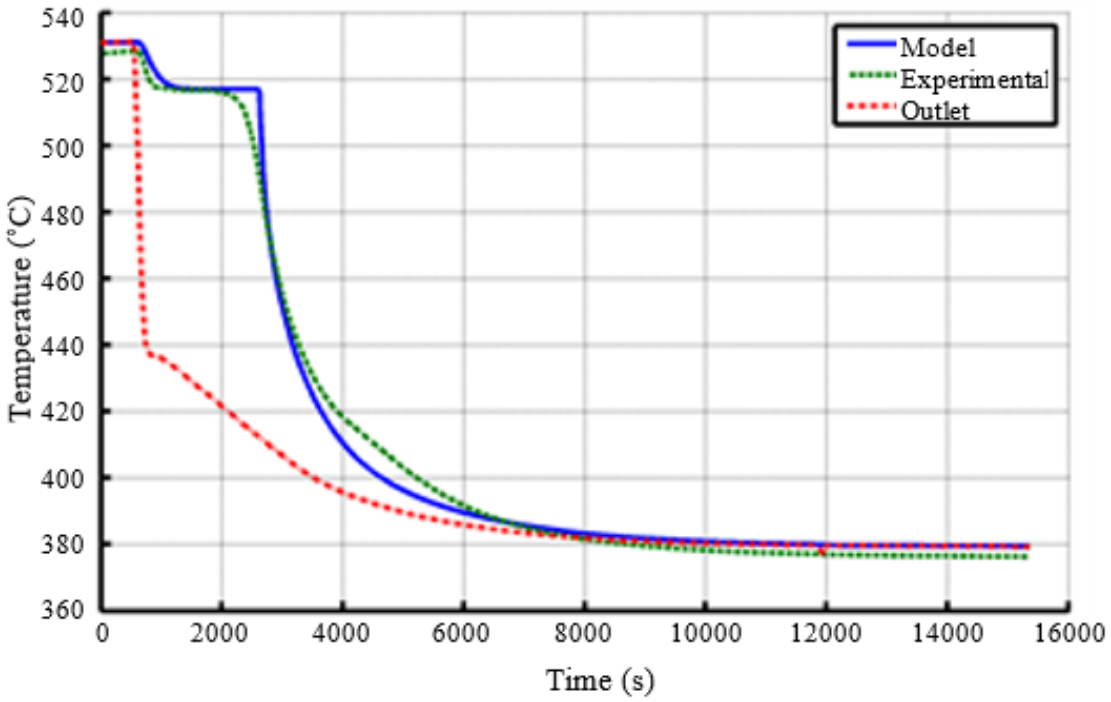

Figure 4.15 Modeled and experimental temperatures at the center of capsule during discharging

4.7 Improvements and Modifications[1]

As explained earlier, due to the bended section (Figure 4.16) in the system, the airflow was significantly faster on the outside (outer bend side), near capsule A, than on the inside(inner bend) of the system, near capsule D. To make this more uniform or even more center oriented, and to minimize the heat transfer losses from the walls, a thorough investigation was conducted to study the present flow conditions and neutralize the effect due to bending as many compact TES systems come with bent sections [176].

[1] The content of 4.7.1 was published in Moloney F, Wickramaratne C, Almatrafi E, Goswami DY, Stefanakos E, Guldiken R. Flow conditioning techniques for a bent pipe in a constrained latent heat storage system. ASME Int. Mech. Eng. Congr. Expo. Proc., vol. 7, 2016. doi:10.1115/IMECE201665730. Permission is included in Appendix C.

4.7.1 Flow Conditioning for the System

When a fluid, which is fully developed, flows through an elbow, the velocity, and subsequently the centrifugal force, is highest at the axis of the pipe. As the fluid passes through the bend, the fluid at the axis moves towards the outer bend, creating rotating cells, also known as Dean Vortices, perpendicular to the flow [177]. This secondary flow causes the flow to shift to the outer bend side of the pipe. In turbulent airflow, Wendt et al. [178] observed that after 2D in a straight pipe after a single bend, there was a local minimum velocity at the center of the pipe. After 10D, the maximum velocity was located towards the outer bend [178]. It can take up to a distance equal to 36 times the diameter (36D) for flow abnormalities to fully disperse after a disturbance [179,180].

To reduce this distance and redirect the flow, specially designed flow conditioners can be installed. There have been many studies investigating various arrangements of flow conditioners [178–190]. However, in many cases, it takes more than 10D to improve flow.

A flow straightener is effective at removing swirl but not at improving the velocity profile. Common flow straighteners are tube bundles and straight vanes. A flow conditioner, on the other hand, is a device that removes swirl and improves the flow within a short distance. Perforated plates are a common type of flow conditioner as they are easily constructed and installed [183]. Swirlers are devices that create predetermined disturbances in order to absorb any other effects [179]. Ahmadi [179] tested several different innovative designs of swirlers. These were effective at improving the velocity profile and the discharge coefficient through an orifice [179].

Many different designs of diffuser plate flow conditioners have been tested. The most commonly tested ones are the Mitsubishi Heavy Industries (MHI), Spearman (NEL), and Laws

plate. Spearman et al. [180,189] tested turbulent flow in water with these three plates in addition to an unchamfered and a chamfered Laws plate after a single 90˚ bend. Placing the plate 4D after a single 90-degree bend, velocity profiles were measured. The MHI plate was effective at removing secondary flows but not at improving the symmetry of the flow [189]. The NEL plate performed the best after 3D. The unchamfered and chamfered Laws plate provided suitable velocity profiles at 11D and 6D after the flow conditioner, respectively [180].

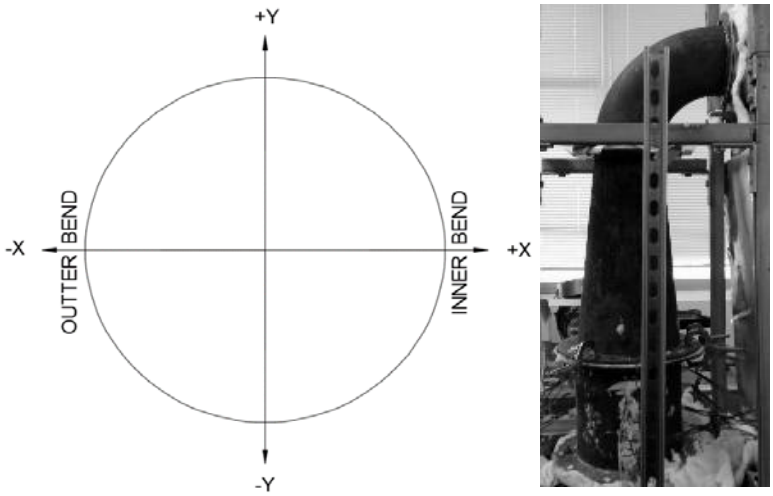

Figure 4.16 Coordinate reference to the bend(left), photo of the actual bent section (right)

Shao [191] tested and modeled the flow of water through a straight pipe with a gate blocking half of the flow. Computational Fluid Dynamics (CFD) was used to model different configurations of Laws plates. The geometry, porosity, and thickness of the plate affect the performance of the flow conditioner [191].

An alternative way to control the flow through an elbow is to use a twisting vane before the start of the bend. Cheng Fluid Systems invented such a vane, the Cheng Rotation Vane (CRV®), which causes the fluid to rotate slightly along its axis through the bend [3]. As the flow rotates

through the bend, the angle, at which the centrifugal force acts on the fluid in respect to the fluid, changes, preventing asymmetrical flow.

These specialized perforated plates have thus been extensively studied for mild disturbances, but not positioned directly after single 90-degree bends to improve flow within 3D lengths of a bend with the heated or compressible flow.

4.7.1.1 Testing Procedure

In the current system, the air was passed through heaters then through a single 90-degree elbow, with a bend ratio of 1.5, followed by an increasing diameter pipe before entering the storage tank. The top of the tank was three times the diameter (3D) of the elbow below the bend.

The tested flow conditioners were installed directly after the bend, before the diffuser cone. The rotational vane was placed inside the horizontal pipe directly before the bend. Different flow rates were provided by the blower (Dayton 115V, 2860 RPM) which was attached to a variable switch. Using an E-Instruments VT 100 anemometer, the velocity was measured across two cross-sections at the end of the diffuser cone and before the location of the storage tank: in the direction spanning from the inner bend to the outer bend (x-direction) and in the perpendicular direction (y-direction). Measurements were taken every one inch at thirty second intervals to record the minimum, maximum, and average velocities at each point. Each flow conditioner was tested at flow rates of 115 m^3/h and 170 m^3/h (inlet) in the ambient environment, 40˚C, and 60˚C. The temperature range tested was limited by the operating conditions of the anemometer. After verifying that the setup contained no leaks, the flow was allowed to stabilize at each temperature before measurements were taken.

4.7.1.2 Tested Flow Conditioners

Several flow conditioners were tested (Figure 4.17). The MHI and the Spearman flow conditioners were designed to allow more flow through the center of the pipe. The MHI plate has 35 holes, all with a diameter of 13% the diameter of the pipe, arranged in a pattern to allow more flow through the center of the pipe. The MHI plate was constructed with a thickness equal to 13% of the pipe diameter [2]. The Spearman plate was constructed according to its specifications with the appropriate thickness (0.12D) [2]. In order to reduce the amount of material needed for high-temperature applications, two plates with a thickness of 0.64 mm were placed 0.12D apart in a double plate configuration.

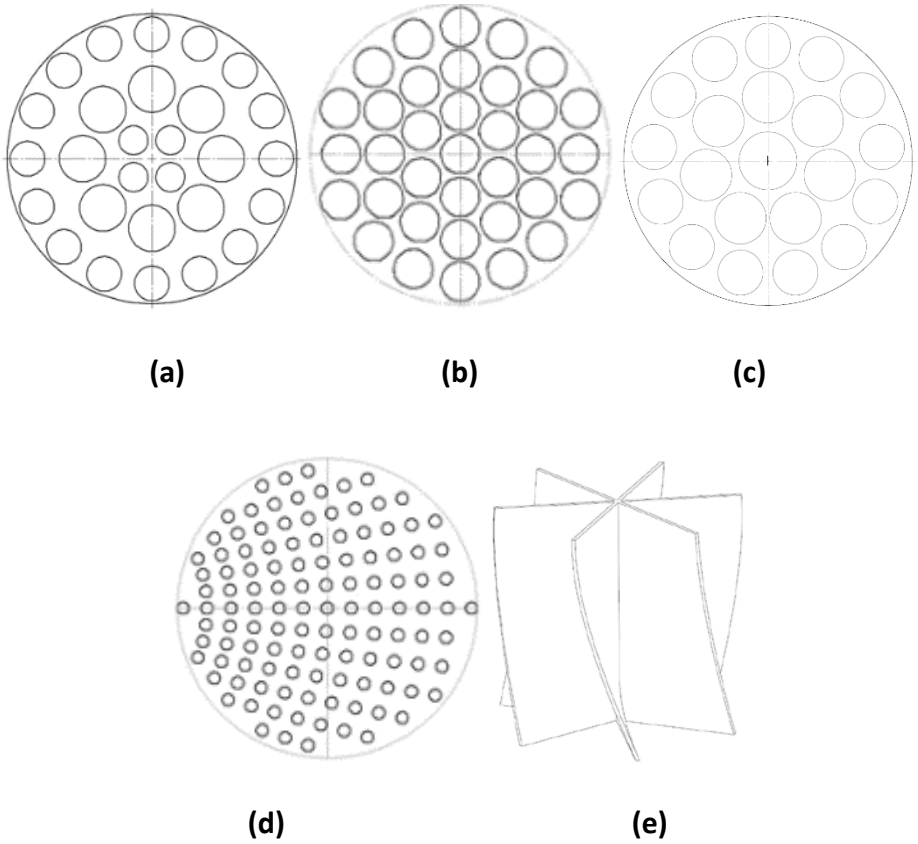

Figure 4.17 Flow conditioners: (a) Spearman plate; (b) MHI plate; (c) Laws plate; (d) Graded porosity plate; (e) Twisted vane type

Additionally, two plates were constructed out of 0.64 mm thick aluminum that provided an increasing porosity across its diameter in the direction of the inner bend. A rotational vane, similar to the CRV, was constructed out of aluminum. The vanes were twisted by 40 degrees.

4.7.1.3 Uncertainty Analysis

The uncertainty of the anemometer was ±0.18 m/s for velocities up to 6 m/s. The positioning of the anemometer was within 0.01m in any direction. The Omega k-type thermocouples had a manufacturer uncertainty of ±0.3^{o}C in the tested temperature range. The thermocouples were also calibrated in a separately closed furnace up to 80^{o}C.

4.7.1.4 Experimental Results

For the set operating conditions, 18 readings were recorded (9 each in x and y-direction, for a single flow conditioner. Non-dimensional parameters were used for the analysis and U_{avg} were calculated from all the 18 velocities at that particular setting. The system was first tested without any flow conditioners. As evident in Figure 4.18, the flow distribution was skewed to the outside of the curve. Along the x-direction, the flow was high near the walls and reduced at the center. These trends were evident at all temperatures and consistent with the trends observed by Spearman in water at 5D after the bend [2]. Velocity profiles for the lower flowrate were steeper and more skewed towards the pipe walls.

The temperature had very little impact on the normalized velocity profiles in the tested range (Appendix B). The vane and graded porosity plates over corrected the flow, directing it towards the inner bend (Appendix B). The results of the conditioners that showed promise are discussed here.

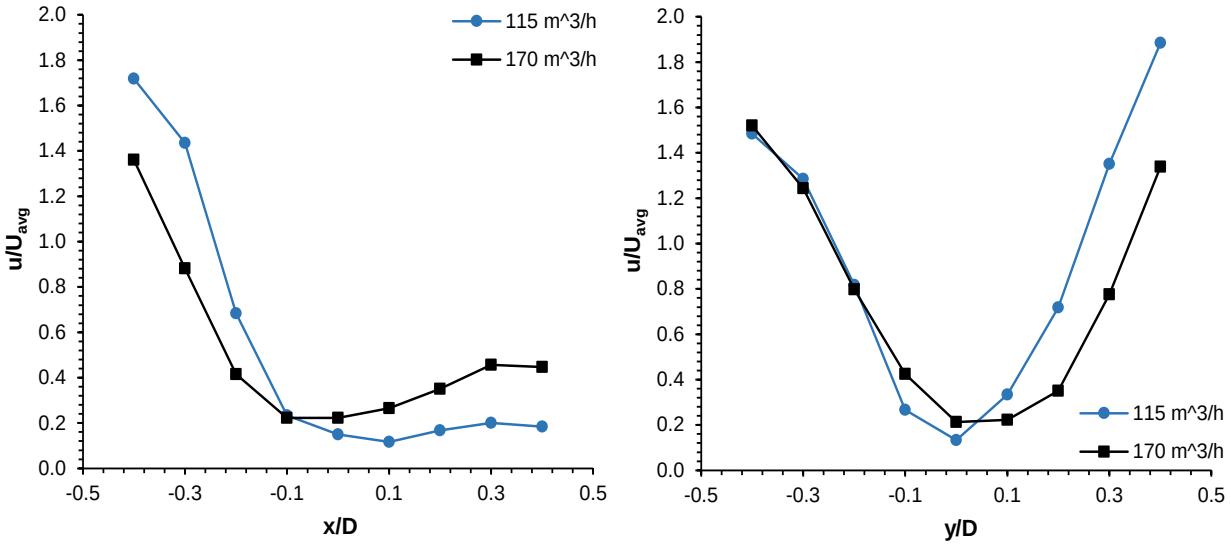

Figure 4.18 Velocity profile for different flow rates with no correction along

The Laws plate showed symmetrical results in the y-direction, but skewed results in the x-direction, as evident in Figure 4.19 (a). The double Spearman plate made the flow more uniform and symmetrical than the control experiments in the x-direction (Figure 4.19 (b)). However, the velocity profile increased across the y-direction, indicating a swirl or irregularity to the flow. The best performing plates were the MHI and Spearman plates. Both plates successfully improved the velocity profile across the x and y-directions (Figure 4.19 (c) & Figure 4.19 (d)) and 6d). The MHI plate produced more dispersed flow than the Spearman and was found to be the best flow conditioner among the tested flow conditioners.

Although this system had turbulent flow at the inlet of the bend (Reynolds numbers over 10,000), the velocity profiles with the Spearman and MHI plates resemble a laminar distribution, but this is not a fully developed flow. The flow conditioner restricts the flow, and the diffuser cone reduces the velocity. As a result, the peak of velocity profile has shifted to the center of the pipe in comparison to the original setup. Numerical models were developed for the flow conditioners using ANSYS and verified with the experimental data.

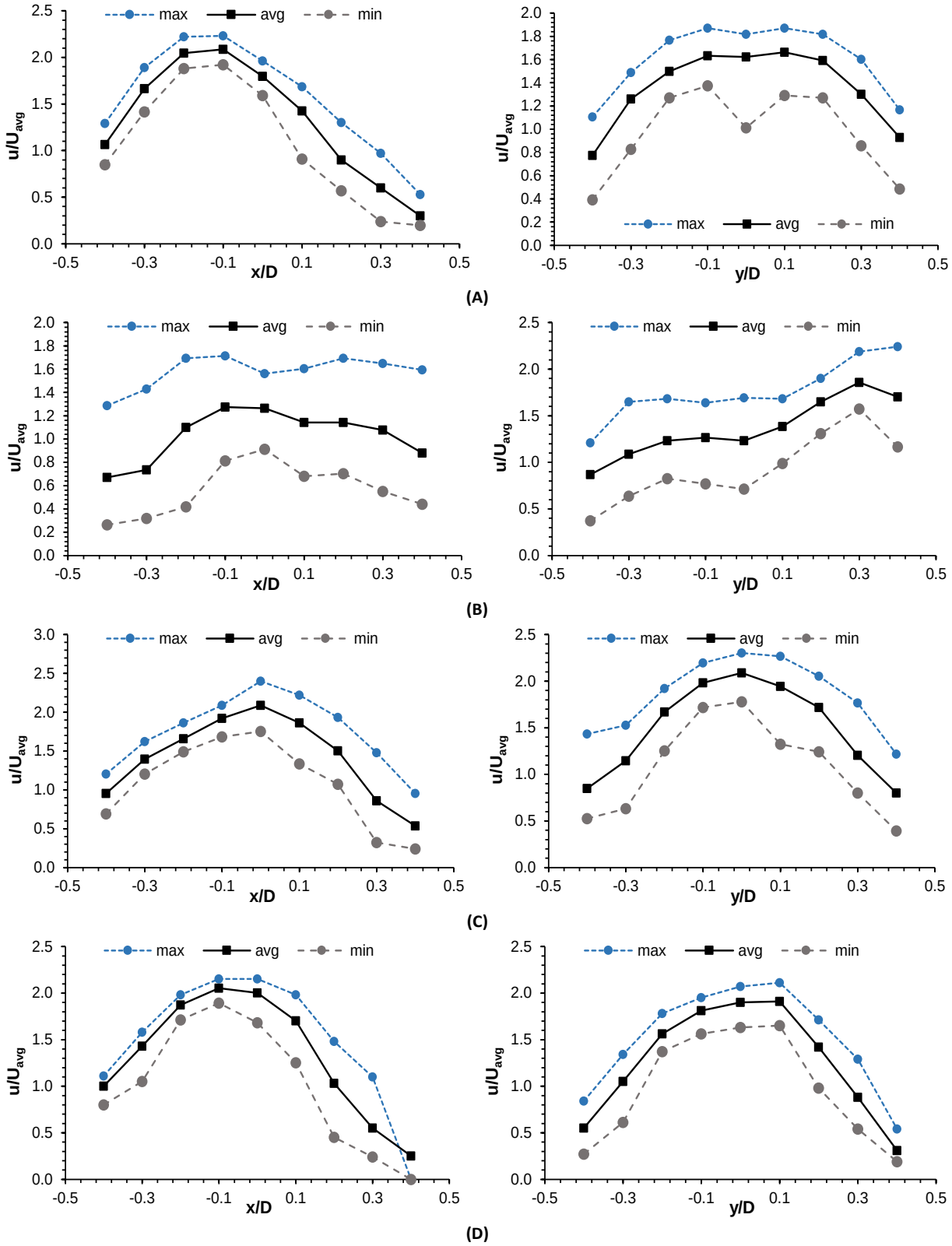

Figure 4.19 Velocity profile in ambient conditions: (a) Laws plate; (b) Double spearman plate; (c) MHI plate; (d) Spearman plate

4.7.1.5 Model Validation

An ANSYS/FLUENT model was developed using the boundary conditions obtained by the experimental setup. All conservation equations including mass, momentum, and energy were discretized using the finite volume method. All the cases analyzed show Reynolds numbers above 10,000, and the standard k-epsilon model was used to model the turbulent flow. Standard wall function was used for near-wall treatment. The second order upwind criteria were used for the discretization of pressure, momentum, turbulent kinetic energy and turbulent dissipation rate. The pressure-velocity coupling was established by using the SIMPLE algorithm. The flow resistance from the heaters was not considered. The measured pressure of the tank corresponding to the model outlet was uniform throughout the outlet plane. An experimental average inlet velocity of 2.46 m/s was used as the model inlet velocity, and the turbulent intensity at the inlet was calculated from the Reynolds number at the inlet using the following equation.

$$I = 0.16Re^{-1/8}$$

Hydraulic diameter for the inlet was 0.158m. The actual outlet of the experimental setup was different than the model created. The pressure outlet boundary condition in the model was set to the gauge pressure measured (130 pa), at the storage tank during the experiments. The air density was 1.225 kg/m3 and the dynamic viscosity was 1.789e-6 kg/m-s.The converged solution contained residuals less than 1e−6. Grid independence was checked by varying the mesh size until the converged results did not vary. The selected mesh had elements in the range of 400,000. A three-dimensional tetrahedron variable size mesh was used and had 81310 nodes and 417530 elements. Grid independence was checked by varying the mesh size until the converged results

did not vary. The converged solution contained residuals less than 1e−6. The average skewness was 0.23, and orthogonal quality was 0.85.

Figure 4.20 shows the velocity distribution along the XZ plane. At 3D after the flow conditioner, the velocity is more dispersed and is between 1 and 2 m/s.

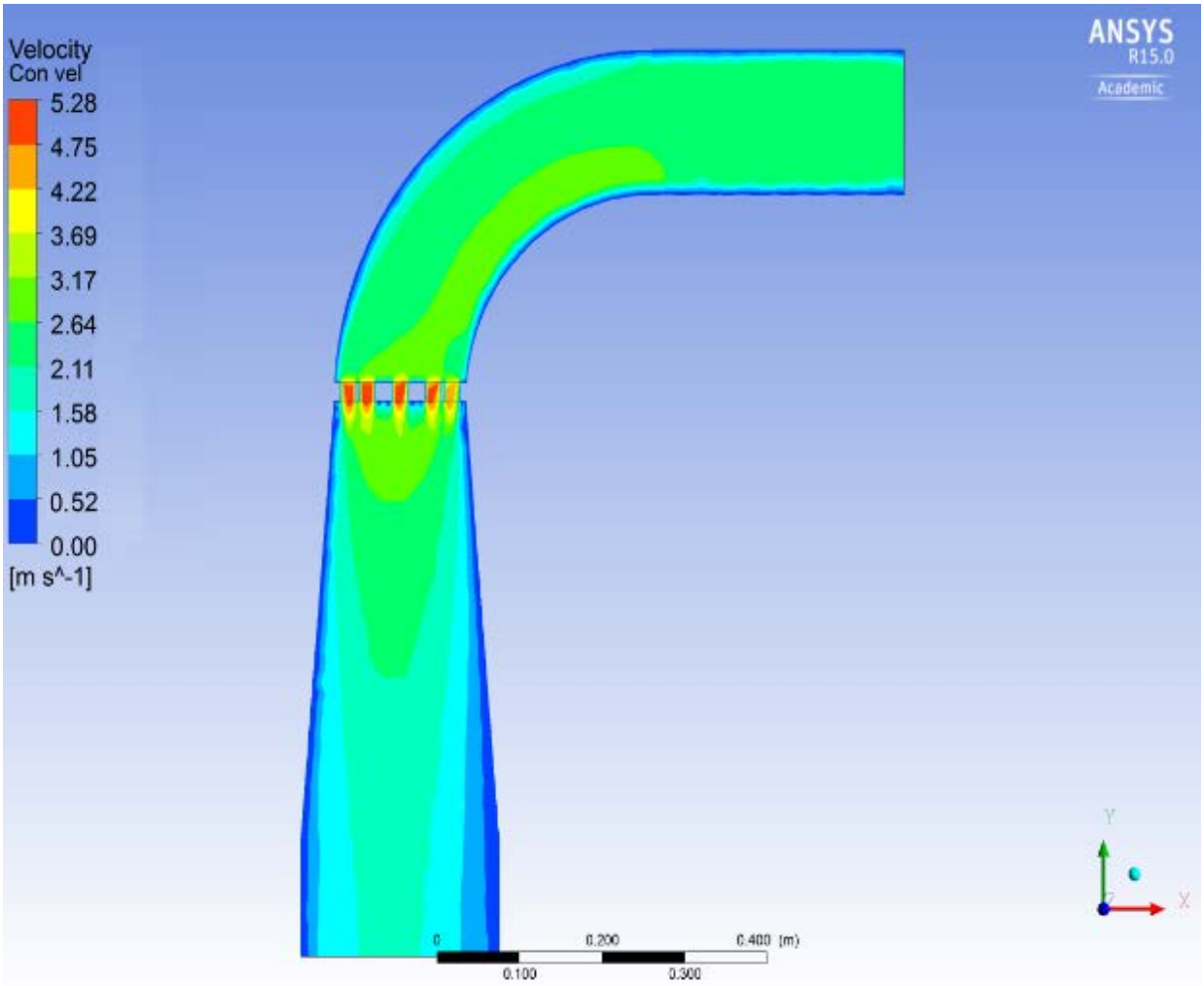

Figure 4.20 Velocity profile along XZ plane for MHI plate

The model shows a reasonable agreement with the experimental data in the x and y-directions, as evident in Figure 4.20. The model slightly overpredicted the maximum velocities for the Spearman plate.

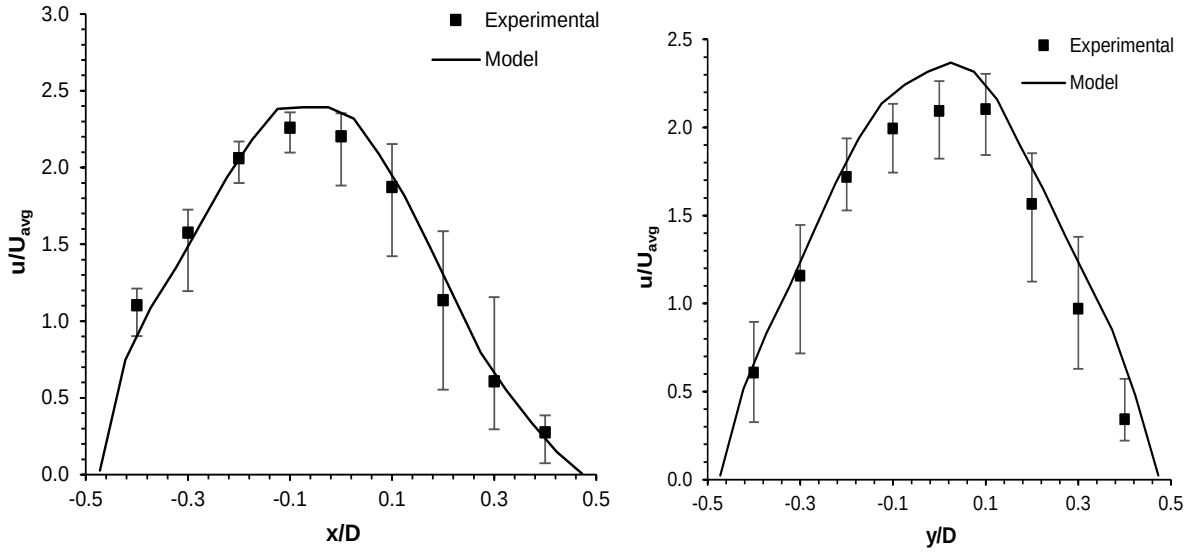

(a)

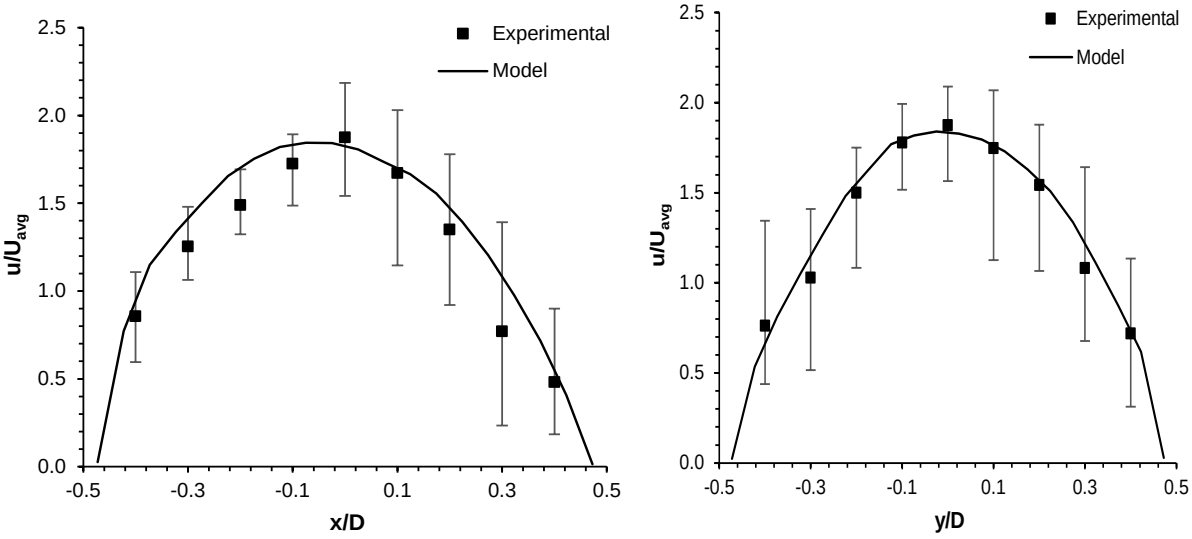

(b)

Figure 4.21 Model vs experimental velocity profiles for: (a) Spearman plate; (b) MHI plate

4.7.1.6 Conclusions from the Experiment

For TES, ensuring that the maximum flow is at the center of the tank minimizes heat loss through the walls, thus improving the efficiency of the system. The MHI and Spearman plates both significantly improved the velocity profiles of the air flow after 3D from the elbow. Both

plates produced a maximum velocity near the center of the pipe as opposed to along the outer wall. The MHI plate produced more dispersed flow than the Spearman.

More testing should be performed with these flow conditioners to analyze the effect of temperatures between 300°C and 500°C on the velocity profile. Further investigation of a double Spearman plate constructed with two thin plates should be performed to optimize the distance separating the two plates, thus reducing the amount of material and cost in respect to a standard Spearman plate. The optimal orientation of the graded porosity plate can be further investigated to produce a symmetrical velocity profile. Additionally, the heated flow can be modeled in CFD to predict the flow distribution for elevated temperatures.

Finally, MHI plate was machined using carbon steel and installed in the system to neutralize the flow irregularities

4.7.2 Discharge Heater Addition

To address the limitation in the discharge temperature, a 2kW Sylvania brand air heater was added to the discharge heater bank. Additional housing was added to the compartment due to the limitations of the spacing availability. With the new discharge heaters expected symmetric operating conditions (20°C above and below the melting point) were achieved for the selected flow rates.

4.7.3 Radiation Shields

To reduce losses due to radiation, radiation shields were added to the bent and cone sections of the system. The added systems were designed and manufactured in-house by thin polished aluminum sheets.

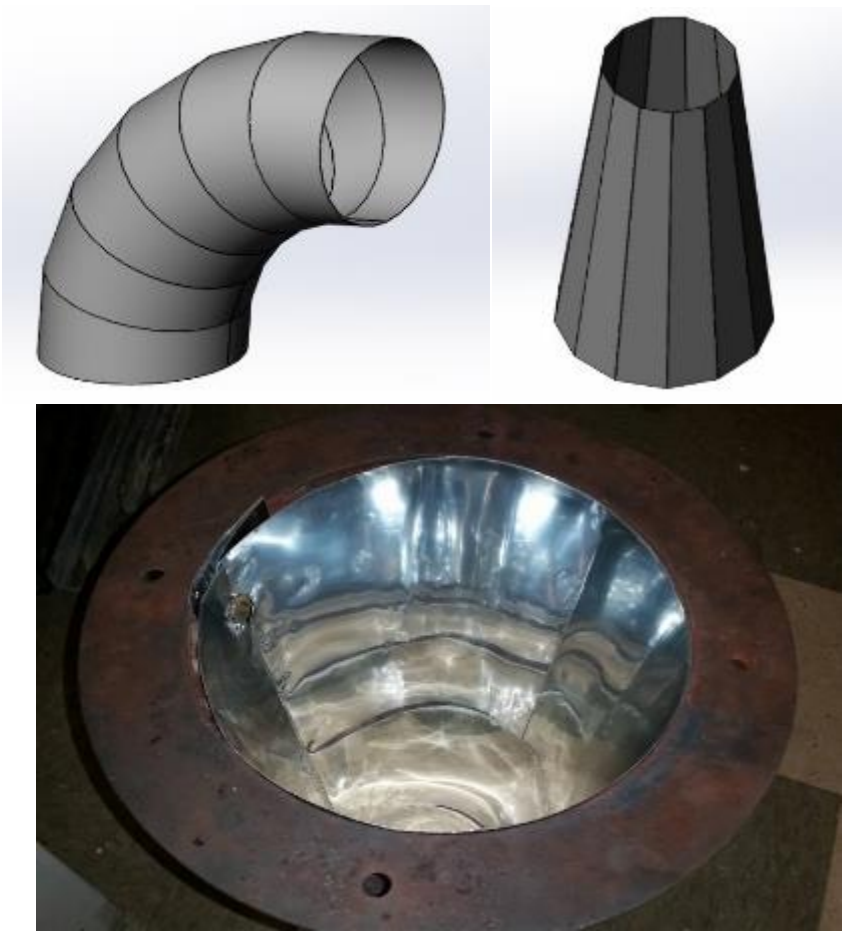

Figure 4.22 Design of radiation shields for bent (top left), cone (top right) sections and the actual picture after installation(bottom)

4.8 Results of the Modified System

Comparing the data with the earlier configuration, temperature variation across the bed (radial variation) was significantly reduced (Figure 4.23). This was a result of the flow conditioning. Melting time difference of A and D capsule, which was as large as 2 hours for the previous system, was reduced to 20 minutes.

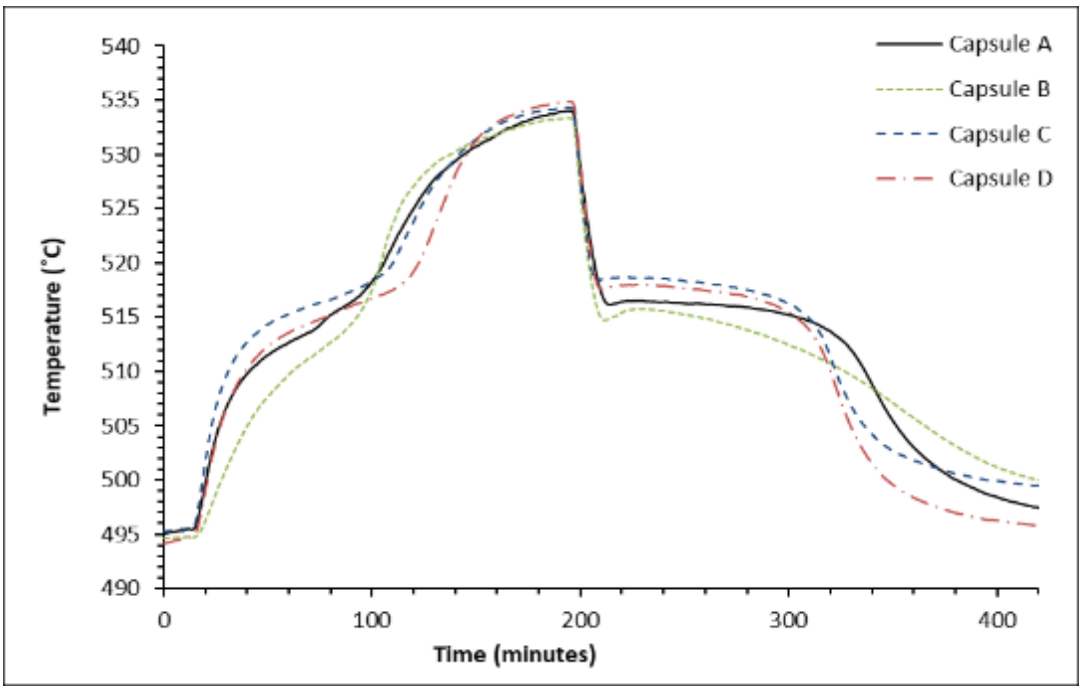

Figure 4.23 Capsule center temperature during one run at 138 m^3/h for the modified system

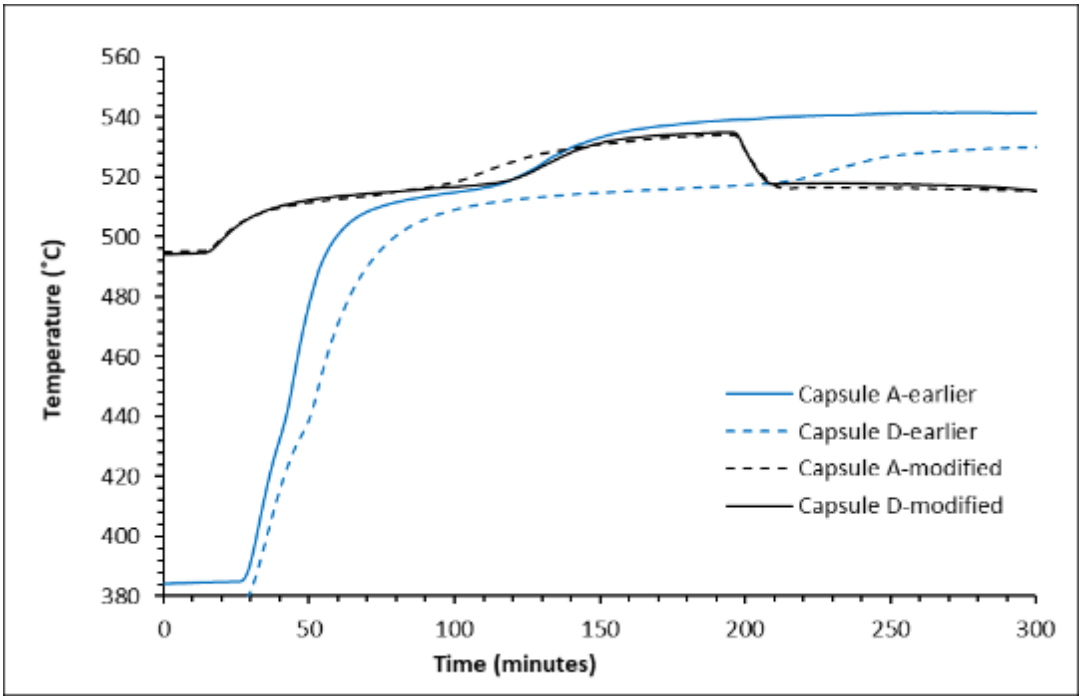

Figure 4.24 A(Left) & D(right) comparison of earlier and modified system

Even though the system was modified, the improvements were not reflected in the data. The overall full cycle efficiency did not increase. This is mainly a result of the narrowing down of the operating temperature in the discharge cycle. As explained earlier, the discharge cycle took little more than one and half hours to stabilize when it was operating between 535°C and 380°C. So during the solidification, which was the major part of the discharge cycle, the heat transfer was happening between 515°C (phase change temperature of the PCM) and 380°C (set discharge temperature) temperatures. In the case of the modified system, the charging and discharging temperatures were set for 20 degrees above and below. During the solidification, the heat transfer was happening between 515°C and 495°C temperatures, and the difference is small (20°C) compared to an earlier difference of 135°C. As a result, the discharge cycle was taking more than three and half hours to stabilize. The total charge-discharge cycle duration was increased compared to the earlier conditions. Total time increase for the full cycle was considerably large and in the range of close to 30%. The effects of modifications were nullified by the extension of cycle time. As a result, the full cycle overall heat loss was high in the modified configuration. However, the exergy to energy ratio of the modified system was around 98% which was a drastic improvement from the earlier value of 89%.

CHAPTER 5: PROPOSED NOVEL THERMAL ENERGY STORAGE SYSTEM

Spherical shaped PCM capsules have shown better heat transfer properties compared to cylindrical systems [192]. In the past, several numerical studies were done for the spherical shape EPCMs [193–196]. Archibold et al.[197–199] investigated the melting and solidification of spherical capsules in high-temperature range LHTES applications. Only Zheng et al. [41] reported an experimental fabrication of spherically shaped capsules for high-temperature PCM applications. He fabricated spherically shaped capsules of 2mm diameter with copper as the PCM. Shell material was made from a combination of chromium and nickel, which were electroplated to a thickness of 100 μm and 500 μm respectively. The capsules successfully survived for 1000 thermal cycles, but this process of electroplating nickel and chromium is expensive.

In the case of cylindrical capsules, the fabrication process is much simpler because of the commercial availability of premade cylindrical tubes. The lab-scale LHTES system described in chapter four was with cylindrical capsules. But the system initially (before implementing flow conditioners) showed uneven heating inside the tank due to the flow irregularities. With a packed-bed spherical setup, flow irregularities would have been comparatively small as these irregularities typically get dispersed due to the packing arrangement. But the fabrication process of spherical capsules is not as straightforward as the cylindrical capsule. The goal of the new

design is to get the benefits of the spherical shape capsules and incorporate into a bulk-manufacturable design.

5.1 Stress Development and Optimization of Thickness

It is essential to optimize the thickness of the capsule to minimize the cost considering the operating conditions. This LHTES design was focused on a high pressure and high-temperature application. Temperature range of 500 - 600oC and pressure of 50 MPa were selected as the operating conditions. Pressure calculation comparing with the common cylindrical configurations were carried out and is given in detail in the appendix B. The material chosen was again Ni-coated carbon steel. The thickness was selected considering conservative conditions. Yield point (370 MPa) was considered in determining the thickness rather than the ultimate tensile strength of carbon steel. The safety factor selected was 1.5. For the selected conditions, a thickness of 1.5 mm was sufficient for a 1" inch (25.4 mm) diameter capsule. In the case of a cylindrical capsule, hoop stress was twice that of spherical and therefore capsule thickness was increased to 3mm for the same operating conditions. Axial stress for this is low, and the failure stress was due to the hoop stress. So it was evident that encapsulation material requirement was larger for the cylindrical case.

5.2 Proposed Design

This design was modeled using Solidworks as shown in the figures. The plate thickness considered here is 1.5 mm, and this thickness can be easily pressed and formed. Figure 5.1 shows a carbon steel sheet of many hemispherical shapes. Spherical salt pellets of Na2SO4-KCl or any PCM that melts in the range of 500oC to 600oC are placed on a multi hemispherical shaped sheet

(Figure 5.2). An identical but inversed metal sheet is placed on top of the capsules and welded to the other sheet with a fusion welding mechanism.

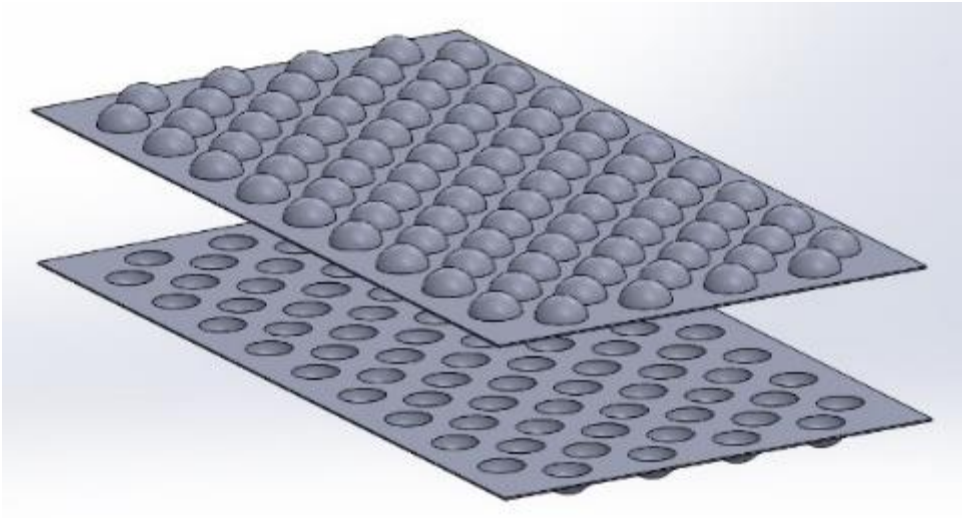

Figure 5.1 Two identical sheets of multi hemispherical shapes

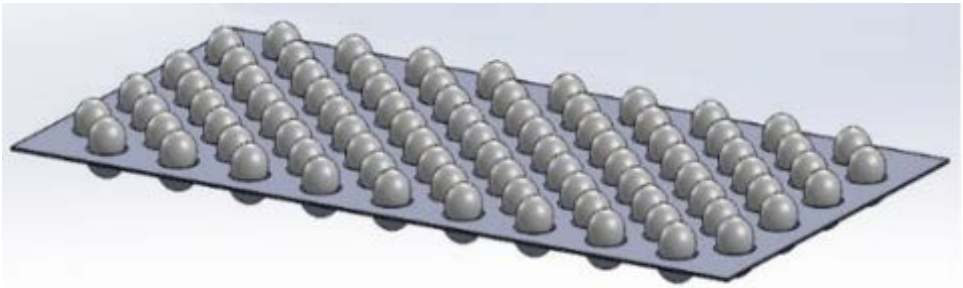

Figure 5.2 Spherical salt pellets placed on the multi hemispherical shape sheet

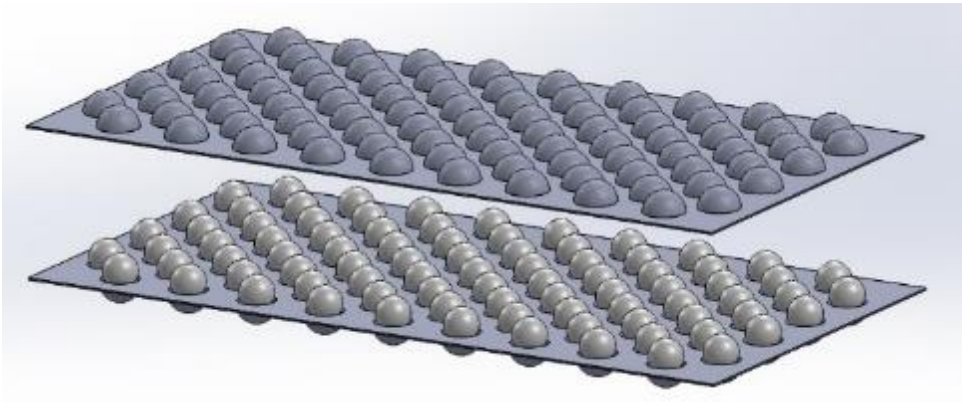

Figure 5.3 Closing with the same type of hemispherically pressed sheet

5.3 LHTES System

A LHTES system of these capsules is similar to a spherical capsule packed bed system (Figure 5.5). The only difference is caused by the secondary flows generated inside the packed bed. The secondary flow of the sheet capsules, even though the shapes are same, are limited by columns of the sheet (Figure 5.4). Therefore, dispersion of flow unevenness in the tank is restricted. In this system, it is essential to have a certain amount of flow uniformity at the inlet unlike a case of packed bed system. As we already experienced a case of flow unevenness in a lab-scale LHTES system (chapter 4), we can tackle this problem with the use of flow conditioners. MHI plate or CRV vane type flow conditioner can be used if the flow entering the LHTES system is uneven.

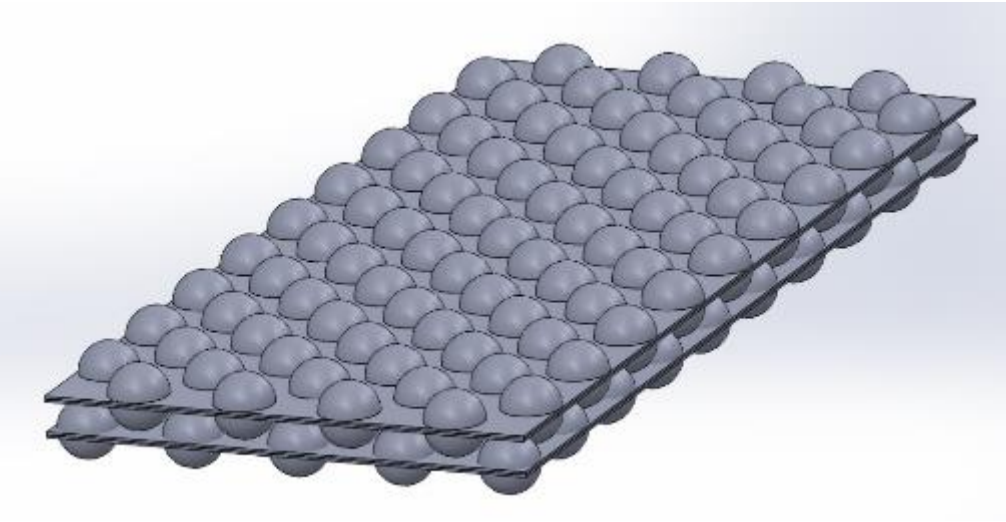

Figure 5.4 Layered arrangement

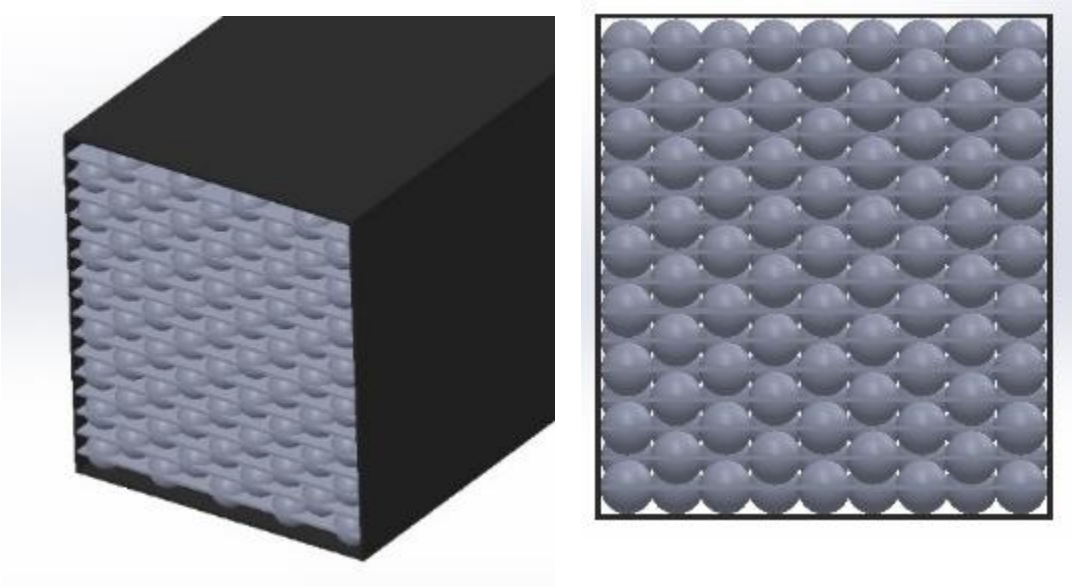

Figure 5.5 Packed bed setup

5.4 Method of Manufacturing

Carbon steel is an inexpensive material, and sheet metal forming is a well-established and low-cost technology. A die is needed for pressing and forming the hemispherical shapes. High-speed steel (HSS) is a good affordable material for the die. The ductility of carbon steel is high and a surface hardened die of HSS can produce a very large number of pressed sheets.

Spherical salt pellets can be made with cheap polyvinyl chloride (PVC) molds. In the post-formed encapsulation explained in the chapter 3.5.1, the method of making the salt pellet was with the use of a PVC mold and a press machine.

Welding and sealing process should be done in a low pressure environment. An argon or nitrogen high environment is also suited for this. This is to ensure that sealing happens in a low oxygen environment, in order to prevent corrosion inside the capsule when the salt is molten. If the length of the sheet is long, the fusion welding machine should either be large or should allow

part by part welding. It is essential to optimize the size of the sheet especially considering this process. If the requirement is for large sheets, an extra joining process can be added rather easily without complicating the welding and sealing process. As the final step, 150 µm to 200 µm thick nickel is electroplated for additional protection.

This method can be easily adopted for low-temperature PCMs without nickel electroplating. Industrial scalability of the mentioned process is considerably high compared to a spherical capsule fabrication process.

CHAPTER 6: CONCLUSION AND FUTURE WORK

6.1 Summary and Conclusion

The main focus of this study was to examine and develop a reliable LHTES system for high-temperature applications. Lack of research on LHTES systems and PCM containment methods for temperatures above 500°C has driven the study to find a reliable encapsulation method for PCMs for temperature above 500°C, and experimentally investigate the performance of a high-temperature LHTES system.

Macro-encapsulation techniques were developed for two temperature ranges: 500°C – 600°C and 600°C above. Three different PCMs; NaCl (801°C), NaCl-KCl (657°C), Na_2SO_4-KCl (515°C), were investigated and tested for compatibility with macro-encapsulation. Low-cost ceramics with excellent chemical stability under molten-salt conditions were selected as the encapsulants for NaCl and NaCl-KCl eutectic. An optimum ceramic composition, feldspar (50%), kaolin (16.67%), 16.67 ball clay (16.67%), silica (16.67%), was identified after several experiments. The processing procedure for these materials was discerned by systematic studies of porosity distribution and materials compatibility. The ceramic materials, when sintered at 800°C, reacted with molten NaCl, whereas the same ceramic composition, when sintered at 1190°C, did not show any reaction with the molten NaCl. Ceramic capsules were fabricated and sintered at 1190°C, and the desired PCM was poured into it through a hole.

A novel technique of sealing was introduced through in-situ layered eutectic formation. Sealing was done at a temperature above the eutectic melting point of the salt mixture but below the individual melting points of each salt. The fabricated capsule survived more than 500 thermal cycles without showing degradation in their thermo-physical properties. Alumina (99%) based capsule of NaCl-KCl was tested successfully for 1000 thermal cycles with a PCM weight loss percentage of less than 5 %. Based on these results, it can be concluded that the developed ceramic materials have good potential for use in high temperature (>500 ^{o}C) LHTES applications

A lab-scale packed-bed system was designed and developed to investigate an industry scalable LHTES system suitable for supplementing heat to a steam-powered cycle. Metallic cylindrical capsules were filled with a eutectic of sodium sulfate (Na2SO4) and potassium chloride (KCl) as the phase change material (PCM) for energy storage. The system consisted of a cylindrical storage tank with the cylindrical capsules arranged vertically.

The system showed flow irregularities due to the presence of bent sections. Several flow conditioners were experimentally tested for the making the flow uniform. The MHI and Spearman plates both significantly improved the velocity profiles of the air flow after 3D distance from the elbow. Both plates produced a maximum velocity near the center of the pipe with MHI showing slightly more dispersed flow than Spearman. ANSYS model was developed to investigate different flow conditioners. The model had a good agreement with the experimental data.

An innovative spherical shaped multi pack design was proposed for large-scale manufacturing. A new technique was proposed while adopting the benefits of the spherical capsules and reducing the manufacturing difficulties. The adoptability of this technique for higher

or lower temperature LHTES applications depends on the properties of the selected sheet metal. Any formable metal sheet can be used considering the compatibility with PCM and HTF.

6.2 Future Work

Future work on ceramic encapsulation should focus on PCMs melting around 1000°C. Sintering using very high temperatures (over 1300°C) and low dwell times, while not increasing the processing energy, needs to be analyzed.

The effect of temperatures over 500˚C on the velocity profile can be investigated to improve the flow irregularities in a compact system. Further investigation of a double Spearman plate constructed with two thin plates should be performed to optimize the distance separating the two plates, thus reducing the amount of material and cost as compared to a standard Spearman plate. The optimal orientation of the graded porosity plate can further be investigated to produce a symmetrical velocity profile. Additionally, the heated flow can be modeled in CFD to predict the flow distribution for elevated temperatures.

For the proposed new spherical shaped PCM design, the process of vacuum or low pressure welding needs to be investigated. Embrittlement, creeping and graphitization of carbon steel at elevated temperatures should be further analyzed for temperatures above 500°C.

REFERENCES

[1] Sozen, Mehmet; Vafai, Kambiz; Kennedy LA. Thermal charging and discharging of sensible and latent heat storage packed beds. J Thermophys Heat Transf 1991;5:623–5.

[2] Kuravi S, Trahan J, Goswami DY, Rahman MM, Stefanakos EK. Thermal energy storage technologies and systems for concentrating solar power plants. Prog Energy Combust Sci 2013;39:285–319. doi:10.1016/j.pecs.2013.02.001.

[3] Hasnain SM. Review on sustainable thermal energy storage technologies, Part I: heat storage materials and techniques. Energy Convers Manag 1998;39:1127–38.

[4] Nomura T, Okinaka N, Akiyama T. Technology of Latent Heat Storage for High Temperature Application: A Review. Isij Int 2010;50:1229–39. doi:10.2355/isijinternational.50.1229.

[5] Sharma A, Tyagi VV, Chen CR, Buddhi D. Review on thermal energy storage with phase change materials and applications. Renew Sustain Energy Rev 2009;13:318–45. doi:10.1016/j.rser.2007.10.005.

[6] Ezan MA, Ozdogan M, Gunerhan H, Erek A, Hepbasli A. Energetic and exergetic analysis and assessment of a thermal energy storage (TES) unit for building applications. Energy Build 2010;42:1896–901. doi:10.1016/j.enbuild.2010.05.025.

[7] Erek A, Dincer I. A New Approach to Energy and Exergy Analyses of Latent Heat Storage Unit. Heat Transf Eng 2009;30:506–15. doi:10.1080/01457630802529271.

[8] Başçetinçelik A, öztürk HH, Paksoy HÖ, Demirel Y. Energetic and exergetic efficiency of latent heat storage system for greenhouse heating. Renew Energy 1999;16:691–4. doi:10.1016/S0960-1481(98)00253-5.

[9] Jegadheeswaran S, Pohekar SD, Kousksou T. Exergy based performance evaluation of latent heat thermal storage system: A review. Renew Sustain Energy Rev 2010;14:2580–95. doi:10.1016/j.rser.2010.07.051.

[10] Konuklu Y, Ostry M, Paksoy HO, Charvat P. Review on using microencapsulated phase change materials (PCM) in building applications. Energy Build 2015;106:134–55. doi:10.1016/j.enbuild.2015.07.019.

[11] Castellón C, Medrano M, Roca J, Nogués M, Castell A, Cabeza LF. Use of Microencapsulated Phase Change Materials in Building Applications. Ashrae 2008.

[12] Kamal R. Optimization and Performance Study of Select Heating Ventilation and Air Conditioning Technologies for Commercial Buildings. University of South Florida, 2017. doi:10.13140/RG.2.2.19262.79686.

[13] Hasnain SM. Review on sustainable thermal energy storage technologies, Part I: heat storage materials and techniques. Energy Convers Manag 1998;39:1127–38. doi:10.1016/S0196-8904(98)00025-9.

[14] Hasnain SM. Review on sustainable thermal energy storage technologies, Part II: cool thermal storage. Energy Convers Manag 1998;39:1139–53. doi:10.1016/S0196-8904(98)00024-7.

[15] Medrano M, Gil A, Martorell I, Potau X, Cabeza LF. State of the art on high-temperature thermal energy storage for power generation. Part 2—Case studies. Renew Sustain Energy Rev 2010;14:56–72. doi:10.1016/j.rser.2009.07.036.

[16] Laing D, Bahl C, Bauer T, Lehmann D, Steinmann WD. Thermal energy storage for direct steam generation. Sol Energy 2011;85:627–33. doi:10.1016/j.solener.2010.08.015.

[17] Maruoka, N.; Sato, K.; Yagi, J-I.; Akiyama T. Development of PCM for Recovering High Temperature Waste Heat and Utilization for Producing Hydrogen by Reforming Reaction of Methane. ISIJ Int 2002;42:215–9. doi:10.2355/isijinternational.42.215.

[18] Tian Y, Zhao CY. A review of solar collectors and thermal energy storage in solar thermal applications. Appl Energy 2013;104:538–53. doi:10.1016/j.apenergy.2012.11.051.

[19] Stamatiou A, Obermeyer M, Fischer LJ, Schuetz P, Worlitschek J. Investigation of unbranched, saturated, carboxylic esters as phase change materials. Renew Energy 2017;108:401–9. doi:10.1016/j.renene.2017.02.056.

[20] Xu B, Li P, Chan C. Application of phase change materials for thermal energy storage in concentrated solar thermal power plants: A review to recent developments. Appl Energy 2015;160:286–307. doi:10.1016/j.apenergy.2015.09.016.

[21] Jacob R, Belusko M, Inés Fernández A, Cabeza LF, Saman W, Bruno F. Embodied energy and cost of high temperature thermal energy storage systems for use with concentrated solar power plants. Appl Energy 2016;180:586–97. doi:10.1016/j.apenergy.2016.08.027.

[22] Huang X, Alva G, Jia Y, Fang G. Morphological characterization and applications of phase change materials in thermal energy storage: A review. Renew Sustain Energy Rev 2017;72:128–45. doi:10.1016/j.rser.2017.01.048.

[23] Kenisarin MM. High-temperature phase change materials for thermal energy storage. Renew Sustain Energy Rev 2010;14:955–70. doi:10.1016/j.rser.2009.11.011.

[24] Agyenim F, Hewitt N, Eames P, Smyth M. A review of materials, heat transfer and phase change problem formulation for latent heat thermal energy storage systems (LHTESS). Renew Sustain Energy Rev 2010;14:615–28. doi:10.1016/j.rser.2009.10.015.

[25] Zhang X, Wen R, Huang Z, Tang C, Huang Y, Liu Y, et al. Enhancement of thermal conductivity by the introduction of carbon nanotubes as a filler in paraffin/expanded perlite form-stable phase-change materials. Energy Build 2017;149:463–70. doi:10.1016/j.enbuild.2017.05.037.

[26] Velraj R, Seeniraj RV, Hafner B, Faber C, Schwarzer K. Heat Transfer Enhancement in a Latent Heat Storage System. Sol Energy 1999;65:171–80. doi:10.1016/S0038-092X(98)00128-5.

[27] Liu M, Saman W, Bruno F. Review on storage materials and thermal performance enhancement techniques for high temperature phase change thermal storage systems. Renew Sustain Energy Rev 2012;16:2118–32. doi:10.1016/j.rser.2012.01.020.

[28] Regin a. F, Solanki SC, Saini JS. Heat transfer characteristics of thermal energy storage system using PCM capsules: A review. Renew Sustain Energy Rev 2008;12:2438–58. doi:10.1016/j.rser.2007.06.009.

[29] Zalba B, Marín JM, Cabeza LF, Mehling H. Review on thermal energy storage with phase change: materials, heat transfer analysis and applications. Appl Therm Eng 2003;23:251–83. doi:10.1016/S1359-4311(02)00192-8.

[30] Kumaresan V, Velraj R, Das SK. The effect of carbon nanotubes in enhancing the thermal transport properties of PCM during solidification. Heat Mass Transf Und Stoffuebertragung 2012;48:1345–55. doi:10.1007/s00231-012-0980-3.

[31] Xiao X, Zhang P, Li M. Thermal characterization of nitrates and nitrates/expanded graphite mixture phase change materials for solar energy storage. Energy Convers Manag 2013;73:86–94. doi:10.1016/j.enconman.2013.04.007.

[32] Sari A, Alkan C, Karaipekli A, Uzun O. Microencapsulated n-octacosane as phase change material for thermal energy storage. Sol Energy 2009;83:1757–63. doi:10.1016/j.solener.2009.05.008.

[33] Hawlader MN a, Uddin MS, Khin MM. Microencapsulated PCM thermal-energy storage system. Appl Energy 2003;74:195–202. doi:10.1016/S0306-2619(02)00146-0.

[34] Alam TE, Dhau J, Goswami DY, Rahman MM, Stefankos E. Experimental Investigation of a Packed-Bed Latent Heat Thermal Storage System with Encapsulated Phase Change Material. IMECE2014 2014:1–6.

[35] Bellan S, Alam TE, González-Aguilar J, Romero M, Rahman MM, Goswami DY, et al. Numerical and experimental studies on heat transfer characteristics of thermal energy storage system packed with molten salt PCM capsules. Appl Therm Eng 2015;90:970–9. doi:10.1016/j.applthermaleng.2015.07.056.

[36] Cho SH, Kim SW, Kim DY, Lee JH, Hur JM. Hot corrosion behavior of magnesia-stabilized ceramic material in a lithium molten salt. J Nucl Mater 2017;490:85–93. doi:10.1016/j.jnucmat.2017.04.012.

[37] Pitié F, Zhao C-Y, Cáceres G. Thermo-mechanical analysis of ceramic encapsulated phase-change-material (PCM) particles 2011;c:2117–24. doi:10.1039/c0ee00672f.

[38] Fukahori R, Nomura T, Zhu C, Sheng N, Okinaka N, Akiyama T. Thermal analysis of Al–Si alloys as high-temperature phase-change material and their corrosion properties with ceramic materials. Appl Energy 2016;163:1–8. doi:10.1016/j.apenergy.2015.10.164.

[39] Grigor'ev ON. CERAMICS AND CERMETS BASED ON NONOXIDE REFRACTORY COMPOUNDS. Powder Metall Met Ceram 2013;51:697–708.

[40] Bhardwaj A. Metallic Encapsulation for High Temperature (>500 °C) Thermal Energy Storage Applications. University of South Florida, 2015. doi:10.1017/CBO9781107415324.004.

[41] Zhang G, Li J, Chen Y, Xiang H, Ma B, Xu Z, et al. Encapsulation of copper-based phase change materials for high temperature thermal energy storage. Sol Energy Mater Sol Cells 2014;128:131–7. doi:10.1016/j.solmat.2014.05.012.

[42] Fernandes D, Pitié F, Cáceres G, Baeyens J. Thermal energy storage: "How previous findings determine current research priorities." Energy 2012;39:246–57. doi:10.1016/j.energy.2012.01.024.

[43] Fernandez AI, Martnez M, Segarra M, Martorell I, Cabeza LF. Selection of materials with potential in sensible thermal energy storage. Sol Energy Mater Sol Cells 2010;94:1723–9. doi:10.1016/j.solmat.2010.05.035.

[44] Nallusamy N, Sampath S, Velraj R. Experimental investigation on a combined sensible and latent heat storage system integrated with constant/varying (solar) heat sources. Renew Energy 2007;32:1206–27. doi:10.1016/j.renene.2006.04.015.

[45] Yang M, Yang X, Yang X, Ding J. Heat transfer enhancement and performance of the molten salt receiver of a solar power tower. Appl Energy 2010;87:2808–11. doi:10.1016/j.apenergy.2009.04.042.

[46] Kearney D, Herrmann U, Nava P, Kelly B, Mahoney R, Pacheco J, et al. Assessment of a molten salt heat transfer fluid in a parabolic trough solar field. J Sol Energy Eng 2003;125:170–6. doi:10.1115/1.1565087.

[47] Kearney D, Kelly B, Herrmann U, Cable R, Pacheco J, Mahoney R, et al. Engineering aspects of a molten salt heat transfer fluid in a trough solar field. Energy 2004;29:861–70. doi:10.1016/S0360-5442(03)00191-9.

[48] Domanski, Roman, Fellah G. Thermoeconomic Analysis of Sensible Heat, Thermal Energy Storage Systems. Appl Therm Eng 1998;18:693–704.

[49] Brosseau D, Edgar M, Kelton JW, Chisman K, Ray D, Emms B. Testing of Thermocline Filler Materials and Molten-Salt Heat Transfer Fluids for Thermal Energy Storage Systems in Parabolic Trough Power Plants. Sol Energy 2004;127:587–95. doi:10.1115/ISEC2004-65144.

[50] De Jong AJ, Van Vliet L, Hoegaerts C, Roelands M, Cuypers R. Thermochemical Heat Storage - From Reaction Storage Density to System Storage Density. Energy Procedia 2016;91:128–37. doi:10.1016/j.egypro.2016.06.187.

[51] Agrafiotis C, Becker A, Roeb M, Sattler C. Exploitation of thermochemical cycles based on solid oxide redox systems for thermochemical storage of solar heat. Part 5: Testing of porous ceramic honeycomb and foam cascades based on cobalt and manganese oxides for hybrid sensible/thermochemical heat s. Sol Energy 2016;139:676–94. doi:10.1016/j.solener.2016.09.013.

[52] Gil A, Medrano M, Martorell I, Lázaro A, Dolado P, Zalba B, et al. State of the art on high temperature thermal energy storage for power generation. Part 1—Concepts, materials and modellization. Renew Sustain Energy Rev 2010;14:31–55. doi:10.1016/j.rser.2009.07.035.

[53] Liu L, Su D, Tang Y, Fang G. Thermal conductivity enhancement of phase change materials for thermal energy storage: A review. Renew Sustain Energy Rev 2016;62:305–17. doi:10.1016/j.rser.2016.04.057.

[54] Farid MM, Khudhair AM, Razack SAK, Al-Hallaj S. A review on phase change energy storage: Materials and applications. Energy Convers Manag 2004;45:1597–615. doi:10.1016/j.enconman.2003.09.015.

[55] Chen C, Wang L, Huang Y. Morphology and thermal properties of electrospun fatty acids/polyethylene terephthalate composite fibers as novel form-stable phase change materials. Sol Energy Mater Sol Cells 2008;92:1382–7. doi:10.1016/j.solmat.2008.05.013.

[56] Liu H, Awbi HB. Performance of phase change material boards under natural convection. Build Environ 2009;44:1788–93. doi:10.1016/j.buildenv.2008.12.002.

[57] Bruno F, Belusko M, Liu M, Tay NHS. 9 – Using solid-liquid phase change materials (PCMs) in thermal energy storage systems. Woodhead Publishing Limited; 2015. doi:10.1533/9781782420965.2.201.

[58] Zalba B, Marín JM, Cabeza LF, Mehling H. Review on thermal energy storage with phase change: materials, heat transfer analysis and applications. Appl Therm Eng 2003;23:251–83. doi:10.1016/S1359-4311(02)00192-8.

[59] Goswami DY, Jotshi CK, Olszewski M. Analysis Of Thermal Energy Storage In Cylindrical PCM Capsules Exbedded In A Metal Matrix. Proc. 25th Intersoc. Energy Convers. Eng. Conf., vol. 4, IEEE; n.d., p. 257–62. doi:10.1109/IECEC.1990.716498.

[60] Wickramaratne C, Moloney F, Pirasaci T, Kamal R, Goswami DY, Stefanakos E, et al. Experimental Study on Thermal Storage Performance of Cylindrically Encapsulated PCM in a Cylindrical Storage Tank With Axial Flow. ASME 2016 Power Conf., ASME; 2016, p. V001T08A014. doi:10.1115/POWER2016-59427.

[61] Silva PD, Gonçalves LC, Pires L. Transient behaviour of a latent-heat thermal-energy store: Numerical and experimental studies. Appl Energy 2002;73:83–98. doi:10.1016/S0306-2619(02)00060-0.

[62] Adine HA, El Qarnia H. Numerical analysis of the thermal behaviour of a shell-and-tube heat storage unit using phase change materials. Appl Math Model 2009;33:2132–44. doi:10.1016/j.apm.2008.05.016.

[63] Zhao D, Tan G. Numerical analysis of a shell-and-tube latent heat storage unit with fins for air-conditioning application. Appl Energy 2015;138:381–92. doi:10.1016/j.apenergy.2014.10.051.

[64] Lacroix M. Study of the heat transfer behavior of a latent heat thermal energy storage unit with a finned tube. Int J Heat Mass Transf 1993;36:2083–92. doi:10.1016/S0017-9310(05)80139-5.

[65] Gong Z, Majumdar A. Finite-element analysis of cyclic heat transfer in a shell-and-tube latent heat energy storage exchanger. Appl Therm Eng 1997;17:583–91. doi:10.1016/S1359-4311(96)00054-3.

[66] Jegadheeswaran S, Pohekar SD. Performance enhancement in latent heat thermal storage system: A review. Renew Sustain Energy Rev 2009;13:2225–44. doi:10.1016/j.rser.2009.06.024.

[67] Ibrahim NI, Al-Sulaiman FA, Rahman S, Yilbas BS, Sahin AZ. Heat transfer enhancement of phase change materials for thermal energy storage applications: A critical review. Renew Sustain Energy Rev 2017;74:26–50. doi:10.1016/j.rser.2017.01.169.

[68] Incropera FP, DeWitt DP, Bergman TL, Lavine AS. Introduction to Conduction. Fundam Heat Mass Transf 2007:997. doi:10.1016/j.applthermaleng.2011.03.022.

[69] Velraj R, Seeniraj R V., Hafner B, Faber C, Schwarzer K. Experimental analysis and numerical modelling of inward solidification on a finned vertical tube for a latent heat storage unit. Sol Energy 1997;60:281–90. doi:10.1016/S0038-092X(96)00167-3.

[70] Stritih U. An experimental study of enhanced heat transfer in rectangular PCM thermal storage. Int J Heat Mass Transf 2004;47:2841–7. doi:10.1016/j.ijheatmasstransfer.2004.02.001.

[71] Hosseinizadeh SF, Tan FL, Moosania SM. Experimental and numerical studies on performance of PCM-based heat sink with different configurations of internal fins. Appl. Therm. Eng., vol. 31, Pergamon; 2011, p. 3827–38. doi:10.1016/j.applthermaleng.2011.07.031.

[72] Rathod MK, Banerjee J. Thermal performance enhancement of shell and tube Latent Heat Storage Unit using longitudinal fins. Appl Therm Eng 2015;75:1084–92. doi:10.1016/j.applthermaleng.2014.10.074.

[73] Rahimi M, Ranjbar AA, Ganji DD, Sedighi K, Hosseini MJ, Bahrampoury R. Analysis of geometrical and operational parameters of PCM in a fin and tube heat exchanger. Int Commun Heat Mass Transf 2014;53:109–15. doi:10.1016/j.icheatmasstransfer.2014.02.025.

[74] Al-Abidi AA, Mat S, Sopian K, Sulaiman MY, Mohammad AT. Internal and external fin heat transfer enhancement technique for latent heat thermal energy storage in triplex tube heat exchangers. Appl Therm Eng 2013;53:147–56. doi:10.1016/j.applthermaleng.2013.01.011.

[75] Al-Abidi AA, Mat S, Sopian K, Sulaiman MY, Mohammad AT. Numerical study of PCM solidification in a triplex tube heat exchanger with internal and external fins. Int J Heat Mass Transf 2013;61:684–95. doi:10.1016/j.ijheatmasstransfer.2013.02.030.

[76] Mat S, Al-Abidi AA, Sopian K, Sulaiman MY, Mohammad AT. Enhance heat transfer for PCM melting in triplex tube with internal-external fins. Energy Convers Manag 2013;74:223–36. doi:10.1016/j.enconman.2013.05.003.

[77] Choi JC, Kim SD, Han GY. Heat transfer characteristics in low-temperature latent heat storage systems using salt-hydrates at heat recovery stage. Sol Energy Mater Sol Cells 1996;40:71–87. doi:10.1016/0927-0248(95)00084-4.

[78] Erek A, Ilken Z, Acar MA. Experimental and numerical investigation of thermal energy storage with a finned tube. Int J Energy Res 2005;29:283–301. doi:10.1002/er.1057.

[79] Agyenim F, Eames P, Smyth M. A comparison of heat transfer enhancement in a medium temperature thermal energy storage heat exchanger using fins. Sol Energy 2009;83:1509–20. doi:10.1016/j.solener.2009.04.007.

[80] Liu Z, Sun X, Ma C. Experimental investigations on the characteristics of melting processes of stearic acid in an annulus and its thermal conductivity enhancement by fins. Energy Convers Manag 2005;46:959–69. doi:10.1016/j.enconman.2004.05.012.

[81] Shabgard H, Bergman TL, Sharifi N, Faghri A. High temperature latent heat thermal energy storage using heat pipes. Int J Heat Mass Transf 2010;53:2979–88. doi:10.1016/j.ijheatmasstransfer.2010.03.035.

[82] Nithyanandam K, Pitchumani R. Computational studies on a latent thermal energy storage system with integral heat pipes for concentrating solar power. Appl Energy 2013;103:400–15. doi:10.1016/j.apenergy.2012.09.056.

[83] Shabgard H, Robak CW, Bergman TL, Faghri A. Heat transfer and exergy analysis of cascaded latent heat storage with gravity-assisted heat pipes for concentrating solar power applications. Sol Energy 2012;86:816–30. doi:10.1016/j.solener.2011.12.008.

[84] Robak CW, Bergman TL, Faghri A. Enhancement of latent heat energy storage using embedded heat pipes. Int J Heat Mass Transf 2011;54:3476–84. doi:10.1016/j.ijheatmasstransfer.2011.03.038.

[85] Shabgard H, Allen MJ, Sharifi N, Benn SP, Faghri A, Bergman TL. Heat pipe heat exchangers and heat sinks: Opportunities, challenges, applications, analysis, and state of the art. Int J Heat Mass Transf 2015;89:138–58. doi:10.1016/j.ijheatmasstransfer.2015.05.020.

[86] Hu BW, Wang Q, Liu ZH. Fundamental research on the gravity assisted heat pipe thermal storage unit (GAHP-TSU) with porous phase change materials (PCMs) for medium temperature applications. Energy Convers Manag 2015;89:376–86. doi:10.1016/j.enconman.2014.10.017.

[87] Sharifi N, Wang S, Bergman TL, Faghri A. Heat pipe-assisted melting of a phase change material. Int J Heat Mass Transf 2012;55:3458–69. doi:10.1016/j.ijheatmasstransfer.2012.03.023.

[88] Zheng Y. Thermal energy storage with encapsulated phase change materials for high temperature applications 2015:189.

[89] Gong ZX, Mujumdar AS. Cyclic heat transfer in a novel storage unit of multiple phase change materials. Appl Therm Eng 1996;16:807–15. doi:10.1016/1359-4311(95)00088-7.

[90] Cui H, Yuan X, Hou X. Thermal performance analysis for a heat receiver using multiple phase change materials. Appl Therm Eng 2003;23:2353–61. doi:10.1016/S1359-4311(03)00210-2.

[91] Fang M, Chen G. Effects of different multiple PCMs on the performance of a latent thermal energy storage system. Appl Therm Eng 2007;27:994–1000. doi:10.1016/j.applthermaleng.2006.08.001.

[92] Mosaffa AH, Infante Ferreira CA, Talati F, Rosen MA. Thermal performance of a multiple PCM thermal storage unit for free cooling. Energy Convers Manag 2013;67:1–7. doi:10.1016/j.enconman.2012.10.018.

[93] Mosaffa AH, Garousi Farshi L, Infante Ferreira CA, Rosen MA. Energy and exergy evaluation of a multiple-PCM thermal storage unit for free cooling applications. Renew Energy 2014;68:452–8. doi:10.1016/j.renene.2014.02.025.

[94] Peiró G, Gasia J, Miró L, Cabeza LF. Experimental evaluation at pilot plant scale of multiple PCMs (cascaded) vs. single PCM configuration for thermal energy storage. Renew Energy 2015;83:729–36. doi:10.1016/j.renene.2015.05.029.

[95] Farid MM, Kim Y, Kansawa A. Thermal Performance of a Heat Storage Module Using PCM's With Different Melting Temperature: Experimental. J Sol Energy Eng 1990;112:125. doi:10.1115/1.2929644.

[96] Myers PD, Yogi Goswami D, Stefanakos E. Molten Salt Spectroscopy for Quantification of Radiative Absorption in Novel Metal Chloride-Enhanced Thermal Storage Media. J Sol Energy Eng 2015;137:41002. doi:10.1115/1.4029934.

[97] Cárdenas B, León N. High temperature latent heat thermal energy storage: Phase change materials, design considerations and performance enhancement techniques. Renew Sustain Energy Rev 2013;27:724–37. doi:10.1016/j.rser.2013.07.028.

[98] Mettawee EBS, Assassa GMR. Thermal conductivity enhancement in a latent heat storage system. Sol Energy 2007;81:839–45. doi:10.1016/j.solener.2006.11.009.

[99] Ho CJ, Gao JY. An experimental study on melting heat transfer of paraffin dispersed with Al2O3 nanoparticles in a vertical enclosure. Int J Heat Mass Transf 2013;62:2–8. doi:10.1016/j.ijheatmasstransfer.2013.02.065.

[100] Motahar S, Nikkam N, Alemrajabi AA, Khodabandeh R, Toprak MS, Muhammed M. Experimental investigation on thermal and rheological properties of n-octadecane with dispersed TiO2 nanoparticles. Int Commun Heat Mass Transf 2014;59:68–74. doi:10.1016/j.icheatmasstransfer.2014.10.016.

[101] Cui Y, Liu C, Hu S, Yu X. The experimental exploration of carbon nanofiber and carbon nanotube additives on thermal behavior of phase change materials. Sol Energy Mater Sol Cells 2011;95:1208–12. doi:10.1016/j.solmat.2011.01.021.

[102] Zhang N, Yuan Y, Yuan Y, Cao X, Yang X. Effect of carbon nanotubes on the thermal behavior of palmitic-stearic acid eutectic mixtures as phase change materials for energy storage. Sol Energy 2014;110:64–70. doi:10.1016/j.solener.2014.09.003.

[103] Shaikh S, Lafdi K, Hallinan K. Carbon nanoadditives to enhance latent energy storage of phase change materials. J Appl Phys 2008;103:94302. doi:10.1063/1.2903538.

[104] Wang J, Xie H, Xin Z. Thermal properties of paraffin based composites containing multi-walled carbon nanotubes. Thermochim Acta 2009;488:39–42. doi:10.1016/j.tca.2009.01.022.

[105] Teng TP, Cheng CM, Cheng CP. Performance assessment of heat storage by phase change materials containing MWCNTs and graphite. Appl. Therm. Eng., vol. 50, Pergamon; 2013, p. 637–44. doi:10.1016/j.applthermaleng.2012.07.002.

[106] Fan LW, Fang X, Wang X, Zeng Y, Xiao YQ, Yu ZT, et al. Effects of various carbon nanofillers on the thermal conductivity and energy storage properties of paraffin-based nanocomposite phase change materials. Appl Energy 2013;110:163–72. doi:10.1016/j.apenergy.2013.04.043.

[107] Harish S, Orejon D, Takata Y, Kohno M. Thermal conductivity enhancement of lauric acid phase change nanocomposite with graphene nanoplatelets. Appl Therm Eng 2015;80:205–11. doi:10.1016/j.applthermaleng.2015.01.056.

[108] Zeng J-L, Zhu F-R, Yu S-B, Zhu L, Cao Z, Sun L-X, et al. Effects of copper nanowires on the properties of an organic phase change material. Sol Energy Mater Sol Cells 2012;105:174–8. doi:10.1016/j.solmat.2012.06.013.

[109] Myers PD, Alam TE, Kamal R, Goswami DY, Stefanakos E. Nitrate salts doped with CuO nanoparticles for thermal energy storage with improved heat transfer. Appl Energy 2016;165:225–33. doi:10.1016/j.apenergy.2015.11.045.

[110] Gasia J, Miró L, Cabeza LF. Materials and system requirements of high temperature thermal energy storage systems: A review. Part 2: Thermal conductivity enhancement techniques. Renew Sustain Energy Rev 2016;60:1584–601. doi:10.1016/j.rser.2016.03.019.

[111] Chieruzzi M, Cerritelli GF, Miliozzi A, Kenny JM, Torre L. Heat capacity of nanofluids for solar energy storage produced by dispersing oxide nanoparticles in nitrate salt mixture directly at high temperature. Sol Energy Mater Sol Cells 2017;167:60–9. doi:10.1016/j.solmat.2017.04.011.

[112] Luo Y, Du X, Awad A, Wen D. Thermal energy storage enhancement of a binary molten salt via in-situ produced nanoparticles. Int J Heat Mass Transf 2017;104:658–64. doi:10.1016/j.ijheatmasstransfer.2016.09.004.

[113] Mahdi JM, Nsofor EC. Melting of PCM with nanoparticles in a triplex-tube thermal energy storage system. vol. 122, Amer. Soc. Heating, Ref. Air-Conditoning Eng. Inc.; 2016, p. 215–24.

[114] Myers PD. Additives for Heat Transfer Enhancement in High Temperature Thermal Energy Storage Media: Selection and Characterization. 2015.

[115] Chen J, Yang D, Jiang J, Ma A, Song D. Research Progress of Phase Change Materials (PCMs) Embedded with Metal Foam (a Review). Procedia Mater Sci 2014;4:389–94. doi:10.1016/j.mspro.2014.07.579.

[116] Srivatsa PVSS, Baby R, Balaji C. Numerical Investigation of PCM Based Heat Sinks with Embedded Metal Foam/Crossed Plate Fins. Numer Heat Transf Part A Appl 2014;66:1131–53. doi:10.1080/10407782.2014.894371.

[117] Tian Y, Zhao CY. A numerical investigation of heat transfer in phase change materials (PCMs) embedded in porous metals. Energy 2011;36:5539–46. doi:10.1016/j.energy.2011.07.019.

[118] Wang W, Yang X, Fang Y, Ding J, Yan J. Enhanced thermal conductivity and thermal performance of form-stable composite phase change materials by using β-Aluminum nitride. Appl Energy 2009;86:1196–200. doi:10.1016/j.apenergy.2008.10.020.

[119] Mills A, Farid M, Selman JR, Al-Hallaj S. Thermal conductivity enhancement of phase change materials using a graphite matrix. Appl Therm Eng 2006;26:1652–61. doi:10.1016/j.applthermaleng.2005.11.022.

[120] Fleming E, Wen S, Shi L, Da Silva AK. Experimental and theoretical analysis of an aluminum foam enhanced phase change thermal storage unit. Int J Heat Mass Transf 2015;82:273–81. doi:10.1016/j.ijheatmasstransfer.2014.11.022.

[121] Dukhan N, Bodke S. An improved PCM heat storage technology utilizing metal foam. 2010 12th IEEE Intersoc. Conf. Therm. Thermomechanical Phenom. Electron. Syst. ITherm 2010, IEEE; 2010, p. 1–7. doi:10.1109/ITHERM.2010.5501364.

[122] Zhong Y, Guo Q, Li S, Shi J, Liu L. Heat transfer enhancement of paraffin wax using graphite foam for thermal energy storage. Sol Energy Mater Sol Cells 2010;94:1011–4. doi:10.1016/j.solmat.2010.02.004.

[123] Sari A, Karaipekli A. Thermal conductivity and latent heat thermal energy storage characteristics of paraffin/expanded graphite composite as phase change material. Appl Therm Eng 2007;27:1271–7. doi:10.1016/j.applthermaleng.2006.11.004.

[124] Zhong Y, Li S, Wei X, Liu Z, Guo Q, Shi J, et al. Heat transfer enhancement of paraffin wax using compressed expanded natural graphite for thermal energy storage. Carbon N Y 2010;48:300–4. doi:10.1016/j.carbon.2009.09.033.

[125] Siahpush A, O'Brien J, Crepeau J. Phase Change Heat Transfer Enhancement Using Copper Porous Foam. J Heat Transfer 2008;130:82301. doi:10.1115/1.2928010.

[126] Wu ZG, Zhao CY. Experimental investigations of porous materials in high temperature thermal energy storage systems. Sol Energy 2011;85:1371–80. doi:10.1016/j.solener.2011.03.021.

[127] Zhao CY, Wu ZG. Heat transfer enhancement of high temperature thermal energy storage using metal foams and expanded graphite. Sol Energy Mater Sol Cells 2011;95:636–43. doi:10.1016/j.solmat.2010.09.032.

[128] Zhong L, Zhang X, Luan Y, Wang G, Feng Y, Feng D. Preparation and thermal properties of porous heterogeneous composite phase change materials based on molten salts/expanded graphite. Sol Energy 2014;107:63–73. doi:10.1016/j.solener.2014.05.019.

[129] Zhang P, Xiao X, Meng ZN, Li M. Heat transfer characteristics of a molten-salt thermal energy storage unit with and without heat transfer enhancement. Appl Energy 2015;137:758–72. doi:10.1016/j.apenergy.2014.10.004.

[130] Fukai J, Kanou M, Kodama Y, Miyatake O. Thermal conductivity enhancement of energy storage media using carbon fibers. Energy Convers Manag 2000;41:1543–56. doi:10.1016/S0196-8904(99)00166-1.

[131] Hamada Y, Ohtsu W, Fukai J. Thermal response in thermal energy storage material around heat transfer tubes: Effect of additives on heat transfer rates. Sol Energy 2003;75:317–28. doi:10.1016/j.solener.2003.07.028.

[132] Khalifa A, Tan L, Date A, Akbarzadeh A. A numerical and experimental study of solidification around axially finned heat pipes for high temperature latent heat thermal energy storage units. Appl Therm Eng 2014;70:609–19. doi:10.1016/j.applthermaleng.2014.05.080.

[133] Khalifa A, Tan L, Date A, Akbarzadeh A. Performance of suspended finned heat pipes in high-temperature latent heat thermal energy storage. Appl Therm Eng 2015;81:242–52. doi:10.1016/j.applthermaleng.2015.02.030.

[134] Sharifi N, Bergman TL, Allen MJ, Faghri A. Melting and solidification enhancement using a combined heat pipe, foil approach. Int J Heat Mass Transf 2014;78:930–41. doi:10.1016/j.ijheatmasstransfer.2014.07.054.

[135] Xie YQ, Song J, Chi PT, Yu JZ. Performance Enhancement of Phase Change Thermal Energy Storage Unit Using Fin and Copper Foam. Appl Mech Mater 2012;260–261:137–41. doi:10.4028/www.scientific.net/AMM.260-261.137.

[136] Allen MJ, Sharifi N, Faghri A, Bergman TL. Effect of inclination angle during melting and solidification of a phase change material using a combined heat pipe-metal foam or foil configuration. Int J Heat Mass Transf 2015;80:767–80. doi:10.1016/j.ijheatmasstransfer.2014.09.071.

[137] Zhang HL, Baeyens J, Degrève J, Cáceres G, Segal R, Pitié F. Latent heat storage with tubular-encapsulated phase change materials (PCMs). Energy 2014;76:66–72. doi:10.1016/j.energy.2014.03.067.

[138] Salunkhe PB, Shembekar PS. A review on effect of phase change material encapsulation on the thermal performance of a system. Renew Sustain Energy Rev 2012;16:5603–16. doi:10.1016/j.rser.2012.05.037.

[139] Stekli J, Irwin L, Pitchumani R. Technical Challenges and Opportunities for Concentrating Solar Power With Thermal Energy Storage. J Therm Sci Eng Appl 2013;5:21011. doi:10.1115/1.4024143.

[140] Liu C, Rao Z, Zhao J, Huo Y, Li Y. Review on nanoencapsulated phase change materials: Preparation, characterization and heat transfer enhancement. Nano Energy 2015;13:814–26. doi:10.1016/j.nanoen.2015.02.016.

[141] Lane GA. Solar heat storage : latent heat materials. CRC Press; 1983.

[142] Fuensanta M, Paiphansiri U, Romero-Sánchez MD, Guillem C, López-Buendía ÁM, Landfester K. Thermal properties of a novel nanoencapsulated phase change material for thermal energy storage. Thermochim Acta 2013;565:95–101. doi:10.1016/j.tca.2013.04.028.

[143] Tumirah K, Hussein MZ, Zulkarnain Z, Rafeadah R. Nano-encapsulated organic phase change material based on copolymer nanocomposites for thermal energy storage. Energy 2014;66:881–90. doi:10.1016/j.energy.2014.01.033.

[144] Fang Y, Yu H, Wan W, Gao X, Zhang Z. Preparation and thermal performance of polystyrene/n-tetradecane composite nanoencapsulated cold energy storage phase change materials. Energy Convers Manag 2013;76:430–6. doi:10.1016/j.enconman.2013.07.060.

[145] Fang Y, Liu X, Liang X, Liu H, Gao X, Zhang Z. Ultrasonic synthesis and characterization of polystyrene/n-dotriacontane composite nanoencapsulated phase change material for thermal energy storage. Appl Energy 2014;132:551–6. doi:10.1016/j.apenergy.2014.06.056.

[146] Fukahori R, Nomura T, Zhu C, Sheng N, Okinaka N, Akiyama T. Macro-encapsulation of metallic phase change material using cylindrical-type ceramic containers for high-temperature thermal energy storage. Appl Energy 2016;170:324–8. doi:10.1016/j.apenergy.2016.02.106.

[147] Wei J, Kawaguchi Y, Hirano S, Takeuchi H. Study on a PCM heat storage system for rapid heat supply 2005. doi:10.1016/j.applthermaleng.2005.02.014.

[148] Zheng Y, Zhao W, Sabol JC, Tuzla K, Neti S, Oztekin A, et al. Encapsulated phase change materials for energy storage – Characterization by calorimetry. Sol Energy 2013;87:117–26. doi:10.1016/j.solener.2012.10.003.

[149] Kenisarin M, Mahkamov K. Solar energy storage using phase change materials. Renew Sustain Energy Rev 2007;11:1913–65. doi:10.1016/j.rser.2006.05.005.

[150] Pielichowska K, Pielichowski K. Phase change materials for thermal energy storage. Prog Mater Sci 2014;65:67–123. doi:10.1016/j.pmatsci.2014.03.005.

[151] Hoshi A, Mills DR, Bittar A, Saitoh TS. Screening of high melting point phase change materials (PCM) in solar thermal concentrating technology based on CLFR. Sol Energy 2005;79:332–9. doi:10.1016/j.solener.2004.04.023.

[152] Myers PD, Goswami DY. Thermal energy storage using chloride salts and their eutectics. Appl Therm Eng 2016;109:889–900. doi:10.1016/j.applthermaleng.2016.07.046.

[153] Mohamed SA, Al-Sulaiman FA, Ibrahim NI, Zahir MH, Al-Ahmed A, Saidur R, et al. A review on current status and challenges of inorganic phase change materials for thermal energy storage systems. Renew Sustain Energy Rev 2017;70:1072–89. doi:10.1016/j.rser.2016.12.012.

[154] Burst JF. The application of clay minerals in ceramics. Appl Clay Sci 1991;5:421–43. doi:10.1016/0169-1317(91)90016-3.

[155] Robelin C, Chartrand P, Pelton AD. Thermodynamic evaluation and optimization of the (NaNO3+KNO3+Na2SO4+K2SO4) system. J Chem Thermodyn 2015;83:12–26. doi:10.1016/j.jct.2014.10.024.

[156] Goswami DY, Jotshi CK, Olszewski M. Analysis Of Thermal Energy Storage In Cylindrical PCM Capsules Exbedded In A Metal Matrix. Proc 25th Intersoc Energy Convers Eng Conf 1990;4:257–62. doi:10.1109/IECEC.1990.716498.

[157] Saitoh T, Kato K. Experiment on melting in heat storage capsule with close contact and natural convection. Exp Therm Fluid Sci 1993;6:273–81. doi:10.1016/0894-1777(93)90068-T.

[158] Wang J, Ouyang Y, Chen G. Experimental study on charging processes of a cylindrical heat storage employing multiple-phase-change materials. Int J Energy Res 2001;25:439–47. doi:10.1002/er.695.

[159] Chen S-L, Chen C-L, Tin C-C, Lee T-S, Ke M-C. An experimental investigation of cold storage in an encapsulated thermal storage tank. Exp Therm Fluid Sci 2000;23:133–44. doi:10.1016/S0894-1777(00)00045-5.

[160] Regin AF, Solanki SC, Saini JS. Latent heat thermal energy storage using cylindrical capsule: Numerical and experimental investigations. Renew Energy 2006;31:2025–41. doi:DOI: 10.1016/j.renene.2005.10.011.

[161] Castell A, Solé C, Medrano M, Roca J, Cabeza LF, García D. Natural convection heat transfer coefficients in phase change material (PCM) modules with external vertical fins. Appl Therm Eng 2008;28:1676–86. doi:10.1016/j.applthermaleng.2007.11.004.

[162] Bareiss M, Beer H. Influence of natural convection on the melting process in a vertical cylindrical enclosure. Lett Heat Mass Transf 1980;7:329–38.

[163] Solomon GR, Velraj R. Analysis of the heat transfer mechanisms during energy storage in a Phase Change Material filled vertical finned cylindrical unit for free cooling application. Energy Convers Manag 2013;75:466–73. doi:10.1016/j.enconman.2013.06.044.

[164] Sridharan P. Aspect Ratio Effect on Melting and Solidification During Thermal Energy Storage. 2013.

[165] Shmueli H, Ziskind G, Letan R. Melting in a vertical cylindrical tube: Numerical investigation and comparison with experiments. Int J Heat Mass Transf 2010;53:4082–91. doi:10.1016/j.ijheatmasstransfer.2010.05.028.

[166] Jones BJ, Sun D, Krishnan S, Garimella S V. Experimental and numerical study of melting in a cylinder. Int J Heat Mass Transf 2006;49:2724–38. doi:10.1016/j.ijheatmasstransfer.2006.01.006.

[167] Shokouhmand H, Kamkari B. Experimental investigation on melting heat transfer characteristics of lauric acid in a rectangular thermal storage unit. Exp Therm Fluid Sci 2013;50:201–22. doi:10.1016/j.expthermflusci.2013.06.010.

[168] Papanicolaou E, Belessiotis V. Transient natural convection in a cylindrical enclosure at high Rayleigh. Int J Heat Mass Transf 2002;45:1425–44. doi:10.1016/S0017-9310(01)00258-7.

[169] Zivkovic B, Fujii I. Analysis of isothermal phase change of phase change material within rectangular and cylindrical containers. Sol Energy 2001;70:51–61. doi:10.1016/S0038-092X(00)00112-2.

[170] Farid M, Kim Y, Honda T, Kanzawa A. The Role of Natural Convection During Melting and Solidification of PCM in a Vertical Cylinder. Chem Eng Commun 1989;84:43–60. doi:10.1080/00986448908940334.

[171] Myers PD, Yogi Goswami D, Stefanakos E. Molten Salt Spectroscopy for Quantification of Radiative Absorption in Novel Metal Chloride-Enhanced Thermal Storage Media. J Sol Energy Eng 2015;137:41002. doi:10.1115/1.4029934.

[172] Myers PD. Additives for Heat Transfer Enhancement in High Temperature Thermal Energy Storage Media: Selection and Characterization. University of South Florida, 2015.

[173] Alam TE. Experimental Investigation of Encapsulated Phase Change Materials for Thermal Energy Storage. University of South Florida, 2015.

[174] Wheeler, Anthony J. ; Ganji AR. Introduction to engineering experimentation. 3rd ed. Prentice Hall; 2009.

[175] Pirasaci T, Goswami DY. Influence of design on performance of a latent heat storage system for a direct steam generation power plant. Appl Energy 2016;162:644–52. doi:10.1016/j.apenergy.2015.10.105.

[176] Moloney F, Wickramaratne C, Almatrafi E, Goswami DY, Stefanakos E, Guldiken R. Flow conditioning techniques for a bent pipe in a constrained latent heat storage system. ASME Int. Mech. Eng. Congr. Expo. Proc., vol. 7, 2016. doi:10.1115/IMECE201665730.

[177] Kalpakli A. Experimental study of turbulent flows through pipe bends. Stockholm, Sweden: 2012.

[178] Wendt G, Mickan B, Kramer R, Dopheide D. Systematic investigation of pipe flows and installation effects using laser Doppler anemometry—Part I. Profile measurements downstream of several pipe configurations and flow conditioners. Flow Meas Instrum 1996;7:141–9. doi:10.1016/S0955-5986(97)00003-4.

[179] Ahmadi A. Experimental Study of a New Flow Conditioner on Disturbed Flow in Orifice Plate Metering. J Fluids Eng 2009;131:51104. doi:10.1115/1.3114677.

[180] Spearman EP, Sattary JA, Reader-Harris MJ. Comparison of velocity and turbulence profiles downstream of perforated plate flow conditioners. Flow Meas Instrum 1996;7:181–99.

[181] Cheng Fluid Systems. CRV Flow Conditioning Technology 2015. http://www.chengfluid.com/flow_conditioner/crv®_flow_conditioner (accessed January 1, 2015).

[182] Gallagher JE, Beaty RE, Lanasa PJ. Flow conditioner for more accurate measurement of fluid flow. 5,495,872, 1996.

[183] Laribi B, Wauters P, Aichouni M. Comparative Study of Aerodynamic Behaviour of Three Flow Conditioners. Eur J Mech Environ Eng 2003;48.

[184] Laws EM, Ouazzane a. K. A further investigation into flow conditioner design yielding compact installations for orifice plate flow metering. Flow Meas Instrum 1995;6:187–99. doi:10.1016/0955-5986(95)00007-9.

[185] Laws EM. United States Patent - Flow Conditioner. 5,341,848, 1994.

[186] Manshoor B, Rosidee NF, Amir K. An Effect of Fractal Flow Conditioner Thickness on Turbulent Swirling Flow. Appl Mech Mater 2013;315:93–7. doi:10.4028/www.scientific.net/AMM.315.93.

[187] Ouazzane AK, Benhadj R. Flow conditioners design and their effects in reducing flow metering errors. Sens Rev 2002;22:223–31. doi:10.1108/02602280210433061.

[188] Schlüter T, Merzkirch W. PIV measurements of the time-averaged flow velocity downstream of flow conditioners in a pipeline. Flow Meas Instrum 1996;7:173–9. doi:10.1016/S0955-5986(96)00016-7.

[189] Spearman EP, Sattary J a., Reader-Harris MJ. A study of flow through a perforated-plate/orifice-meter package in two different pipe configurations using laser Doppler velocimetry. Flow Meas Instrum 1991;2:83–8. doi:10.1016/0955-5986(91)90015-J.

[190] Xiong W, Kalkühler K, Merzkirch W. Velocity and turbulence measurements downstream of flow conditioners. Flow Meas Instrum 2003;14:249–60. doi:10.1016/S0955-5986(03)00031-1.

[191] Shao Z. Numerical and experimental evaluation of flow through perforated plates. Rand Afrikaans University, 2001.

[192] Wei J, Kawaguchi Y, Hirano S, Takeuchi H. Study on a PCM heat storage system for rapid heat supply. Appl Therm Eng 2005;25:2903–20. doi:10.1016/j.applthermaleng.2005.02.014.

[193] Veerappan M, Kalaiselvam S, Iniyan S, Goic R. Phase change characteristic study of spherical PCMs in solar energy storage. Sol Energy 2009;83:1245–52. doi:10.1016/j.solener.2009.02.006.

[194] Ismail KAR, Henríquez JR. Solidification of pcm inside a spherical capsule. Energy Convers Manag 2000;41:173–87. doi:10.1016/S0196-8904(99)00101-6.

[195] Sattari H, Mohebbi A, Afsahi MM, Azimi Yancheshme A. Simulation par MFN du processus de fusion des matériaux à changement de phase dans une capsule sphérique. Int J Refrig 2017;73:209–18. doi:10.1016/j.ijrefrig.2016.09.007.

[196] Karthikeyan S, Velraj R. Numerical investigation of packed bed storage unit filled with PCM encapsulated spherical containers - A comparison between various mathematical models. Int J Therm Sci 2012;60:153–60. doi:10.1016/j.ijthermalsci.2012.05.010.

[197] Archibold AR, Rahman MM, Yogi Goswami D, Stefanakos EK. The effects of radiative heat transfer during the melting process of a high temperature phase change material confined in a spherical shell. Appl Energy 2015;138:675–84. doi:10.1016/j.apenergy.2014.10.086.

[198] Archibold AR, Gonzalez-Aguilar J, Rahman MM, Yogi Goswami D, Romero M, Stefanakos EK. The melting process of storage materials with relatively high phase change temperatures in partially filled spherical shells. Appl Energy 2014;116:243–52. doi:10.1016/j.apenergy.2013.11.048.

[199] Archibold AR, Rahman MM, Goswami DY, Stefanakos EK. Analysis of heat transfer and fluid flow during melting inside a spherical container for thermal energy storage. Appl Therm Eng 2014;64:396–407. doi:10.1016/j.applthermaleng.2013.12.016.

APPENDIX A: NOMENCLATURE

A.1 Acronyms

PCM	Phase change material
TES	Thermal energy storage
LHTES	Latent heat thermal energy storage
SHTES	Sensible heat thermal energy storage
EPCM	Encapsulated phase change material
HTF	Heat transfer fluid
HP	Heat pipe
TTHX	Triplex tube heat exchangers
EG	Expanded graphite
MWCNT	Multi-walled carbon nanotubes
GNP	Graphene nanoplatelets
FTIR	Fourier transform infrared spectroscopy
TGA	Thermogravimetric analysis
DSC	Differential scanning calorimetry
EDS	Energy Dispersive Spectroscopy
IR	Infrared Radiation
TIG	Tungsten inert gas
CFD	Computational fluid dynamics
MHI	Mitsubishi Heavy Industries
CRV	Cheng Rotation Vane
$NaNO_3$	Sodium nitrate.
KNO_3	Potassium nitrate
NaCl	Sodium chloride
KCl	Potassium chloride
Na_2SO_4	Sodium sulfate
Ch	Charge
DCh	Discharge
C_p	Specific Heat
E	Energy (kJ)
Ex	Exergy (kJ)
$\dot{m}$	Mass Flowrate (kg/s)
t	Time (s)
T	Temperature (K)

Wt	Weight
hrs	Hours
T_o	Ambient Temperature (K)
D	Diameter
I	Turbulence intensity
Re	Reynolds number
u	velocity (m/s)
U_{avg}	Average velocity (m/s)
X	Distance from pipe center along x-direction (m)
Y	Distance from pipe center along y-direction (m)

A.2 Greek Letters

η	Efficiency (%)
ρ	Density (kg/m3)
μ	Dynamic viscosity (kg/m-s)
σ_{random}	Random Error
$\sigma_{systematic}$	Systematic Error
ε	Void Fraction

A.3 Subscripts

i	Initial
f	Final
avg	Average

APPENDIX B: SUPPLEMENTAL INFORMATION

B.1 General Equations for Stress Calculations

$$\sigma_{axial} = (p_i r_i^2 - p_o r_o^2)/(r_o^2 - r_i^2) \quad (1)$$

$$\sigma_{hoop} = [(p_i r_i^2 - p_o r_o^2) / (r_o^2 - r_i^2)] - [r_i^2 r_o^2 (p_o - p_i) / (r^2 (r_o^2 - r_i^2))] \quad (2)$$

$$\sigma_{radial} = [(p_i r_i^2 - p_o r_o^2) / (r_o^2 - r_i^2)] + [r_i^2 r_o^2 (p_o - p_i) / (r^2 (r_o^2 - r_i^2))] \quad (3)$$

where,

σ_{axial} = stress in axial direction

σ_{hoop} = stress(hoop) in circumferential direction

σ_{radial} = stress in radial direction

p_i = internal pressure

p_o = external pressure

r_i = internal radius

r_o = external radius

r = radius to point in cylinder wall ($r_i < r < r_o$)

B.2 Stress Comparison of Cylindrical and Spherical Capsule

Table B.1 Stress calculation for cylindrical and spherical capsule

Outer diameter	**1.00**	**Inch**
Inner diameter	**0.88**	**Inch**
Cylinder Length	100	cm
Capsule Thickness	**0.15**	**cm**
Cylinder Outer radius	1.27	cm
Cylinder Inner Radius in cm	1.12	cm
Radius (inner)/thickness ratio	7.47	
Elastic limit (Yield stress)	**370**	**MPa**
Poisson's Ratio	0.29	
Tensile Strength, Ultimate	540	MPa
Density	7.87	g/cc
Modulus of Elasticity	200	GPa
Ouside Pressure(P-out)	**50.00**	**Mpa**
Inside pressure(P-in)	0.10	Mpa
R-out=	0.0127	m
R-in	0.0112	m
Maximum Stressv point	0.0112	m
Circumferencial(Hoop) stress - cylinder	**-449.10**	**Mpa**
Axial Stress - cylinder	**-224.60**	**Mpa**
Hoop stress in same Dia Sperical capsule	**-224.55**	**MPa**

B.3 Sealing Pressure Calculation

Table B.2 Sealing pressure calculation

	For PCM of NaCl	Amount	Unit
Initial	**Capsule inner Diameter**	**1.00**	Inch
	20050	2.54	cm
	Capsule Volume	8.58	cm^3
	Room temperature	25.00	C
	PCM density at room temperature	**2.13**	(g/cm³)
	Initial pressure	1.00	atm
	Density at melting temperature	**1.56**	(g/cm³)
	Maximum mass that can fill (0% void when in liquid)	13.35	g
	Necessary void	26.95%	
	Void space kept @ room temperature	**30.00%**	
	PCM Volume @ room temperature	6.01	cm^3
	Air volume @ room temperature	2.57	cm^3
	PCM mass in the capsule	**12.79**	g
Sealing	**PCM sealing temperature**	**25.00**	C
	Density at sealing temperature	**2.13**	(g/cm³)
	PCM volume at sealing	6.00	cm^3
	Ceramic capsule expansion	0.00	cm^3
	Total Capsule volume at sealing	8.58	cm^3
	Air volume at sealing	**2.58**	cm^3
Cycling	highest temperature(Cycling)	830.00	C
	Thermal expansion coefficient of ceramic	7.00E-07	/C (Alumina)**
	Ceramic capsule expansion	0.01	cm^3
	Total Capsule Volume @ highest temperature	**8.59**	cm^3
	PCM Volume at highest temperature	**8.22**	cm^3
	Air Volume at highest temperature	**0.37**	cm^3
	PCM volume increase	36.9%	
	Final Air volume	0.37	cm^3
	Total air volume reduction	85.5%	
	Gas Constnat(m)	0.2869	J/(g. K)
	Gas Constant(n)	8.3144598	J/(mol.K)
	Air mass initially	0.003051	g
	N_2 mass	0.002318	g
	O_2 mass	0.000732	g
	Air mass at sealing	0.003056	g
	Final Pressure	2593043.40	pa
		25.59	atm
		25.59	pv/t method

B.4 Additional Flow Conditioning Data

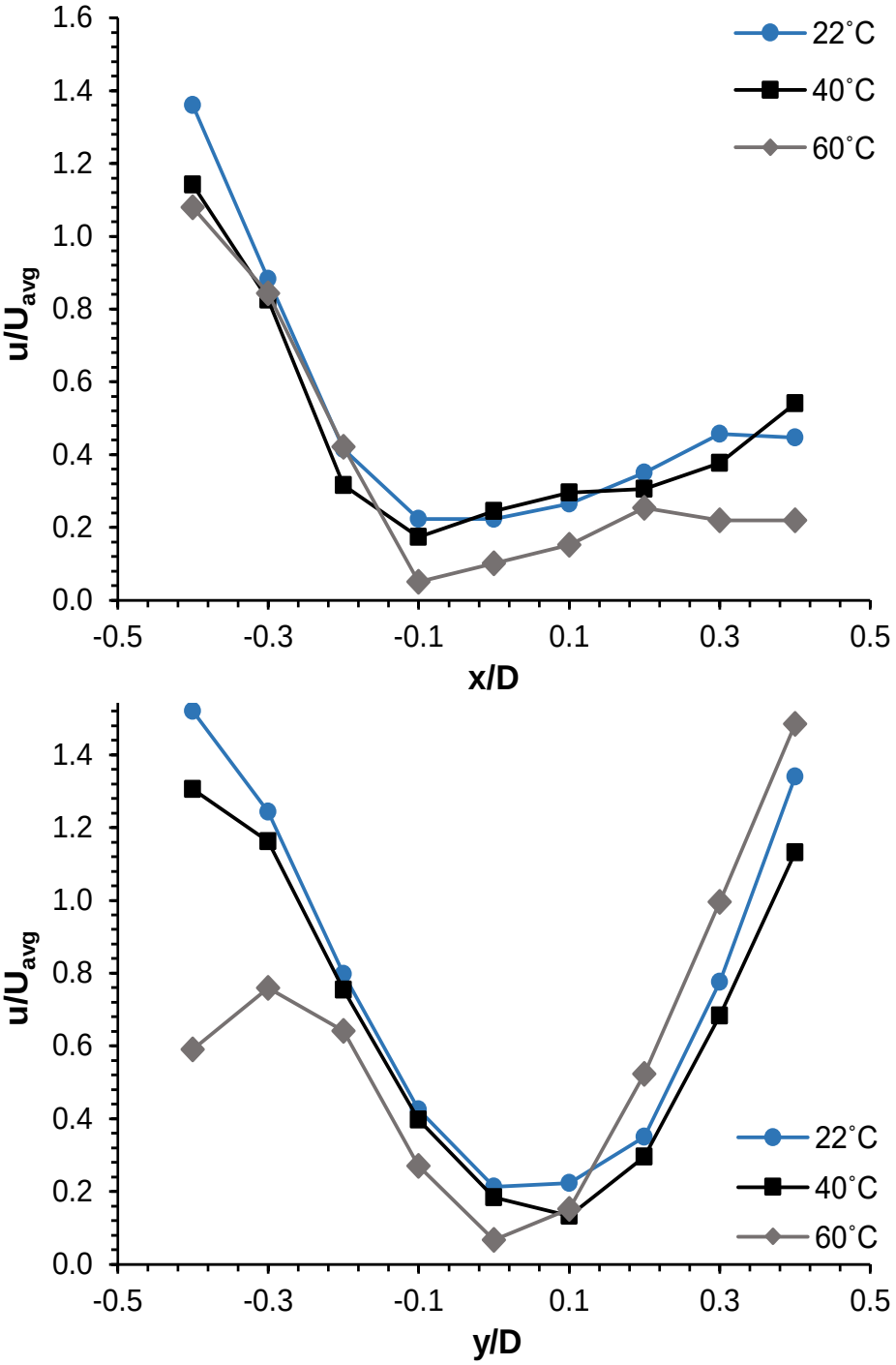

Figure B.1 Velocity profile for heated flow (x and y direction) with no corrections

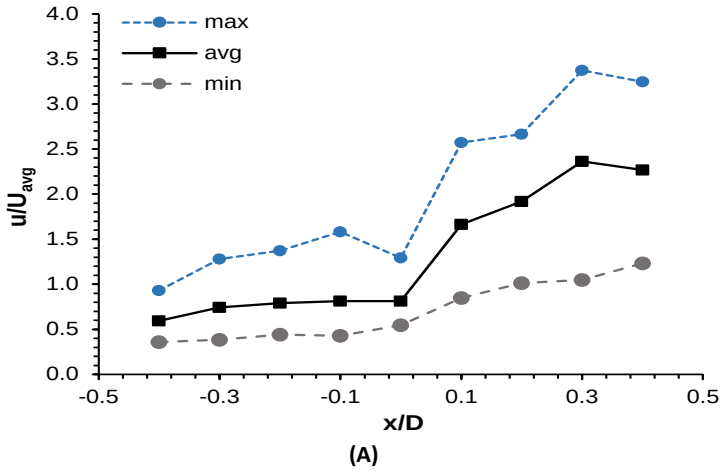

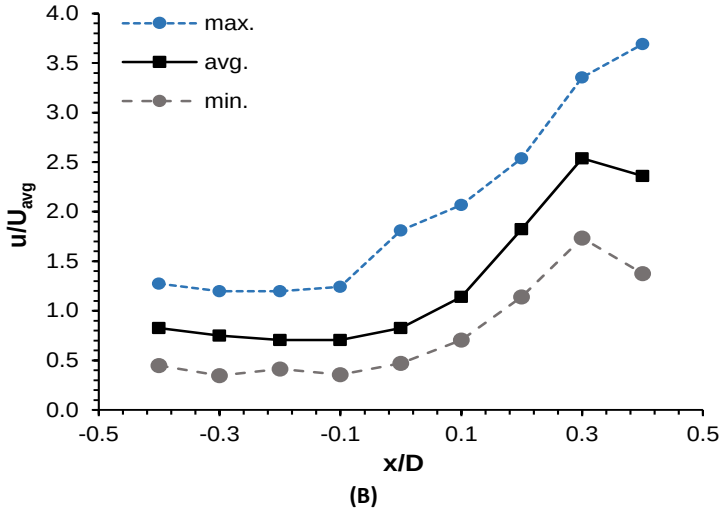

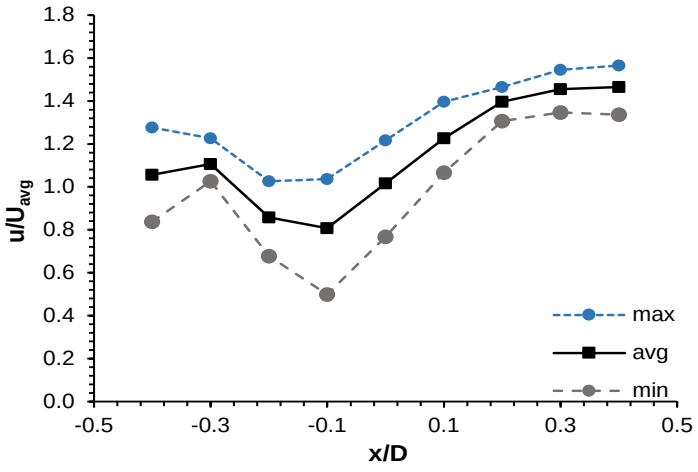

(C)

Figure B.2 Velocity profile in ambient conditions along x-direction (X/D) with: (A) Low graded porosity plate; (B) High graded porosity plate; (C) Twisted vane

APPENDIX C: COPYRIGHTS

This is the copyright permission given by Elsevier for figure 2.1 in section 2.2.1.

Order Completed

Thank you for your order.

This Agreement between Chatura Wickramratne ("You") and Elsevier ("Elsevier") consists of your license details and the terms and conditions provided by Elsevier and Copyright Clearance Center.

Your confirmation email will contain your order number for future reference.

Printable details.

License Number	4192010958122
License date	Sep 18, 2017
Licensed Content Publisher	Elsevier
Licensed Content Publication	Renewable and Sustainable Energy Reviews
Licensed Content Title	A review of materials, heat transfer and phase change problem formulation for latent heat thermal energy storage systems (LHTESS)
Licensed Content Author	Francis Agyenim,Neil Hewitt,Philip Eames,Mervyn Smyth
Licensed Content Date	Feb 1, 2010
Licensed Content Volume	14
Licensed Content Issue	2
Licensed Content Pages	14
Type of Use	reuse in a thesis/dissertation
Portion	figures/tables/illustrations
Number of figures/tables/illustrations	1
Format	both print and electronic
Are you the author of this Elsevier article?	No
Will you be translating?	No
Original figure numbers	Fig. 3. Heat transfer enhancement methods employed in phase change material research.
Title of your thesis/dissertation	High Temperature Thermal Energy Storage
Expected completion date	Dec 2017
Estimated size (number of pages)	100
Requestor Location	Chatura Wickramratne 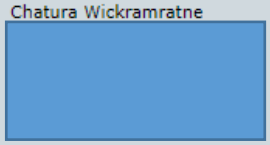
Publisher Tax ID	98-0397604
Total	0.00 USD

ORDER MORE CLOSE WINDOW

This is the copyright permission given by American Society of Mechanical Engineering (ASME) for the content in chapter 4.

Chatura Wickramaratne <chaturaw@mail.usf.edu>

Permission to include a photos and content in a dissertation

Beth Darchi <DarchiB@asme.org> Wed, Oct 4, 2017 at 2:09 PM
To: Chatura Wickramaratne <chaturaw@mail.usf.edu>

Dear Mr. Wickramaratne,
It is our pleasure to grant you permission to use all or any part of the ASME papers:

- Experimental Study on Thermal Storage Performance of Cylindrically Encapsulated PCM in a Cylindrical Storage Tank With Axial Flow, by Chatura Wickramaratne, Francesca Moloney, Tolga Pirasaci, Rajeev Kamal, D. Y. Goswami, Elias Stefanakos and Jaspreet Dhau, Paper No. POWER2016-59427

- Flow Conditioning Techniques for a Bent Pipe in a Constrained Latent Heat Storage System, by Francesca Moloney, Chatura Wickramaratne, Eydhah Almatrafi, D. Y. Goswami, Elias Stefanakos and Rasim Guldiken, Paper No. IMECE2016-65730

cited in your letter for inclusion in a dissertation entitled Experimental Study of High-Temperature Range Latent Heat Thermal Energy Storage to be published by University of South Florida.

Permission is granted for the specific use as stated herein and does not permit further use of the materials without proper authorization. Proper attribution must be made to the author(s) of the materials. **Please note:** if any or all of the figures and/or Tables are of another source, permission should be granted from that outside source or include the reference of the original source. ASME does not grant permission for outside source material that may be referenced in the ASME works.

As is customary, we request that you ensure full acknowledgment of this material, the author(s), source and ASME as original publisher. Acknowledgment must be retained on all pages where figure is printed and distributed.

Many thanks for your interest in ASME publications.

Sincerely,

Beth Darchi

Publishing Administrator

ASME

2 Park Avenue

New York, NY 10016-5990

Tel 1.212.591.7700

darchib@asme.org

ABOUT THE AUTHOR

Chatura Wickramaratne was born in Matara, Sri Lanka on October 10, 1980. He received his bachelor's degree in mechanical engineering from the University of Moratuwa, Sri Lanka, in 2004. He then followed a post graduate diploma course in energy technology from the same university. In 2007 – 2010, he worked as a research and development engineer for Orange Electrics, Sri Lanka, where his work included the development of new products in the category of electrical switches and sockets. From 2010-2011, he worked as an operation manager in a textile company (Hayleys Fabric PLC, Sri Lanka) where his work was related to energy and process optimization. From 2010-2011, he worked as an energy auditing consultant for the Metropolitan Engineering (Pvt) Ltd, Sri Lanka.

He began his doctoral studies in the University of South Florida (USF) in 2012 and started working at the Clean Energy Research Center (CERC) under the guidance of Dr. D. Yogi Goswami. As a part of his PhD work, he developed encapsulation techniques for high temperature phase change materials (PCMs) and analyzed the performance of latent heat thermal energy storage systems.